

UNIVERSITY OF TWENTE

MASTER THESIS

---

# Sustainable Heat Pump Solutions for Dynamic Operational Conditions in Industrial Settings

---

*Author:*

Danique Hemme

*Graduation committee members:*

prof. Dr.-Ing. W. Rohlf

Dr. T. Zhu

Dr. M. Mehrali

R. Poort MSc

Dr. Ir. C. Scholtens

*Master Mechanical Engineering*

Department of Thermal and Fluid Engineering

Faculty of Engineering Technology

March 25, 2025

**UNIVERSITY  
OF TWENTE.**

**TEIJIN ARAMID**

## *Abstract*

The transition towards sustainable industrial energy systems necessitates innovative solutions to enhance energy efficiency and to reduce carbon emissions. This study evaluates the feasibility of integrating heat pump systems into industrial fluid heating and cooling processes at Teijin Aramid's Emmen facility, with a focus on providing process heat for a heating process with a target temperature of 60°C. Given the dynamic fluctuations in temperature and mass flow rates in thermal processes, an optimized heat pump design is required to ensure optimal performance. Currently, conventional heating and cooling methods, such as steam and glycol-based chillers, result in high operational costs and environmental impact, highlighting the need for more energy-efficient alternatives. To improve thermal efficiency within the industrial processes, a comprehensive thermodynamic analysis was conducted to assess the impact of temperature variations, refrigerant selection, and system configuration on overall heat pump performance.

Four heat pump integration concepts were analyzed: independent, centralized, clustered, and cascade configurations. Results indicate that centralized and cascade systems provide the highest efficiency, with coefficient of performance (COP) values of 4.32 and 4.48, respectively. Additionally, mixing of multiple streams before the heat pump inlet, on either the condenser or evaporator side, was found to enhance system performance by reducing exergy destruction and optimizing temperature lift. In contrast, outlet mixing introduced inefficiencies due to increased irreversibilities.

Moreover, refrigerant selection emerged as a critical factor in optimizing both system efficiency and sustainability. R1234ze(Z) and R1233zd(E) demonstrated the most favorable thermodynamic properties, offering high COP and low global warming potential (GWP). For cascade heat pump configurations, R1233zd(E)/R1233zd(E) achieved the highest COP (5.09).

Besides, promising results in terms of energetic performance, economic benefits, and sustainability improvements demonstrate the potential of heat pump technology in industrial applications. However, economic feasibility remains a significant challenge due to high initial capital investments and a five-year payback requirement. While heat pump implementation could reduce energy costs by up to 52%, additional financial subsidies or an extended payback period may be necessary to ensure investment viability.

Overall, this study identifies optimal heat pump configurations and refrigerant choices that enhance energy efficiency, reduce operational costs, and minimize environmental impact in industrial processes. The findings provide first valuable insights into the role of heat pump technology in achieving net-zero emissions targets within energy-intensive industrial sectors.

## *Acknowledgements*

This thesis marks the completion of a challenging and rewarding journey, and I am grateful to everyone who supported me along the way. I would like to take this opportunity to sincerely thank those who contributed to both this research and my personal and academic growth throughout the process.

First, I would like to thank Wilko Rohlf, my supervisor at the university, for his guidance and valuable feedback. His structured approach and insightful advice have helped shape this research, and I greatly appreciate the time and effort he dedicated to our discussions.

I am also grateful to Tingting Zhu for her continuous support, helpful insights, and availability whenever I had questions. Whether during scheduled meetings or last-minute calls, her input was always appreciated.

Thanks to Ron Poort, my daily supervisor at Teijin Aramid, for his continuous support and willingness to answer all my questions, particularly regarding the process and practical aspects. His enthusiasm and occasional pep talks were much appreciated.

I would also like to thank Chris Scholtens, my second supervisor at Teijin, for his sharp questions and constructive feedback. Even though most of our communication was online, his contributions were very valuable.

Lastly, I want to express my gratitude to my family and friends for their continuous support and encouragement. Their patience, understanding, and motivation have been invaluable throughout this journey.

Thank you all for your contributions and support!

# Contents

<b>Abstract</b>	<b>ii</b>
<b>Acknowledgements</b>	<b>iii</b>
<b>1 Introduction</b>	<b>1</b>
1.1 Introduction to sustainable energy in industrial processes . . . . .	2
1.2 Comparable research . . . . .	3
1.3 Thesis outline . . . . .	5
<b>2 Theoretical background</b>	<b>7</b>
2.1 Introduction to heat pumps . . . . .	8
2.2 Theoretical performance of heat pumps . . . . .	9
2.3 Vapor compression heat pumps . . . . .	10
2.3.1 Simple vapor compression cycle . . . . .	10
2.3.2 Cascade cycle . . . . .	13
2.4 Exergy analysis of heat pump systems . . . . .	17
2.5 Refrigerants for sustainable heat pump systems . . . . .	19
2.6 Economic considerations . . . . .	22
<b>3 Analyzing thermal inefficiencies and developing optimal heat pump strategies for industrial applications</b>	<b>23</b>
3.1 Introduction to thermal energy management at Teijin Aramid . . . . .	24
3.1.1 Process challenges and energy inefficiencies . . . . .	26
3.1.2 Thermodynamic evaluation of heat integration opportunities . . . . .	27
3.1.3 Heat pump integration for sustainable process optimization . . . . .	27
3.2 Introduction to heat pump integration concepts . . . . .	30
3.3 List of requirements . . . . .	30
3.4 Development and evaluation of heat pump configurations for process integration	30
3.4.1 Concept 1: Single heat pump per process line (SHP) . . . . .	32
3.4.2 Concept 2: Centralized heat pump system (CHP) . . . . .	33
3.4.3 Concept 3: Heat pump per cluster configuration (HPC) . . . . .	35
3.4.4 Concept 4: Cascade heat pump configuration (CaHP) . . . . .	36
<b>4 Methodology: Thermodynamic modeling and heat pump integration</b>	<b>39</b>
4.1 Thermodynamic model assumptions and approach simple vapor heat pump .	40
4.2 Model validation simple vapor heat pump . . . . .	42
4.3 Thermodynamic model assumptions and approach cascade heat pump . . . .	44
4.4 Model validation cascade heat pump . . . . .	47

<b>5</b>	<b>Thermodynamic analysis</b>	<b>49</b>
5.1	Impact of parameter variation on system performance . . . . .	50
5.1.1	Influence of inlet temperatures . . . . .	50
5.1.2	Influence of mass flow rates . . . . .	51
5.2	Comparative analysis of simple vapor and cascade cycles . . . . .	51
5.3	Screening of refrigerants . . . . .	53
5.3.1	Screening of refrigerants for the simple vapor heat pump integration .	53
5.3.2	Screening of refrigerants for the cascade heat pump . . . . .	54
5.4	Evaluation of COP trends across individual, clustered, and integrated heat pump configurations . . . . .	56
5.4.1	COP variations across individual lines . . . . .	57
5.4.2	COP trends in clustered configurations . . . . .	57
5.4.3	COP performance in system concepts . . . . .	57
5.5	Economic analysis of heat pump configurations . . . . .	58
5.5.1	Operational cost comparison . . . . .	58
5.5.2	Economic feasibility . . . . .	59
5.6	Selection of heat pump configurations for implementation . . . . .	60
<b>6</b>	<b>Effect of mixing on the performance of heat pumps</b>	<b>63</b>
6.1	Introduction to mixing strategies in heat pump systems . . . . .	64
6.2	Thermodynamic principles of mixing . . . . .	67
6.3	Integration of mixing in the heat pump model . . . . .	67
6.4	Results and discussion . . . . .	68
6.4.1	Inlet temperature mixing cases . . . . .	69
6.4.2	Outlet temperature mixing cases . . . . .	72
6.4.3	Inlet mixing extended analysis: Mass flow variation on condenser and evaporator side . . . . .	75
6.4.4	Inlet mixing condenser side extended: Mixing of cascade with simple vapor heat pump . . . . .	82
6.5	Exergy analysis of mixing strategies . . . . .	85
6.5.1	Exergy analysis: Inlet side . . . . .	85
6.5.2	Exergy analysis: Outlet side . . . . .	87
6.6	Conclusion: Influence of mixing strategies on heat pump performance . . . .	89
<b>7</b>	<b>Conclusion</b>	<b>91</b>
7.1	Concluding reflections on research objectives . . . . .	92
7.1.1	Critical process parameters and system performance . . . . .	92
7.1.2	Optimal heat pump configurations for managing dynamic conditions .	92
7.1.3	Impact of refrigerant selection on system efficiency and sustainability .	93
7.1.4	Scalability of heat pump systems under fluctuating production conditions	93
7.1.5	Economic feasibility . . . . .	94
<b>8</b>	<b>Recommendations</b>	<b>95</b>
8.1	Recommendations for Teijin Aramid . . . . .	96
8.2	Recommendations for further reseach . . . . .	97
<b>A</b>	<b>Verification of the thermodynamic model</b>	<b>98</b>

# List of Abbreviations

<b>CAPEX</b>	<b>C</b> apital <b>E</b> xpenditures
<b>CFC</b>	<b>C</b> hloro <b>F</b> luoro <b>C</b> arbons
<b>COP</b>	<b>C</b> oefficient <b>O</b> f <b>P</b> erformance
<b>EEP</b>	<b>E</b> nergy <b>E</b> fficiency <b>P</b> lan
<b>EOS</b>	<b>E</b> quation <b>O</b> f <b>S</b> tate
<b>GWP</b>	<b>G</b> lobal <b>W</b> arming <b>P</b> otential
<b>HC</b>	<b>H</b> ydro <b>C</b> arbons
<b>HCFC</b>	<b>H</b> ydro <b>C</b> hloro <b>F</b> luoro <b>C</b> arbons
<b>HCFO</b>	<b>H</b> ydro <b>C</b> hloro <b>F</b> luoro <b>O</b> lefins
<b>HFC</b>	<b>H</b> ydro <b>F</b> luoro <b>C</b> arbons
<b>HFO</b>	<b>H</b> ydro <b>F</b> luoro <b>O</b> lefins
<b>HTCHP</b>	<b>H</b> igh <b>T</b> emperature <b>C</b> ascade <b>H</b> eat <b>P</b> ump
<b>HTHP</b>	<b>H</b> igh <b>T</b> emperature <b>H</b> eat <b>P</b> ump
<b>IEA</b>	<b>I</b> nternational <b>E</b> nergy <b>A</b> gency
<b>IHX</b>	<b>I</b> ntermediate <b>H</b> eat <b>e</b> Xchanger
<b>LMTD</b>	<b>L</b> ogarithmic <b>M</b> ean <b>T</b> emperature <b>D</b> ifference
<b>NZE</b>	<b>N</b> et <b>Z</b> ero <b>E</b> missions
<b>ODP</b>	<b>O</b> zone <b>D</b> epletion <b>P</b> otential
<b>OPEX</b>	<b>O</b> perating <b>E</b> xpenditures
<b>ROI</b>	<b>R</b> eturn <b>O</b> f <b>I</b> nterest
<b>TAC</b>	<b>T</b> otal <b>A</b> nnual <b>C</b> ost
<b>TEWI</b>	<b>T</b> otal <b>E</b> quivalent <b>W</b> arming <b>I</b> mpact

# List of Symbols

## Symbols:

$C$	Heat capacity	[J/K]
$h$	Specific enthalpy	[J/kg]
$\dot{m}$	Mass flow rate	[kg/s]
$P$	Pressure	[Pa]
$\dot{Q}$	Heat transfer rate	[W]
$S$	Entropy	[J/K]
$s$	Specific entropy	[J/kgK]
$\Delta S$	Entropy drop	[J/K]
$T$	Temperature	[K]
$\Delta T$	Temperature difference	[K]
$\bar{T}$	Logarithmic mean temperature	[K]
$U$	Overall heat transfer coefficient	[W/m <sup>2</sup> K]
$W$	Work	[W]
$\eta$	Efficiency	[-]

## Subscripts:

C	Lower-temperature cycle
c	Condenser side
cond	Condenser
des	Destruction
e	Evaporator side
evap	Evaporator
H	Higher-temperature cycle
i	Inlet
in	Inlet
lm	Logarithmic mean
mix	Mixing
out	Outlet
o	Outlet
ref	Refrigerant
tot	Total

## Chapter 1

# Introduction

*As the global effort to combat climate change intensifies, the need for sustainable energy solutions has become increasingly urgent. The International Energy Agency's (IEA) Net Zero Emissions (NZE) by 2050 Scenario highlights the critical role of energy efficiency and the electrification of industrial processes in reducing carbon emissions. This research focuses on improving energy consumption at Teijin Aramid's Emmen facility, where energy-intensive thermal processes present opportunities for efficiency improvements through the integration of heat pump technology. Heat pumps offer the potential to recover and redistribute thermal energy, reducing reliance on conventional heating and cooling methods while lowering operational costs and environmental impact. The study aims to assess the feasibility of such a system under fluctuating production demands and dynamic operational conditions. By exploring this approach, this chapter contributes to the broader transition toward sustainable industrial energy systems and highlights the role of heat pumps in enhancing energy efficiency.*

## 1.1 Introduction to sustainable energy in industrial processes

The global transition towards sustainable energy systems has become a critical focus in addressing climate change. The International Energy Agency's (IEA) Net Zero Emissions by 2050 Scenario (NZE) outlines a comprehensive pathway for reducing carbon dioxide ( $CO_2$ ) emissions across all sectors, emphasizing energy efficiency, renewable energy integration, and electrification of industrial processes. A key aspect of this transition is the increasing role of electricity in final energy consumption, with its share expected to grow from 20% in 2022 to over 27% by 2030. Achieving this shift will be vital to realizing net zero emissions by mid-century, particularly within energy-intensive sectors like industry, which accounted for 37% of global energy use in 2022 [1]. Achieving this growth will require a compound annual growth rate of 4.1%, underscoring the urgency of electrification in industrial sectors, where optimizing energy consumption is crucial not only for sustainability but also for operational efficiency and competitiveness.

Teijin Aramid, based in Arnhem, is a leading manufacturer of high-performance para-aramid fibers, with a production spinning facility located in Emmen. The company's primary product, Twaron, is a synthetic fiber known for its exceptional tensile strength and heat resistance. Twaron is used in a wide range of applications, including bulletproof vests, aerospace composite materials, automotive components, protective clothing, and ropes and cables. The fiber's unique properties make it a viable alternative to traditional materials like steel or asbestos, offering comparable or superior performance while significantly reducing weight. Committed to sustainability, Teijin Aramid is actively exploring innovative methods to minimize its environmental impact.

This research focuses on optimizing energy consumption at Teijin Aramid's Emmen facility, where energy-intensive processes present opportunities for efficiency improvements through heat pump technology. The production process involves multiple stages that require significant thermal energy inputs, with conventional heating and cooling methods relying on steam and glycol-based chillers. These systems contribute to high operational costs and substantial carbon emissions. To address these challenges, Teijin Aramid is considering the implementation of a heat pump system to enhance heat recovery and thermal management within the facility. This system would leverage a warm process stream as a heat source, extracting energy to elevate another process stream to the required temperature of 60 °C while simultaneously providing cooling. By integrating this approach, the facility could achieve significant reductions in both energy consumption and environmental impact.

The primary objective of this study is to evaluate the feasibility of such a heat pump system, taking into account the fluctuating production demands and dynamic operational conditions at the facility. Conventional heat pump systems, even when specifically adapted to accommodate the dynamic conditions of a single production line, may exhibit limitations in flexibility, particularly in handling frequent variations in temperature and mass flow rates. Heat pumps are generally designed for steady-state operation, and as a result, their efficiency and reliability may be compromised under variable load conditions, such as those observed in Teijin Aramid's production process. Therefore, a comprehensive thermodynamic analysis is conducted to assess the impact of key process variables including temperature variations, mixing strategies, and refrigerant selection on overall heat pump performance. Additionally, both

single-stage vapor compression cycles and cascade heat pump configurations are examined to determine the most efficient system integration strategy. A comparative evaluation of multiple heat pump configurations ranging from decentralized, independent systems to centralized and cascade setups is performed, with key performance indicators such as COP, exergy efficiency, and operational costs taken into account.

By systematically analyzing various heat pump cycles under fluctuating temperature and mass flow conditions, this research seeks to identify the most effective system configuration that achieves an optimal balance between operational efficiency and environmental sustainability. Factors such as process integration, system scalability, and economic viability are examined in detail, with the overarching objective of providing insights into the role of heat pump technology in achieving net-zero energy (NZE) targets.

Once the most efficient heat pump configuration is identified, refrigerant selection plays a critical role in further optimizing system performance. Environmental considerations, thermodynamic properties, and compatibility with existing simulation tools must be carefully evaluated. The study investigates potential refrigerants that align with sustainability targets while ensuring optimal performance under industrial operating conditions.

Ultimately, this research aims to determine optimal configurations and strategies for maximizing heat pump performance while ensuring energy-efficient and sustainable operation. The focus is on achieving the target temperature of 60 °C for the heating process while also evaluating the potential benefits of cooling within the system. This approach ensures that operational requirements are met while enhancing energy efficiency and reducing the facility's environmental impact.

To this end, the study presents a feasibility analysis aimed at assessing the potential of heat pump technology to not only reduce operational costs but also minimize environmental impacts. The central research question guiding this investigation is as follows: *How can heat pump cycles be integrated into industrial fluid heating and cooling processes, characterized by dynamic fluctuations in temperature and mass flow rates, to optimize energy efficiency, operational feasibility, and environmental sustainability in the textile industry?*

## 1.2 Comparable research

A thorough examination of high-temperature heat pump (HTHP) technologies can be found in the paper 'High-temperature heat pumps: Market overview, state of the art, research status, refrigerants, and application potentials' by Arpagaus et al. [2]. It provides a market overview, describes the state of the art currently, and assesses recent advancements in the field of research. The efficiency and environmental impact of the different refrigerants used in these systems are also discussed and evaluated in this paper. Moreover, it investigates the possible uses of HTHPs in sectors like paper, food processing, and chemicals where high-temperature heat is necessary. The authors draw attention to the opportunities and challenges presented by technology as well as the necessity of innovation in order to increase the usability and effectiveness of HTHPs in industrial applications.

The study by Y. Dong and R. Wang [3] investigates the optimal application of cascade high-temperature heat pumps (CHTHPs) by evaluating their performance across different temperature lifts, working fluid pairs, and operational conditions. The research compares four heat pump configurations—single-stage, two-stage, injection-assisted, and cascade—against 289 refrigerant combinations to determine their efficiency based on COP, cost, exergy efficiency, and total equivalent warming impact (TEWI). The findings indicate that cascade configurations are most effective when the temperature lift exceeds 70°C, as they allow for the efficient utilization of ultra-low-grade waste heat while supplying high-temperature process heat. However, for lower temperature lifts, two-stage and single-stage heat pumps become more favorable due to their lower capital costs and reduced exergy losses. The study also employs a multi-criteria decision-making (MCDM) approach to assess the trade-offs between economic, environmental, and safety considerations in selecting the optimal configuration and refrigerant pair.

The research conducted by Wu D. et al. [4] focuses on the critical assessment and application of multiple heat pump systems using each utilizing a range of low Global Warming Potential (GWP) refrigerants. This segment of research is critical for developing more eco-friendly heating and cooling solutions without compromising efficiency. The authors categorize and analyze the performance of systems such as single-stage, multi-stage, and variable refrigerant flow configurations under different operational conditions. This comprehensive overview aids in understanding the specific advantages and limitations associated with each refrigerant type across various system setups. Furthermore, the article presents a matrix that identifies which combinations of refrigerants and heat pump systems have been extensively researched versus those that have not. This framework is particularly valuable for pinpointing research gaps in the field.

The article 'Multi-temperature heat pumps – A literature review' by Cordin Arpagaus et al. [5] delves into advanced heat pump systems designed for multi-temperature applications. It highlights various system configurations like multi-stage compressors and cascades, commonly used in industries requiring differentiated temperature control, such as supermarkets with transcritical  $CO_2$  systems. The review emphasizes innovations like ejectors and separated gas coolers that enhance efficiency, and points to multi-stage compressor cycles as offering the highest efficiencies for substantial energy savings in industrial settings.

The article 'The Challenge of Integrating Non-Continuous Processes – Milk Powder Plant Case Study' by M. Atkins et al. [6] examines the integration challenges of non-continuous processes in a New Zealand dairy factory, particularly focusing on energy efficiency through indirect heat transfer. The study investigates the use of a heat recovery loop and a stratified tank to enhance heat exchange between various semi-continuous plants within the dairy factory. It highlights that direct integration is impractical due to varying operational schedules and proposes a solution that involves adjusting the temperature of the hot fluid in the recirculation loop based on operational conditions to maximize heat recovery. The findings suggest significant potential for energy savings by optimizing the heat recovery process and using thermal storage to buffer operational variations.

The study by J.V.M. Walden and P. Stathopoulos [7] explores the role of heat pump load flexibility in optimizing system integration, economic performance, and energy efficiency within industrial processes. By leveraging time-resolved industrial process data, the research assesses how different levels of part-load operation affect key performance metrics, including Net Present Value (NPV), COP, and heating capacity. The study finds that increasing load flexibility enhances economic viability, as more adaptable systems can respond more efficiently to fluctuating heat demands. However, it also identifies a flexibility threshold (45–55% minimum load), beyond which additional flexibility provides diminishing returns. This insight is particularly relevant for determining the optimal balance between system size, investment cost, and operational efficiency in heat pump integration.

The article titled 'Heat pump integration in non-continuous industrial processes by Dynamic Pinch Analysis Targeting' by J.V.M. Walden et al. [8] introduces a methodology for heat pump design and sizing using simulated annual process data, offering a more dynamic alternative to the Time Average Model (TAM). It evaluates three approaches: (1) conventional TAM, (2) Pinch Analysis optimization, and (3) advanced economic optimization with NPV & IRR included. The findings show that a 33% smaller heat pump can achieve 2.22% lower OPEX, compared to 1.75% in TAM-based systems. Economic performance also improves significantly, with NPV and IRR tripling due to increased operating hours. This demonstrates that dynamic heat pump integration enhances system efficiency and investment profitability.

### 1.3 Thesis outline

This thesis explores the potential for heat integration and recovery at Teijin Aramid's Emmen facility, focusing on the influence of dynamic operational conditions such as fluctuating mass flows and temperatures on energy efficiency. The research examines the challenges that arise due to these variations in process lines and evaluates the most effective heat pump system to optimize performance and improve environmental sustainability in an industrial setting with continuously changing conditions. The main objective of this study is to determine the feasibility and efficiency of heat pump integration under varying process conditions. Specifically, to answer the following research question:

*How can heat pump cycles be integrated into industrial processes in the textile industry, characterized by dynamic fluctuations in temperature and mass flow rates, to optimize energy efficiency, operational feasibility, and environmental sustainability?*

To achieve this, the project aims to accomplish the following objectives:

- Analyze the key process parameters, such as temperature variations, mass flow rates, and energy consumption, that impact the selection and design of an optimal heat pump system.
- Determine the optimal heat pump configurations for managing dynamic temperature ranges and mass flow rates in a manufacturing line.
- Evaluate how different refrigerants impact heat pump cycles' efficiency and environmental footprint under fluctuating operational conditions.

- Assess the scalability of heat pump systems using the selected refrigerant when addressing variations in the number of production lines and dynamic fluctuating demands.
- Analyze the anticipated capital and operational expenses (CAPEX and OPEX) of implementing the selected refrigerant in heat pump systems and compare these costs to the expected energy savings and payback period.

The investigation into optimizing and sustaining energy consumption at Teijin Aramid's Emmen facility is structured into distinct project stages, with each phase detailed in its respective chapter.

Chapter 2 provides a theoretical foundation on heat pump technology, including vapor compression cycles, exergy analysis, and thermodynamic equations. Additionally, it explores refrigerant selection for sustainable industrial applications, considering environmental impact and thermodynamic performance.

Chapter 3 presents a case study on thermal energy management at Teijin Aramid's Emmen facility. It outlines various system concepts ranging from decentralized to centralized and cascade setups and discusses their theoretical advantages, limitations, and expected impacts on energy efficiency and operational feasibility.

Chapter 4 focuses on the thermodynamic modeling and validation of heat pump systems. A mathematical framework is developed for both the simple vapor compression cycle and the cascade heat pump configuration. The models are validated using reference thermodynamic data to ensure accuracy and applicability in industrial conditions.

Chapter 5 conducts a performance analysis of heat pump systems under varying operational conditions. The influence of key parameters such as inlet temperatures, mass flow rates, and pressure ratios on system efficiency is examined. Furthermore, an economic analysis is conducted to evaluate cost implications, payback periods, and the financial feasibility of heat pump integration.

Chapter 6 investigates the effect of mixing on heat pump performance, analyzing temperature and mass flow variations. Various mixing strategies are modeled to quantify their impact on system stability, energy efficiency, and exergy losses. The findings provide guidelines for optimizing heat pump operation under fluctuating production conditions.

Chapter 7 summarizes key findings on heat pump performance, energy efficiency, and operational impacts. It assesses the feasibility of heat pump implementation at Teijin Aramid and identifies the most effective system configurations.

Chapter 8 provides recommendations for future research and practical implementation at Teijin Aramid, outlining key areas for further investigation and operational improvements.

## Chapter 2

# Theoretical background

*The transition toward sustainable and energy-efficient industrial systems necessitates a thorough understanding of the principles and technologies that enable their implementation. This chapter provides the theoretical foundation required to analyze and optimize heat pump systems for industrial applications, focusing on thermodynamic and operational characteristics. The chapter explores the mechanisms of heat pumps, covering energy transfer processes, performance metrics like COP, and efficiency considerations. Configurations including the simple vapor compression and cascade cycles are examined to demonstrate their applicability across various operational scenarios. The evaluation of refrigerant selection emphasizes environmentally sustainable options, while exergy analysis is discussed to identify inefficiencies. Economic factors, including CAPEX, OPEX, and payback periods, are also addressed to contextualize the integration of heat pumps within industrial systems.*

## 2.1 Introduction to heat pumps

In a heat pump, thermal energy is transferred from a lower-temperature source  $T_C$  to a higher-temperature sink  $T_H$  through the input of external work  $\dot{W}_{in}$ . This fundamental operation is depicted schematically in Figure 2.1.

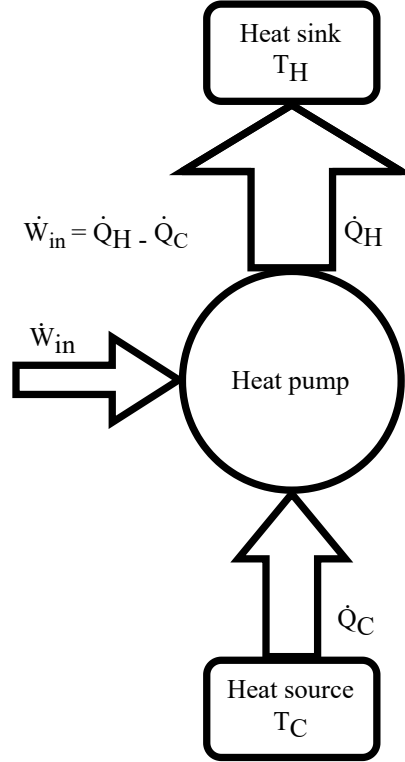


FIGURE 2.1: Schematic of a heat pump transferring heat from a low-temperature source ( $T_C$ ) to a high-temperature sink ( $T_H$ ) with work input ( $\dot{W}_{in}$ ).

Heat pumps operate based on the principles of the first and second laws of thermodynamics. According to the first law of thermodynamics, energy cannot be created or destroyed, emphasizing the principle of energy conservation. For the heat pump cycle, the internal energy change,  $\Delta U$ , must equal zero. This is expressed as:

$$\Delta U = \dot{Q}_C + \dot{W}_{in} + \dot{Q}_H = 0, \quad (2.1)$$

where  $\dot{Q}_C$  denotes the rate of heat transfer from the low-temperature source, and  $\dot{Q}_H$  is the rate of heat transfer to the high-temperature sink, and  $\dot{W}_{in}$  is the rate of work input [9].

The second law of thermodynamics states that heat transfer occurs spontaneously from a higher-temperature body to a lower-temperature body. This behavior is governed by the entropy of the system, which must adhere to the following conditions:

$$\Delta S \geq 0, \quad (2.2)$$

where  $\Delta S$  represents the change in entropy of the system. To achieve the reverse flow of heat from the heat source to the heat sink at elevated temperatures external work is required [9].

## 2.2 Theoretical performance of heat pumps

The performance of heat pumps and refrigeration systems is commonly evaluated using the COP, which quantifies the ratio of thermal energy transferred to the external work input. Industrial heat pumps typically achieve performance values ranging from 2 to 5, meaning they deliver 2 to 5 units of heat energy for each unit of electrical energy consumed [10].

Under ideal, reversible conditions, the maximum theoretical performance is described by the Carnot cycle [9]. The Carnot COP represents the upper limit of efficiency for a heat pump or refrigeration system. For heating and cooling modes, the Carnot COP can be expressed as:

$$\text{COP}_{\text{Carnot}} = \begin{cases} \frac{T_{\text{H}}}{T_{\text{H}} - T_{\text{C}}}, & \text{heating mode} \\ \frac{T_{\text{C}}}{T_{\text{H}} - T_{\text{C}}}, & \text{cooling mode} \end{cases} \quad (2.3)$$

where  $T_{\text{H}}$  and  $T_{\text{C}}$  are the absolute temperatures of the heat sink and heat source, respectively, expressed in Kelvin.

In practical systems, the actual performance in heating and cooling modes is calculated as:

$$\text{COP} = \begin{cases} \frac{\dot{Q}_{\text{H}}}{\dot{W}_{\text{in}}}, & \text{heating mode} \\ \frac{\dot{Q}_{\text{C}}}{\dot{W}_{\text{in}}}, & \text{cooling mode} \end{cases} \quad (2.4)$$

The Lorenz COP ( $\text{COP}_{\text{Lorenz}}$ ) accounts for the variation in temperature of the heat reservoirs during the heat transfer process, commonly referred to as the temperature glide [11]. This makes it a more realistic measure of performance for systems where heat transfer occurs under non-isothermal conditions. The Lorenz COP is defined as:

$$\text{COP}_{\text{Lorenz}} = \frac{\bar{T}_{\text{H}}}{\bar{T}_{\text{H}} - \bar{T}_{\text{C}}}, \quad (2.5)$$

where  $\bar{T}_{\text{H}}$  and  $\bar{T}_{\text{C}}$  are the logarithmic mean temperatures for the heat transfer processes at the sink and source side, respectively. These mean temperatures are calculated using the following:

$$\bar{T} = \begin{cases} \frac{\Delta T_{\text{H}}}{\ln\left(\frac{T_{\text{H,o}}}{T_{\text{H,i}}}\right)}, & \text{sink side (high-temperature side)} \\ \frac{\Delta T_{\text{C}}}{\ln\left(\frac{T_{\text{C,i}}}{T_{\text{C,o}}}\right)}, & \text{source side (low-temperature side)} \end{cases} \quad (2.6)$$

The temperature differences for the heating and cooling processes are defined as:

$$\Delta T = \begin{cases} T_{H,o} - T_{H,i}, & \text{sink side (high-temperature side)} \\ T_{C,i} - T_{C,o}, & \text{source side (low-temperature side)} \end{cases} \quad (2.7)$$

where  $T_{H,o}$  and  $T_{H,i}$  denote the outlet and inlet temperature at the sink side (high-temperature side), while  $T_{C,i}$  and  $T_{C,o}$  correspond to the inlet and outlet temperature at the source side (low-temperature side).

The Lorenz efficiency,  $\eta_{\text{Lorenz}}$ , quantifies the performance of a heat pump or refrigeration system by comparing the actual COP to the theoretical Lorenz COP. This relationship is expressed as:

$$\eta_{\text{Lorenz}} = \frac{\text{COP}}{\text{COP}_{\text{Lorenz}}}, \quad (2.8)$$

where COP refers to the COP for either heating or cooling modes [11].

## 2.3 Vapor compression heat pumps

The vapor compression cycle, in its simplest form, represents a single-stage configuration widely employed in heat pump systems to facilitate heat transfer across moderate temperature differences. This section explores the fundamental principles and thermodynamic behavior of this cycle, as well as its application in industrial and domestic heat pump systems. Additionally, the cascade heat pump system, a configuration designed for larger temperature differences, is introduced. The cascade system consists of two interconnected vapor compression cycles operating at distinct temperature levels, with an intermediate heat exchanger enabling efficient heat transfer. The thermodynamic advantages of the cascade cycle are evaluated, particularly for applications requiring significant temperature lifts.

### 2.3.1 Simple vapor compression cycle

The simple vapor compression cycle also referred to as the single-stage vapor compression cycle, is the most commonly used configuration in heat pump applications [9]. It operates by transferring heat from a low-temperature source to a high-temperature sink. Figure 2.2 illustrates the schematic of this system, which uses R134a as the working fluid. The cycle comprises four main processes: evaporation, compression, condensation, and expansion. The refrigerant absorbs heat ( $\dot{Q}_{\text{in}}$ ) from the low-temperature source in the evaporator, transitions to a high-pressure, high-temperature state in the compressor, releases heat ( $\dot{Q}_{\text{out}}$ ) to the high-temperature sink in the condenser, and finally returns to its initial state through an isenthalpic expansion process in the expansion valve.

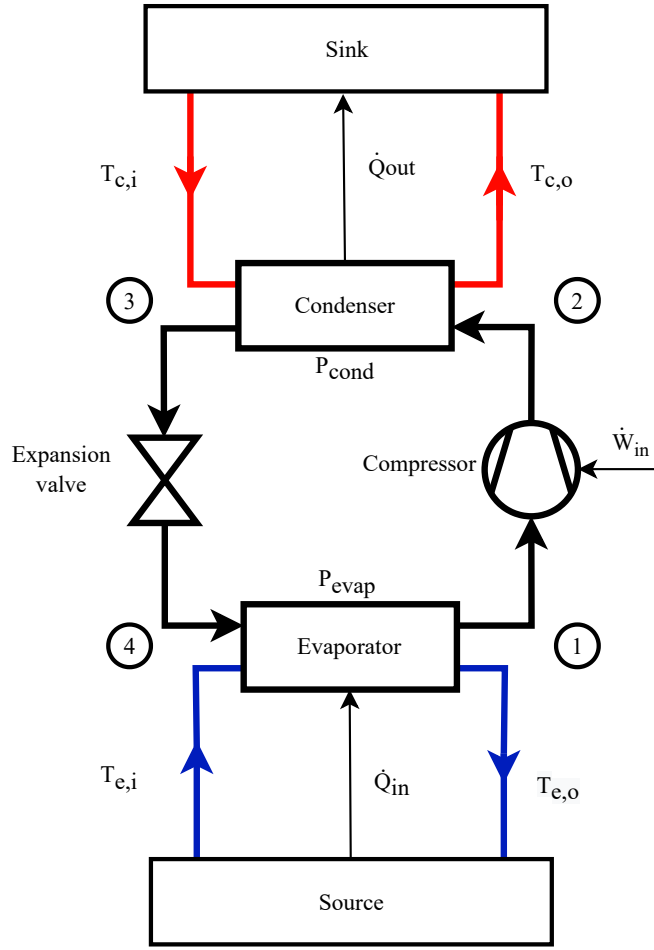


FIGURE 2.2: Schematic of a simple vapor compression heat pump system using R134a, transferring heat from the sink to the source.

**Evaporator** The refrigerant enters the evaporator as a low-pressure, low-temperature liquid. As it absorbs heat from the source, it undergoes a phase change to a low-pressure vapor. The heat absorbed by the refrigerant in the evaporator,  $\dot{Q}_{\text{evap}}$ , is calculated as:

$$\dot{Q}_{\text{evap}} = \dot{m}_{\text{ref}}(h_1 - h_4), \quad (2.9)$$

where,  $h_1$  and  $h_4$  represent the specific enthalpies of the refrigerant at the evaporator inlet and outlet, respectively. The refrigerant exits the evaporator at state 1 and enters at state 4 as shown in Figure 2.2.

The heat transferred from the source fluid to the evaporator, ( $\dot{Q}_{\text{in}}$ ), can be determined using:

$$\dot{Q}_{\text{in}} = \dot{m}_e c_p (T_{e,i} - T_{e,o}), \quad (2.10)$$

where  $\dot{m}_e$  and  $c_p$  denote the mass flow rate and specific heat capacity of the source fluid, respectively. Here,  $T_{e,i}$  and  $T_{e,o}$  represent the temperature of the source fluid at the evaporator inlet and outlet, respectively.

**Compressor** The refrigerant vapor exiting the evaporator at state 1 is compressed to a high-pressure, high-temperature vapor at state 2. The work input required for this process,  $\dot{W}_{\text{in}}$ , is given by:

$$\dot{W}_{\text{in}} = \dot{m}_{\text{ref}}(h_2 - h_1), \quad (2.11)$$

where  $h_1$  and  $h_2$  represent the specific enthalpies at the compressor inlet and outlet, respectively. The isentropic efficiency of the compressor,  $\eta_c$ , is defined as:

$$\eta_c = \frac{h_{2s} - h_1}{h_2 - h_1}, \quad (2.12)$$

where,  $h_{2s}$  is the enthalpy at the compressor outlet under isentropic conditions.

**Condenser** The high-pressure, high-temperature refrigerant releases heat to the sink in the condenser, transitioning from a vapor to a liquid state. The heat released,  $\dot{Q}_{\text{out}}$ , is calculated as:

$$\dot{Q}_{\text{out}} = \dot{m}_c c_p (T_{c,o} - T_{c,i}), \quad (2.13)$$

where  $T_{c,i}$  and  $T_{c,o}$  are the inlet and outlet temperatures of the condenser, and  $\dot{m}_c$  is the mass flow rate of the sink fluid. The heat released by the refrigerant to that absorbed by the condenser,  $\dot{Q}_{\text{cond}}$ , is expressed as:

$$\dot{Q}_{\text{cond}} = \dot{m}_{\text{ref}}(h_2 - h_3), \quad (2.14)$$

where  $h_2$  and  $h_3$  are the specific enthalpies at the condenser inlet (state 2) and condenser outlet (state 3), respectively.

**Expansion Valve** The refrigerant exits the condenser at state 3 as a high-pressure liquid and enters the expansion valve. During this isenthalpic process, the refrigerant's pressure and temperature drop significantly, and it exits the valve at state 4 before re-entering the evaporator to complete the cycle.

**Energy balance and COP formulation** The energy balance of the cycle is governed by:

$$\dot{Q}_{\text{out}} = \dot{Q}_{\text{in}} + \dot{W}_{\text{in}}. \quad (2.15)$$

This equation ensures that the heat released to the sink equals the sum of the heat absorbed from the source and the work input.

In Equation (2.4) COP is defined as the ratio of useful heat transfer to the work input and can be expressed in terms of enthalpy differences:

$$\text{COP} = \begin{cases} \frac{h_3 - h_2}{h_2 - h_1}, & \text{heating mode} \\ \frac{h_1 - h_4}{h_2 - h_1}, & \text{cooling mode} \end{cases} \quad (2.16)$$

**Thermodynamic representation** The thermodynamic behavior of the refrigerant is typically illustrated using pressure-enthalpy (p-h) and temperature-entropy (T-s) diagrams, as

shown in Figure 2.3. These diagrams depict the four primary processes of the cycle: evaporation, compression, condensation, and expansion, providing insights into the pressure, temperature, enthalpy, and entropy changes of the refrigerant throughout the cycle.

The (log)p-h diagram, shown on the left, plots the pressure of the refrigerant on a logarithmic scale against its specific enthalpy. This diagram is particularly useful for understanding the energy transfer in the system, as it shows the heat and work interactions of the refrigerant during each process. The first process is compression (1 to 2), where the pressure and enthalpy increase due to the work input; condensation (2 to 3), where the refrigerant releases heat at constant high pressure; expansion (3 to 4), where pressure and temperature drop without a change in enthalpy; and evaporation (4 to 1), where the refrigerant absorbs heat at constant low pressure, completing the cycle.

The T-s diagram, shown on the right, plots the temperature of the refrigerant against its specific entropy. This diagram provides insight into the thermodynamic efficiency of the cycle by illustrating the relationship between heat transfer and entropy changes. The compression process (1 to 2) shows an increase in both temperature and entropy, condensation (2 to 3) occurs at constant temperature with decreasing entropy, and expansion (3 to 4) is represented by a vertical line indicating a drop in temperature with constant entropy, and evaporation (4 to 1) involves heat absorption at nearly constant temperature, increasing entropy [9].

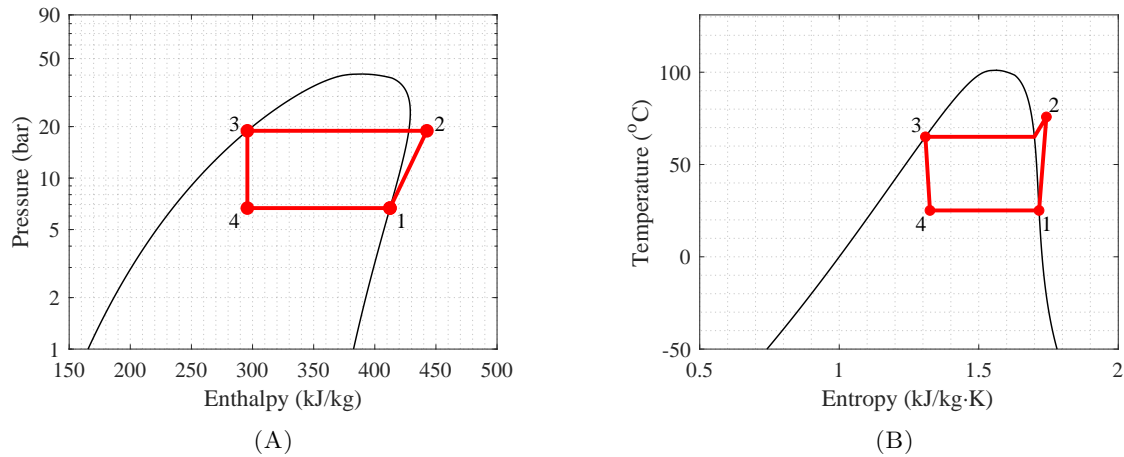


FIGURE 2.3: P-h diagram (A) and T-s diagram (B) of R134a refrigerant with a condensation temperature of  $65^{\circ}\text{C}$  and an evaporation temperature of  $25^{\circ}\text{C}$ .

### 2.3.2 Cascade cycle

The cascade heat pump system is an advanced configuration designed to handle significant temperature differences that exceed the operational limits of a single-stage vapor compression cycle. It integrates two interconnected cycles: a low-temperature cycle (cycle A) and



as it passes through the evaporator. The heat absorbed,  $\dot{Q}_{\text{in}}$ , is expressed as:

$$\dot{Q}_{\text{in}} = \dot{m}_A(h_1 - h_4), \quad (2.17)$$

where  $h_1$  and  $h_4$  are the specific enthalpies of the refrigerant at the evaporator outlet and inlet, respectively. The refrigerant exits the evaporator at state 1 and enters the compressor, where it undergoes compression to a high-pressure vapor at state 2. The work input for this process,  $\dot{W}_{\text{in,A}}$ , is calculated as:

$$\dot{W}_{\text{in,A}} = \dot{m}_A(h_2 - h_1). \quad (2.18)$$

The high-pressure vapor releases heat in the IHX, transitioning to a high-pressure liquid. The heat released by the refrigerant,  $\dot{Q}_{\text{IHX,A}}$ , is given by:

$$\dot{Q}_{\text{IHX,A}} = \dot{m}_A(h_2 - h_3) \quad (2.19)$$

where  $h_2$  and  $h_3$  are the specific enthalpies of the refrigerant entering and exiting the IHX on the low-temperature side. After releasing heat, the refrigerant undergoes isenthalpic expansion through an expansion valve, reducing its pressure and temperature before re-entering the evaporator at state 4.

**High-temperature cycle (Cycle B)** The high-temperature cycle absorbs heat from the IHX, where the refrigerant enters at state 5 as a low-pressure liquid and exits as a low-pressure vapor at state 6. The heat absorbed,  $\dot{Q}_{\text{IHX,B}}$ , is calculated as:

$$\dot{Q}_{\text{IHX,B}} = \dot{m}_B(h_5 - h_8), \quad (2.20)$$

where  $h_5$  and  $h_8$  represent the specific enthalpies of the refrigerant entering and exiting the IHX on the high-temperature side. The refrigerant is then compressed to a high-pressure vapor at state 7. The work input for this process,  $\dot{W}_{\text{in,B}}$ , is given by:

$$\dot{W}_{\text{in,B}} = \dot{m}_B(h_6 - h_5). \quad (2.21)$$

The high-pressure vapor releases heat to the sink in the condenser, transitioning to a high-pressure liquid at state 8. The heat released,  $\dot{Q}_{\text{out}}$ , is expressed as:

$$\dot{Q}_{\text{out}} = \dot{m}_B(h_6 - h_7), \quad (2.22)$$

where  $h_6$  and  $h_7$  are the specific enthalpies of the refrigerant entering and leaving the condenser. Finally, the refrigerant undergoes isenthalpic expansion, reducing its pressure and temperature before re-entering the IHX at state 5.

**Energy Balance and COP Formulation** The cascade system adheres to the first law of thermodynamics, ensuring that the heat rejected by cycle A equals the heat absorbed by cycle B in the IHX:

$$\dot{m}_B(h_5 - h_8) = \dot{m}_A(h_2 - h_3). \quad (2.23)$$

The COP for the cascade system can be calculated for both cooling and heating modes based on the energy balances within the system and is expressed as:

$$\text{COP} = \begin{cases} \frac{\dot{Q}_{\text{out}}}{\dot{W}_{\text{net}}} = \frac{\dot{m}_{\text{B}}(h_6 - h_7)}{\dot{m}_{\text{B}}(h_6 - h_5) + \dot{m}_{\text{A}}(h_2 - h_1)}, & \text{heating mode} \\ \frac{\dot{Q}_{\text{in}}}{\dot{W}_{\text{net}}} = \frac{\dot{m}_{\text{A}}(h_1 - h_4)}{\dot{m}_{\text{B}}(h_6 - h_5) + \dot{m}_{\text{A}}(h_2 - h_1)}, & \text{cooling mode} \end{cases} \quad (2.24)$$

where  $\dot{W}_{\text{net}}$  represents the total work input, which is the sum of the work inputs for cycles A and B.

**Thermodynamic representation** The thermodynamic behaviour of the cascade heat pump system is depicted through the (log)p-h (pressure-enthalpy) and T-s (temperature-entropy) diagrams, as shown in Figure 2.5. The principles underlying these diagrams are similar to those described for the simple vapor compression cycle. However, the cascade system introduces additional complexities due to the integration of two interconnected cycles, each with distinct thermodynamic states.

In the p-h diagram (A in Figure 2.5), the low-temperature cycle (cycle A) begins with heat absorption in the evaporator (1 to 2), followed by compression (2 to 3), heat transfer to the high-temperature cycle via the intermediate heat exchanger (3 to 4), and expansion (4 to 1). The high-temperature cycle (cycle B) absorbs heat from the IHX (5 to 6), undergoes compression (6 to 7), releases heat to the sink in the condenser (7 to 8), and then expands (8 to 5).

The T-s diagram (B in Figure 2.5) similarly reflects these processes but highlights the thermodynamic efficiency and entropy changes across the cycles. The IHX serves as a key distinction between the two cycles, facilitating heat transfer while maintaining separate pressure and temperature ranges for each stage. A zoomed-in view of the T-s diagram (C in 2.5) emphasizes critical points in the high-temperature region, particularly the entropy and temperature changes during compression (1 to 2 and 5 to 6) [9].

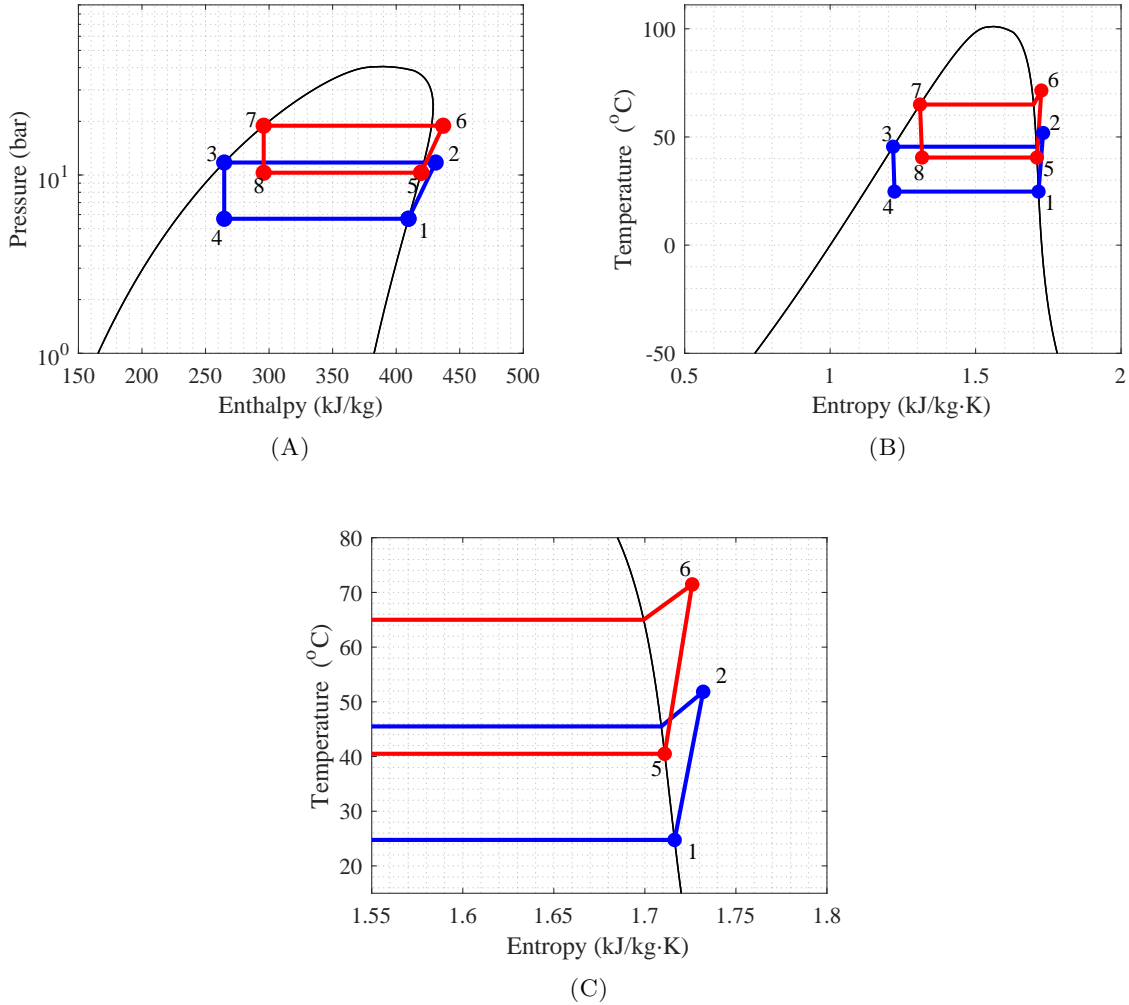


FIGURE 2.5: P-h diagram (A) and T-s diagram (B) for the cascade heat pump system using R134a as the refrigerant in both the upper and lower cycle, with a condensation temperature of  $65^{\circ}\text{C}$  and an evaporation temperature of  $25^{\circ}\text{C}$ . The zoomed-in T-s diagram (C) provides enhanced visibility of the thermodynamic states in both the high- and low-temperature cycles.

## 2.4 Exergy analysis of heat pump systems

Exergy analysis is a thermodynamic tool used to evaluate the quality and efficiency of energy transformations within a system. While energy is conserved according to the first law of thermodynamics, exergy introduces the concept of energy quality, accounting for the system's ability to perform useful work. Unlike energy, exergy is not conserved; it is destroyed due to irreversibilities governed by the second law of thermodynamics [9]. These irreversibilities, arising from processes such as friction, heat transfer across finite temperature differences, and mixing, result in exergy destruction, which directly limits the system's performance. Exergy analysis is therefore instrumental in identifying inefficiencies and potential areas for optimization within heat pumps.

Exergy is defined as the maximum useful work that can be obtained as a system transitions to equilibrium with its surroundings. By quantifying exergy destruction in each component, areas of improvement can be identified to optimize the system's overall efficiency. The exergy destruction within a system component the difference between the exergy entering and leaving the component and can be calculated by

$$\Delta \dot{E}_{\text{component}} = \dot{E}_{\text{in}} - \dot{E}_{\text{out}}, \quad (2.25)$$

where  $\dot{E}_{\text{in}}$  and  $\dot{E}_{\text{out}}$  represents the difference between the exergy entering and leaving a control volume.

**Simple vapor heat pump** The exergy destruction rates for each component in the simple vapor heat pump system discussed in Section 2.3.1 are defined as follows [12]:

$$\Delta \dot{E} = \begin{cases} \dot{m}_{\text{ref}} [(h_1 - h_2) - T_0(s_1 - s_2)] + \dot{W}_{\text{in}}, & \text{Compressor} \\ \dot{m}_{\text{ref}} [(h_2 - h_3) - T_0(s_2 - s_3)] + \dot{m}_c c_p \left[ (T_{c,i} - T_{c,o}) - T_0 \ln \frac{T_{c,i}}{T_{c,o}} \right], & \text{Condenser} \\ \dot{m}_{\text{ref}} [(h_3 - h_4) - T_0(s_3 - s_4)], & \text{Expansion Valve} \\ \dot{m}_{\text{ref}} [(h_4 - h_1) - T_0(s_4 - s_1)] + \dot{m}_e c_p \left[ (T_{e,i} - T_{e,o}) - T_0 \ln \frac{T_{e,i}}{T_{e,o}} \right], & \text{Evaporator.} \end{cases} \quad (2.26)$$

where  $\dot{m}_{\text{ref}}$ ,  $\dot{m}_c$ , and  $\dot{m}_e$  denote the mass flow rates of the refrigerant, the working fluid on the condenser side, and the working fluid on the evaporator side, respectively. The dead-state temperature is represented by  $T_0$ .

The overall exergy efficiency of the heat pump system is calculated as the ratio of the useful exergy delivered to the total exergy input:

$$\eta_{\text{ex}} = \frac{\dot{E}_{\text{use}}}{\dot{W}_{\text{in}} + \Delta \dot{E}_{\text{HS}}}, \quad (2.27)$$

where  $\dot{E}_{\text{use}}$  is the useful exergy delivered to the sink expressed as

$$\dot{E}_{\text{use}} = \dot{m}_c c_p (T_{c,o} - T_{c,i} - T_0 \ln \frac{T_{c,o}}{T_{c,i}}) \quad (2.28)$$

and  $\dot{E}_{\text{HS}}$  represents the exergy destruction on the heat source side:

$$\dot{E}_{\text{HS}} = \dot{m}_e c_p (T_{e,i} - T_{e,o} - T_0 \ln \frac{T_{e,i}}{T_{e,o}}) \quad (2.29)$$

The exergy efficiency highlights how effectively the heat pump converts input work and heat into useful heating or cooling, while accounting for all irreversibilities within the system [12].

**Cascade heat pump** The cascade heat pump system, which consists of two interconnected cycles (low-temperature cycle A and high-temperature cycle B), requires an extended exergy analysis to account for additional components, including the intermediate heat exchanger (IHX). The exergy destruction for each component is given by:

$$\Delta \dot{E} = \begin{cases} \dot{m}_A [(h_4 - h_1) - T_0(s_4 - s_1)] + \dot{m}_e c_p [(T_{e,i} - T_{e,o}) - T_0 \ln \frac{T_{e,i}}{T_{e,o}}], & \text{Evaporator A,} \\ \dot{m}_A [(h_1 - h_2) - T_0(s_1 - s_2)] + \dot{W}_{in,A}, & \text{Compressor A,} \\ \dot{m}_A [(h_2 - h_3) - T_0(s_2 - s_3)], & \text{IHX (A side),} \\ \dot{m}_A [T_0(s_3 - s_4)], & \text{Expansion Valve A,} \\ \dot{m}_B [(h_8 - h_5) - T_0(s_8 - s_5)], & \text{IHX (B side),} \\ \dot{m}_B [(h_5 - h_6) - T_0(s_5 - s_6)] + \dot{W}_{in,B}, & \text{Compressor B,} \\ \dot{m}_B [(h_6 - h_7) - T_0(s_6 - s_7)] + \dot{m}_c c_p [(T_{c,i} - T_{c,o}) - T_0 \ln \frac{T_{c,i}}{T_{c,o}}], & \text{Condenser B,} \\ \dot{m}_B [T_0(s_7 - s_8)], & \text{Expansion Valve B.} \end{cases} \quad (2.30)$$

The total exergy efficiency for the cascade heat pump is:

$$\eta_{ex} = \frac{\dot{E}_{use}}{\dot{W}_{in,A} + \dot{W}_{in,B} + \Delta \dot{E}_{HS}}, \quad (2.31)$$

where  $\dot{E}_{use}$  and  $\dot{E}_{HS}$  are calculated similarly to the single-stage cycle.

## 2.5 Refrigerants for sustainable heat pump systems

Refrigerants are crucial for the performance and environmental impact of vapor compression heat pumps. Regulations increasingly emphasize the selection of refrigerants with zero ozone depletion potential (ODP) and a global warming potential (GWP) below 150 [4], aligning with international agreements such as the Montreal Protocol and the Kigali Amendment. Consequently, the transition toward low-impact refrigerants has progressed, with a focus on sustainability, safety, and efficiency. International classifications, such as ASHRAE 34 and ISO 817, assess refrigerants based on toxicity (A: low, B: high) and flammability (1: non-flammable to 3: highly flammable, including 2L for mildly flammable) [13].

Early refrigerants, including water (H<sub>2</sub>O), carbon dioxide (CO<sub>2</sub>), ammonia (NH<sub>3</sub>), and hydrocarbons (HCs), were selected for their availability and were effective but posed challenges such as toxicity, flammability, and operational constraints. The introduction of synthetic refrigerants, such as chlorofluorocarbons (CFCs) and hydrochlorofluorocarbons (HCFCs), addressed some of these issues but led to high ODP, leading to their phase-out under the Montreal Protocol. Hydrofluorocarbons (HFCs) eliminated ODP concerns but exhibited high GWP, leading to further restrictions. Today, hydrofluoroolefins (HFOs) and hydrochlorofluoroolefins (HCFOs) offer lower environmental impact, while natural refrigerants such as H<sub>2</sub>O,

CO<sub>2</sub>, and NH<sub>3</sub> are being reconsidered due to their minimal ecological footprint. A classification of refrigerants is provided in Figure 2.6, distinguishing between pure and mixed types and further differentiating between natural and synthetic refrigerants.

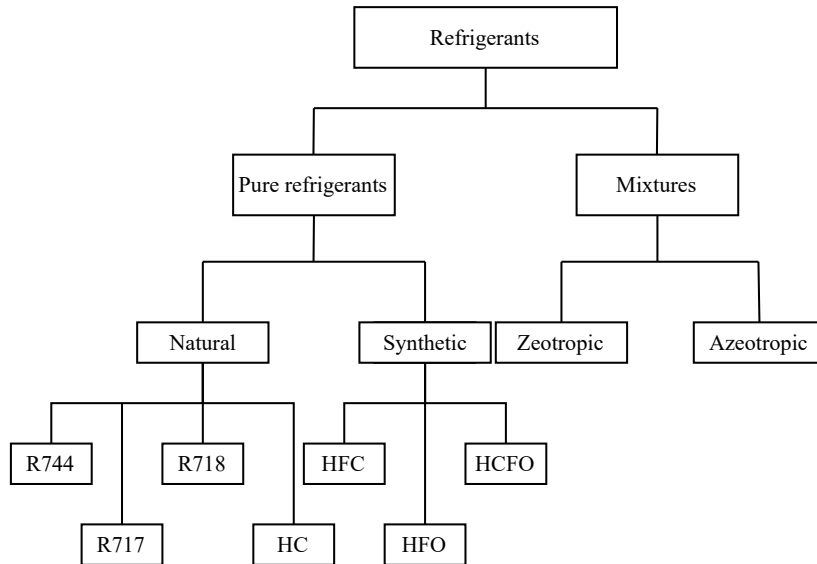


FIGURE 2.6: Classification of refrigerants.

**Natural** Natural refrigerants provide sustainable alternatives, each with distinct advantages and challenges. Ammonia (R717) delivers excellent thermodynamic performance and zero GWP/ODP but has toxicity concerns and material compatibility issues [14]. Carbon dioxide (R744) has a GWP of 1 and zero ODP and has a high efficiency in transcritical cycles but has a low critical temperature of 31 °C and operates at extreme pressures (>100 bar), requiring robust components. Water (R718) is non-toxic and widely available, yet its high boiling point necessitates sub-atmospheric operation for temperatures below 100°C. Hydrocarbons (HCs), such as propane (R290) and isobutane (R600a), exhibit excellent efficiency and ultra-low GWP but are highly flammable (A3 classification), limiting large-scale applications [4].

**Synthetic** Synthetic refrigerants have been developed as alternatives to natural refrigerants, designed to enhance thermodynamic efficiency, safety, and stability while minimizing environmental impact. Key categories include HFCs, HFOs, and HCFOs. However, HFCs are being phased out due to their high GWP. In contrast, HFOs such as R1234yf and R1234ze(E) have GWPs below 20, making them viable replacements, though some variants are mildly flammable (A2L) [4]. HCFOs, including R1233zd(E) and R1224yd(Z), offer high efficiency with low environmental impact and are particularly suited for industrial heat pumps [4].

**Mixtures** Mixtures, classified as either zeotropic or azeotropic, optimize system performance by influencing efficiency, stability, and design. Zeotropic mixtures exhibit a temperature glide during phase change due to differences in component boiling points, which can enhance heat exchanger performance in counterflow configurations but also introduce challenges such as fractionation and non-linearities in two-phase flow [15]. Figure 2.7 illustrates

the non-isothermal phase transition of zeotropic refrigerants compared to pure substances, highlighting their impact on system efficiency. In contrast, azeotropic mixtures behave like pure refrigerants, undergoing phase changes at a constant temperature, ensuring stable thermodynamic properties and simplifying system design, making them ideal for applications requiring precise temperature control.

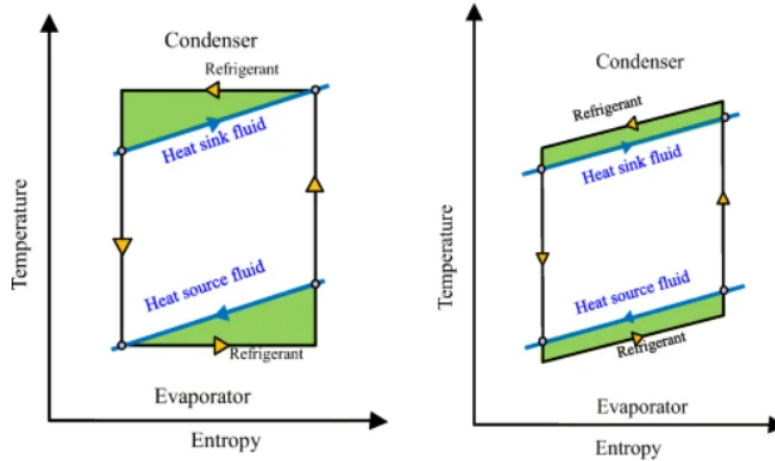


FIGURE 2.7: T-s diagram comparison of heat pumps with pure refrigerant (left) and zeotropic refrigerant (right) [16].

The thermodynamic performance of refrigerants is determined by properties such as critical temperature ( $T_{cr}$ ), critical pressure ( $P_{cr}$ ), and safety classification. Table 2.1 provides an overview of key low-GWP refrigerants and their respective thermodynamic characteristics. Efficient heat pump operation requires a condensation temperature at least  $10 - 15^\circ C$  below  $T_{cr}$  to optimize phase changes and enhance the COP [17]. While high  $P_{cr}$  can reduce system size through increased vapor densities, excessively high pressures pose design and safety challenges [17]. Additionally, maintaining system pressures above atmospheric levels prevents air and moisture ingress, ensuring longevity and reliability [17].

TABLE 2.1: Refrigerant properties derived from [3], highlighting their thermodynamic characteristics, GWP, ODP, and safety classifications.

Type	Refrigerant	T <sub>cr</sub> (°C)	P <sub>cr</sub> (MPa)	NBP (°C)	ODP	GWP	Safety
HFC	R161	102.2	5.09	-37.5	0	12	A3
HFC	R152a	113.3	4.52	-24.0	0	140	A2
HFO	R1234yf	94.7	3.38	-29.0	0	<1	A2L
HFO	R1132(E)	97.4	5.09	-35.7	0	1	A1
HFO	R1243zf	103.8	3.52	-25.5	0	0.8	A2L
HFO	R1234ze(E)	109.4	3.64	-19.0	0	<1	A2L
HFO	R1234ze(Z)	150.1	3.53	9.8	0	<1	A2L
HFO	R1336mzz(E)	137.7	3.15	7.5	0	1	A1
HFO	R1336mzz(Z)	171.3	2.90	33.4	0	2	A1
HCFO	R1224yd(Z)	155.5	3.33	14.0	0.00012	<1	A1
HCFO	R1233zd(E)	166.5	3.62	18.0	0.00034	1	A1
HC	R1270	91.1	4.55	-42.1	0	3	A3
HC	R290	96.7	4.25	-42.0	0	3	A3
HC	R600a	134.7	3.66	-11.0	0	3	A3
HC	R600	152.0	3.80	-0.5	0	3	A3
HC	R601a	187.8	3.38	27.7	0	3	A3
HC	R601	196.6	3.37	36.1	0	3	A3
Natural	R717	132.3	11.33	-33.0	0	0	B2L
Natural	R718	373.9	22.06	100.0	0	0	A1
Natural	R744	31.0	7.38	-78.5	0	1	A1
HFO	R1123	58.6	4.55	-58.1	0	<1	A2L

## 2.6 Economic considerations

The economic feasibility of heat pump systems is commonly assessed through capital expenditures (CAPEX), operating expenditures (OPEX), and the payback period. CAPEX represents the upfront investment costs associated with equipment procurement, installation, and infrastructure modifications, while OPEX encompasses the recurring costs related to energy consumption [18]. A key financial indicator, the payback period, refers to the time required for cumulative cost savings to recover the initial investment. Despite the importance of CAPEX in investment feasibility, accurately estimating it is challenging due to variations in supplier pricing, system configurations, and project conditions. As precise calculations require direct engagement with suppliers, which is beyond this study's scope, the analysis instead focuses on estimating OPEX based on energy input and electricity prices.

For industrial applications, investment decisions are often guided by predefined financial constraints. In the case of Teijin, a multinational company seeking to integrate heat pump technology, a maximum allowable payback period of five years has been established as a decision criterion. Given this constraint, the analysis employs an inverse approach, whereby the maximum allowable CAPEX is inferred based on the projected OPEX savings over the defined payback period. This methodology enables a structured economic assessment while addressing the uncertainties associated with supplier-specific cost estimations.

## Chapter 3

# Analyzing thermal inefficiencies and developing optimal heat pump strategies for industrial applications

*The production process at Teijin Aramid is energy-intensive, relying on glycol-based cooling and steam heating to maintain thermal conditions across multiple production lines. While effective, this setup leads to high energy consumption and a strong dependence on fossil fuels, presenting challenges in efficiency and sustainability. This chapter examines the current thermal energy system, identifying inefficiencies in heating, cooling, and heat recovery. A pinch analysis evaluates the potential for improved energy integration. Based on these findings, several heat pump configurations are proposed to bridge the energy gap between cooling and heating demands. These concepts are assessed for performance, scalability, and feasibility, forming the basis for an optimized heat pump integration strategy.*

### 3.1 Introduction to thermal energy management at Teijin Aramid

The production process at Teijin Aramid consists of multiple individual process lines, each with specific properties and requirements. While the operational parameters of these lines vary, the overall configuration remains consistent. A key section within this production process involves thermal energy management, which is divided into two primary stages, referred to as 'Process 1' and 'Process 2'. These stages are responsible for different thermal processes, with one focusing on cooling and the other on heating. However, the current setup relies on independent cooling and heating mechanisms, leading to inefficiencies in energy utilization. A schematic representation of this system is provided in Figure 3.1.

At present, process 2 requires steam heating, whereas process 1 involves a glycol-based cooling system. While this configuration effectively maintains the necessary thermal conditions, it is highly energy-intensive and dependent on fossil fuels. Furthermore, variability in feed conditions and inconsistencies in heat recovery mechanisms contribute to inefficiencies, limiting overall system performance. These challenges highlight the need for an optimized energy strategy to improve sustainability and operational efficiency within this specific section of the production process.

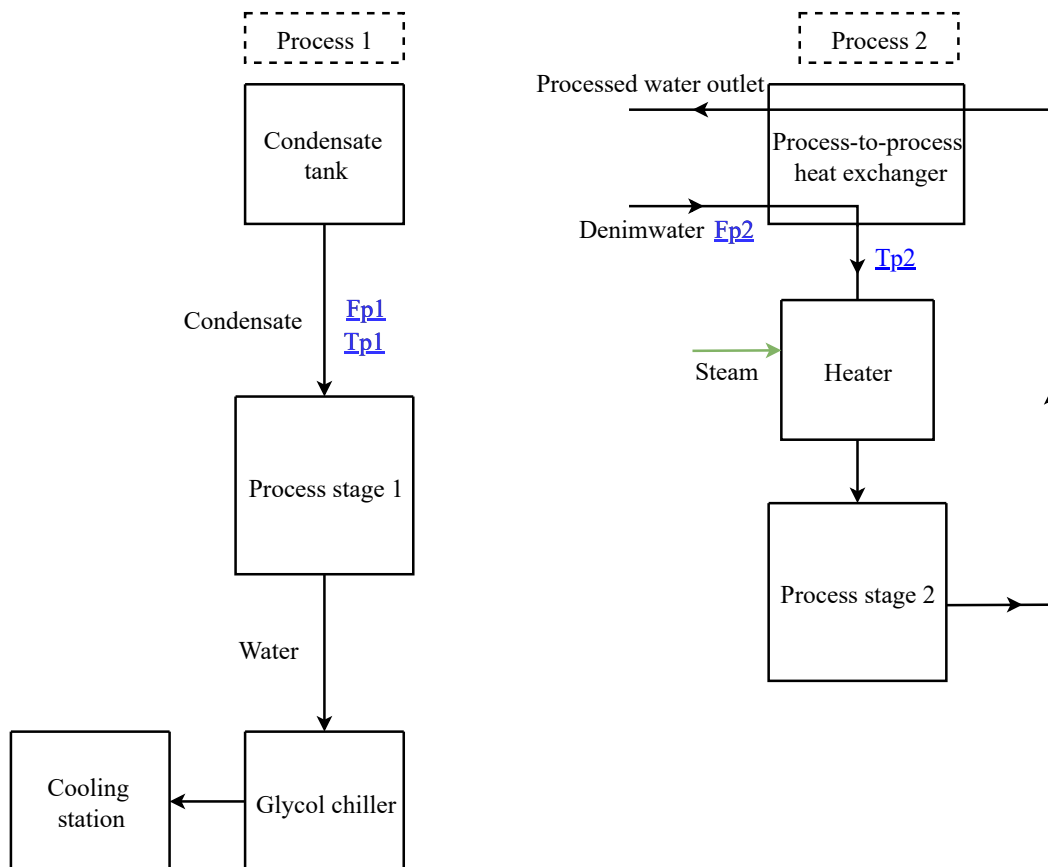


FIGURE 3.1: Schematic overview of process 1 and 2 at Teijin Aramid with associated flows and utilities.

**Process 1** In process 1, condensate from upstream operations is directed to a shared storage tank, supplying multiple process lines. While this configuration ensures that all lines receive condensate at temperature  $T_{p1}$ , variations in upstream evaporation processes, influenced by fluctuations in operating conditions and feed composition, result in fluctuating temperature profiles across the production lines. However, as all lines are supplied from the same tank, these fluctuations are consistently experienced across the system.

Additionally, the mass flow rate ( $F_{p1}$ ) varies between lines and within the lines, reflecting product-specific requirements and differences in production intensity. The exiting process water is directed to a glycol-based chiller system, where it undergoes cooling before being discharged to subsequent process steps.

Although process stage 1 does not inherently require cooling, the process water is eventually cooled further downstream. By pre-cooling the process water earlier in the system, the load on the glycol cooling system is reduced, which leads to lower energy demand and improved efficiency in later cooling steps. The thermal behavior of process 1 is depicted in Figure 3.2, which illustrates mass flow rate variations on the left side (A) and temperature fluctuations on the right side (B) over a 11-day period.

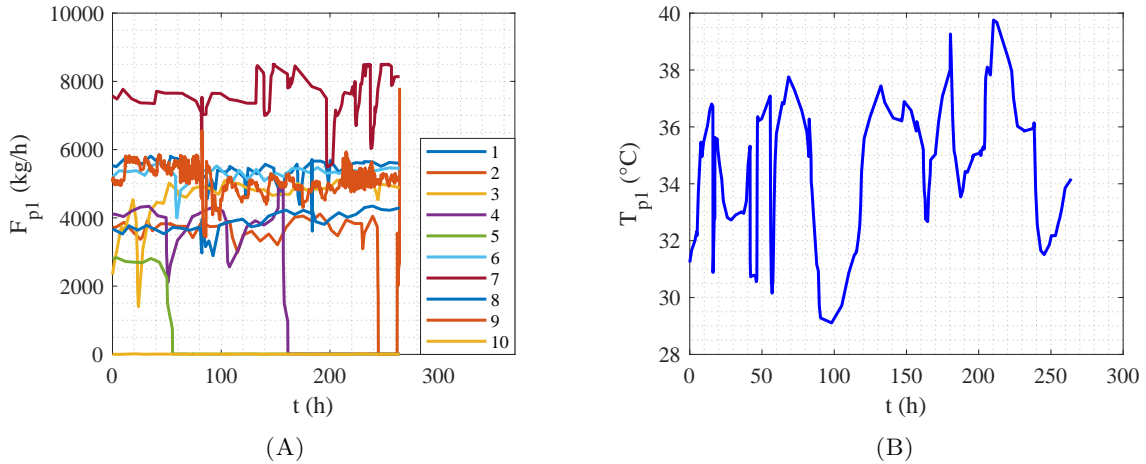


FIGURE 3.2: Trends in process stage 1 over a 11-day period of the (A) condensate flow ( $F_{p1}$ ) and (B) temperature ( $T_{p1}$ ).

**Process 2** In process 2, external water supplied by GETEC [19] is preheated using residual heat from the process in a process-to-process heat exchanger. The preheated water with temperature  $T_{p1}$  is further heated using steam to reach the process temperature of 60°C. The mass flow of incoming water is labeled as  $F_{p2}$ . Variability in water temperature after preheating between production lines results in varying steam usage and energy inefficiencies.

The mass flow trends ( $F_{p2}$ ) across multiple production lines over a 11-day period is depicted in Figure 3.3, demonstrating variations in flow rates due to dynamic operational conditions.

The observed fluctuations highlight the influence of production-specific requirements and system load variations. In contrast, Table 3.1 shows the corresponding temperature values ( $T_{p2}$ ) for each process line, which remain constant throughout the entire period. The differences in temperature across production lines indicate process-specific thermal requirements.

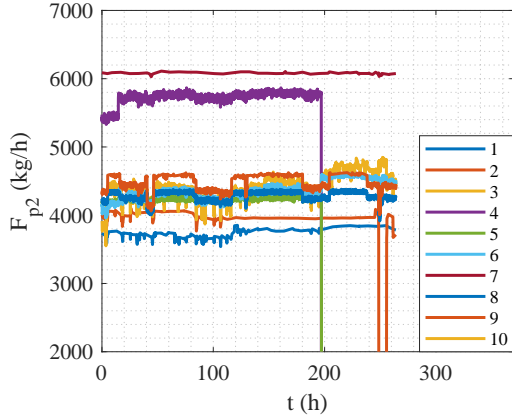


FIGURE 3.3: Trends in process 2 over a 11-day period of the mass flows ( $F_{p2}$ ).

TABLE 3.1: Temperature values for  $T_{p2}$  at different production lines

Production Line	$T_{p2}$ ( $^{\circ}\text{C}$ )
1	53
2	53
3	55
4	33
5	40
6	55
7	40
8	42
9	50
10	47

### 3.1.1 Process challenges and energy inefficiencies

The current system presents several challenges in energy efficiency and heat recovery, leading to increased operational costs and resource inefficiencies.

- High energy consumption in cooling and heating:** The glycol cooling system depends on external cooling utilities to lower the temperature of process 1, which results in significant energy consumption and operational costs. Additionally, the use of steam for process 2 requires substantial energy input, leading to high dependency on fossil fuels and contributing to increased greenhouse gas emissions.
- Lack of heat integration:** The processes operate independently, with no direct heat recovery between process 1 and process 2. As a result, the heat removed from the process 1 stream is not utilized elsewhere in the process, representing a missed opportunity for energy integration. This lack of heat recovery not only increases energy demands but also limits the overall thermal efficiency of the process.
- Fluctuating process conditions:** Variations in temperature profiles and mass flow rates across production lines create inconsistent thermal behavior, reducing the potential for optimization and standardization.
- Inefficiencies in heat exchanger performance:** The process-to-process heat exchanger, which preheats incoming process water, operates with varying outlet temperatures ( $33\text{--}55^{\circ}\text{C}$ ) across process lines. This variability leads to fluctuating steam demand and inefficient heating, likely influenced by differences in heat exchanger effectiveness.

### 3.1.2 Thermodynamic evaluation of heat integration opportunities

A thermodynamic analysis was conducted to assess the potential for heat integration between process 1 and process 2. Pinch analysis, a methodical approach to identifying heat recovery opportunities, was used to evaluate the thermal interactions between hot and cold streams. By analyzing the enthalpy changes and temperature profiles of these streams, the analysis aimed to maximize heat recovery and minimize reliance on external energy sources [20].

The heat capacity flow rate ( $CP$ ) of each stream, representing the energy required to change its temperature by one degree, was calculated as:

$$CP = c_p \dot{m}, \quad (3.1)$$

where  $c_p$  is the specific heat capacity and  $\dot{m}$  is the mass flow rate. The composite curves

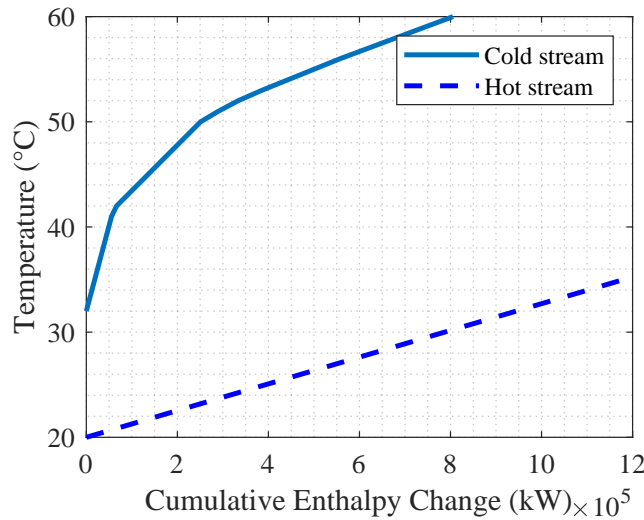


FIGURE 3.4: Composite curve, where the dashed line represents the hot stream and the solid line denotes the cold stream.

for the processes 1 and 2 are presented in Figure 3.4, illustrating the cumulative enthalpy changes of the hot and cold streams. The significant gap between the hot and cold streams reveals the absence of a pinch point, indicating a lack of direct heat recovery within the system. This inefficiency underscores the reliance on external utilities, such as a heat pump, to bridge the thermal gap and improve energy efficiency.

While further heat recovery opportunities may exist within the broader production system, this research does not extend the pinch analysis beyond the identified streams shown in Figure 3.1. The focus remains on optimizing heat integration between these streams to improve the energy efficiency of the thermal process.

### 3.1.3 Heat pump integration for sustainable process optimization

Based on the findings of the pinch analysis, a heat pump was identified as a suitable solution to address energy inefficiencies in process 1 and process 2. As illustrated in Figure 3.5, the

heat pump enables direct heat recovery between these two stages, improving thermal energy management. The system utilizes the evaporator to extract heat from process 1, thereby cooling the process stream, while the condenser transfers this recovered thermal energy to process 2, reducing the need for external heating. On the evaporator side, heat is extracted from the process water stream in process 1 before it undergoes further cooling. The recovered heat is then transferred through the compressor to the condenser side, where it is used to heat the process water entering process 2. This reduces the system's reliance on external steam heating, ensuring that the necessary temperature levels are maintained with improved energy efficiency. The refrigerant flow within the heat pump is depicted with red dashed lines, while the process water flow is shown with solid black lines in Figure 3.5.

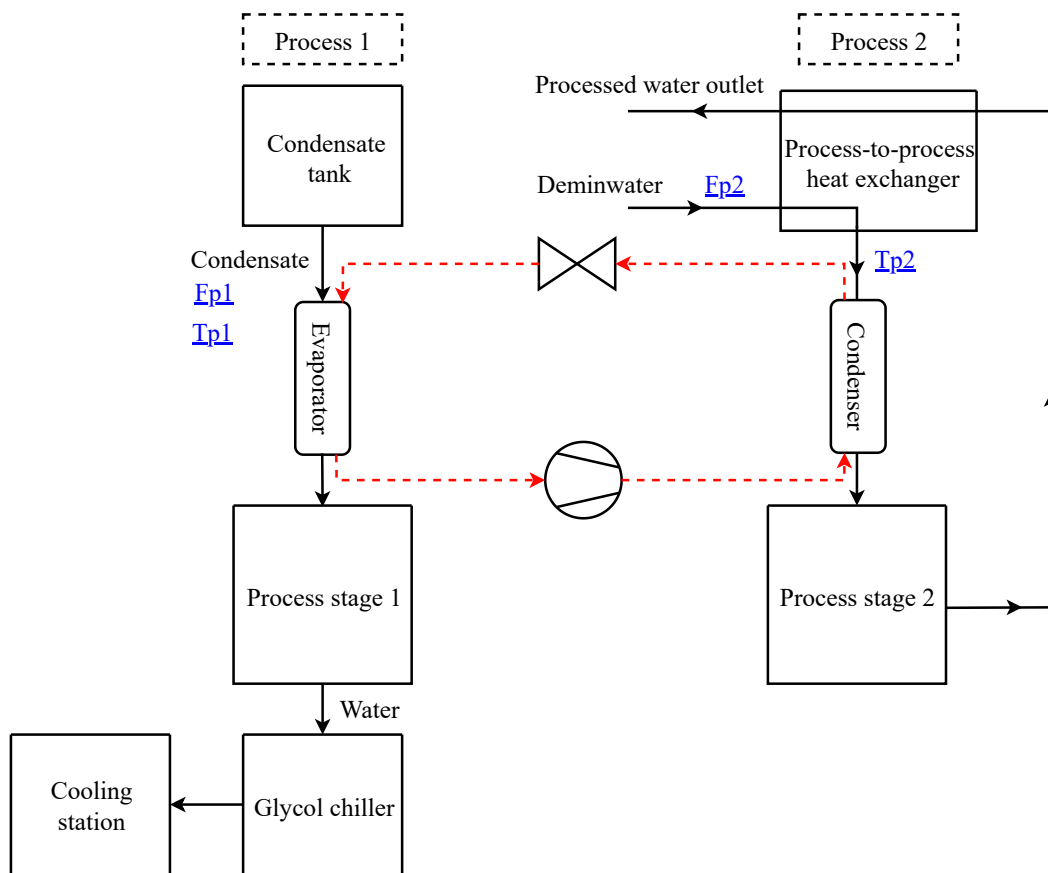


FIGURE 3.5: Schematic representation of heat pump integration within process 1 and process 2.

**Ongoing industrial projects at Teijin Aramid relevant to thermal efficiency** Several ongoing industrial projects at Teijin Aramid are expected to influence the integration and efficiency of the heat pump system. Although these projects are not the primary focus of this research, their outcomes provide valuable insights into energy optimization strategies.

1. **Process-to-Process heat exchanger performance** One of the identified inefficiencies lies in the process-to-process plate heat exchangers, which preheat the process water entering process 2. These heat exchangers recover residual heat, but significant variations in outlet temperature have been observed across the ten production lines.

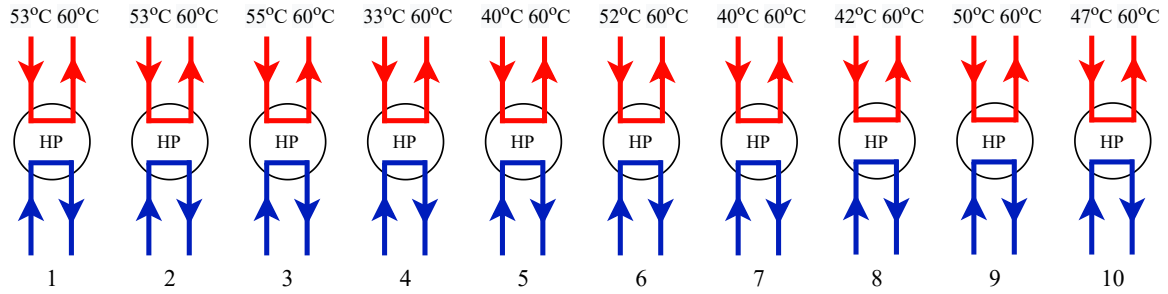


FIGURE 3.6: Temperature variations of preheated water entering the condenser side of the heat pump across the different process lines.

As illustrated in Figure 3.6, outlet temperatures range from 33°C to 55°C, reflecting considerable variability between lines. It is important to note that this figure purely illustrates the temperature lift required for each process line, independent of mass flow rates. The data highlight the varying inlet temperatures at the condenser side of the heat pump, emphasizing the disparity in heating requirements. The outlet temperature of the heat exchanger serves as the inlet temperature for the heat pump condenser. This inconsistency suggests issues such as fouling, incorrect installation, or potential leaks within the heat exchanger.

To mitigate these inefficiencies, several targeted actions were taken during maintenance intervals. These included cleaning the heat exchangers, replacing a unit with a revised one, and performing leakage tests to assess the possibility of leaks. Although no leaks were detected, the cleaning and replacement efforts highlighted opportunities for improving heat exchanger performance.

This variability in preheated water temperatures has a direct impact on the thermal input to the heat pump system, as consistent inlet conditions are essential for optimizing the performance and efficiency of the heat pump. Addressing these discrepancies will indirectly enhance the integration of the heat pump by ensuring stable thermal conditions in the water entering process 2.

2. **Heat recovery optimization in the sulfuric acid recycling system** Another ongoing project, focuses on optimizing heat recovery in the sulfuric acid recycling system. This system recovers and concentrates sulfuric acid by evaporating water and subsequently condensing it, reducing the reliance on external acid supply. To enhance energy efficiency, a heat exchanger was installed to transfer heat from the condensate stream to the acid feed stream, thereby reducing steam consumption and cooling demands.

Currently, this heat exchanger is not in operation, but once reactivated, it is expected to lower the condensate temperature by approximately 2 °C. As a result, the inlet temperature of the evaporator will decrease, which will influence the system's energy efficiency and heat pump performance. This temperature reduction could lead to lower cooling requirements and improve overall energy savings within the process.

## 3.2 Introduction to heat pump integration concepts

Current inefficiencies highlight the need for a more integrated thermal energy approach. While some heat recovery exists, it remains insufficient for balancing cooling and heating demands. A heat pump system presents a viable solution, enabling effective heat reuse while reducing reliance on external energy sources. The following section introduces several conceptual heat pump configurations designed to integrate into the system. Each concept represents a distinct approach to managing heating and cooling demands while considering feasibility and scalability. These configurations are outlined with their key characteristics, providing a foundation for further analysis.

## 3.3 List of requirements

- The heat pump must deliver a heat output of at least 700 kW.
- The system must deliver heat with a temperature of up to 60°C.
- The evaporator must effectively extract heat with a minimum evaporation temperature of 5°C.
- The heat pump should efficiently operate across a load range from 50% to 100% of nominal capacity.
- The buffer system must supply heat when the evaporator flow is insufficient or unavailable.
- The buffer must be charged during periods of low heat demand.
- When the buffer is depleted, steam must be available to meet the heat demand.
- The buffer must charge when its capacity is below 30% and stop charging at 90%-100%.
- During buffer charging, overproduction must not exceed 10% of the direct heat demand.
- The refrigerant must comply with EU F-gas regulations.
- The heat pump must be scalable to support 120% of the current heat demand in future expansions.
- The heat pump must have an operational lifespan of at least 15 years under normal operating conditions.

## 3.4 Development and evaluation of heat pump configurations for process integration

In each concept, a heat pump is strategically integrated between Process 1 and Process 2 to facilitate heat recovery. The heat pump functions by extracting heat from Process 1 on the evaporator side while simultaneously supplying heat to Process 2 on the condenser side. Process 1 receives condensate collected from various upstream evaporation processes, while Process 2 utilizes demineralized water that is pre-heated through a process-to-process heat

exchanger before entering the condenser. The heat pump then further raises the temperature of this water to 60°C, reducing reliance on external heating sources.

The buffer system in the heat pump setup acts as a thermal storage reservoir, providing stability and flexibility to accommodate fluctuations in heat demand and supply. Its primary function is to store excess thermal energy during periods of low demand, a process known as charging, and release stored energy when demand increases, referred to as discharging. This ensures consistent system performance and efficient energy utilization, even when immediate heat supply and demand are not perfectly matched.

During the charging phase, the buffer accumulates surplus energy generated by the heat pump when heating demand on the condenser side is minimal or when the system operates under partial load conditions.

The discharging phase occurs when the heat pump is unable to meet instantaneous heating demands. Under such circumstances, the buffer compensates by releasing stored thermal energy. This is particularly advantageous during peak demand periods, when the heat pump's capacity may be exceeded, or when insufficient flow on the evaporator side limits heat pump operation.

The buffer offers several operational advantages, including enhanced system stability by mitigating fluctuations in heat supply and demand, improved efficiency by enabling the heat pump to operate continuously under optimal conditions, and the capability to handle peak demands without requiring oversized heat pump components. Furthermore, the buffer acts as a redundant energy source during heat pump downtime, ensuring uninterrupted system functionality.

### 3.4.1 Concept 1: Single heat pump per process line (SHP)

In the first concept, each of the ten process lines is equipped with a dedicated heat pump system, featuring separate evaporators and condensers for process 1 and process 2. While Figure 3.7 illustrates only two lines, the actual system includes ten independent setups, each operating autonomously. Heat is extracted from the stream in process 1 via the evaporator and subsequently transferred to the stream in process 2 through the condenser.

This configuration offers a high degree of operational independence, ensuring that each production line functions without being affected by fluctuations in other lines. One notable advantage is system redundancy: in the event of a heat pump failure, only the affected line is impacted, while the remaining systems continue operating uninterrupted. Moreover, tailoring heat pump operation to individual line conditions allows for precise thermal control, optimizing energy efficiency for specific process demands.

However, this approach also has notable drawbacks. The duplication of equipment across ten lines results in higher capital expenditures due to increased installation costs and elevated maintenance complexity. Additionally, the lack of thermal integration between lines leads to limited opportunities for heat recovery, potentially reducing overall system efficiency.

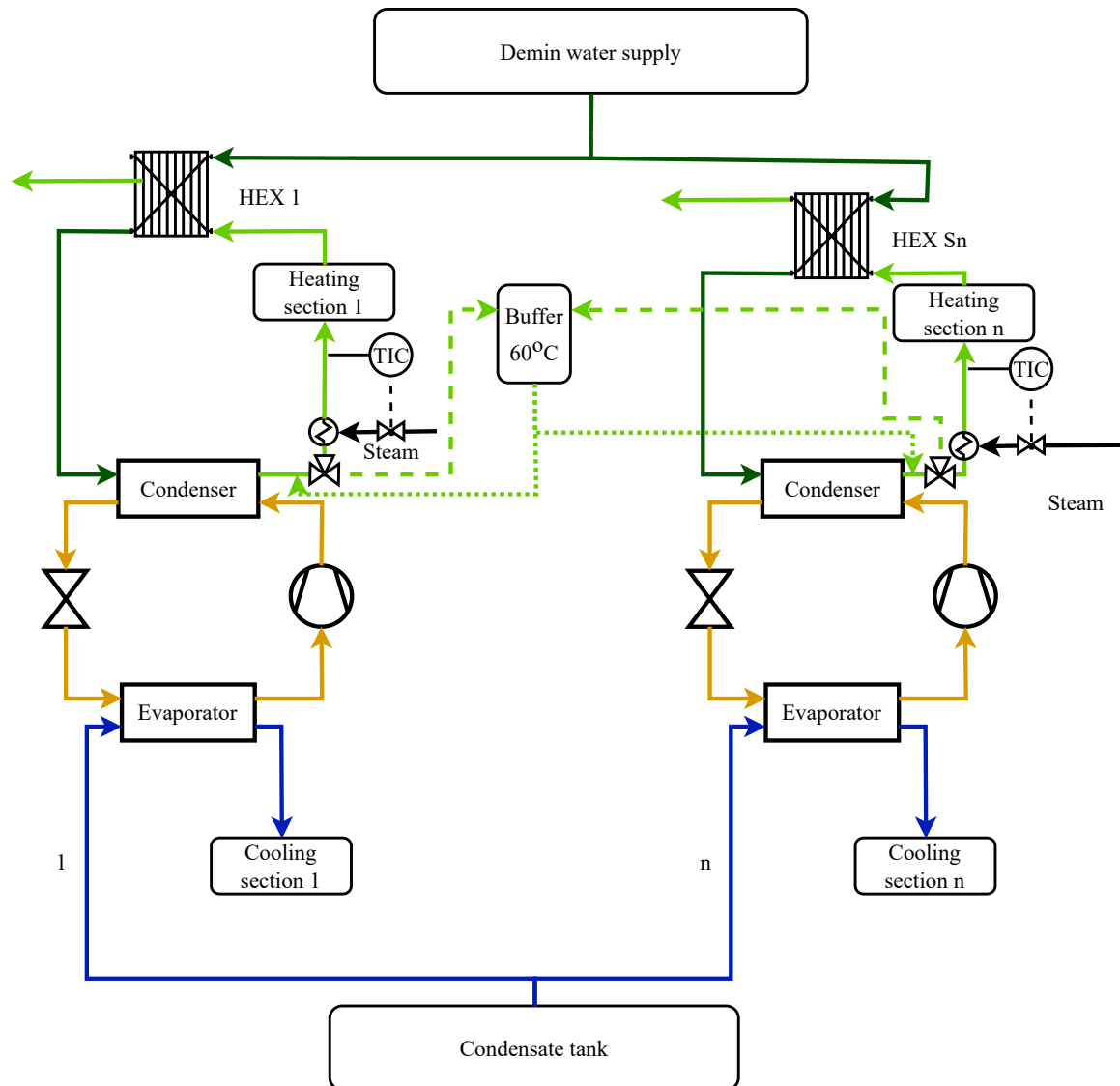


FIGURE 3.7: Concept 1: Single heat pump per production line with integrated buffer and steam backup.

### 3.4.2 Concept 2: Centralized heat pump system (CHP)

In the second concept, process lines keep independent process flows, but the heat exchange is centralized. The fluid stream from all process 1 sections is mixed and directed into a single evaporator system, while all process 2 streams are combined and supplied to a centralized condenser system.

This integrated approach enhances thermal efficiency by averaging temperature fluctuations across lines, leading to a more stable heat pump operation. The shared evaporator and condenser system reduces equipment redundancy, decreasing investment and maintenance costs compared to concept 1. Moreover, centralizing the heat pump system improves heat utilization, increasing overall energy efficiency.

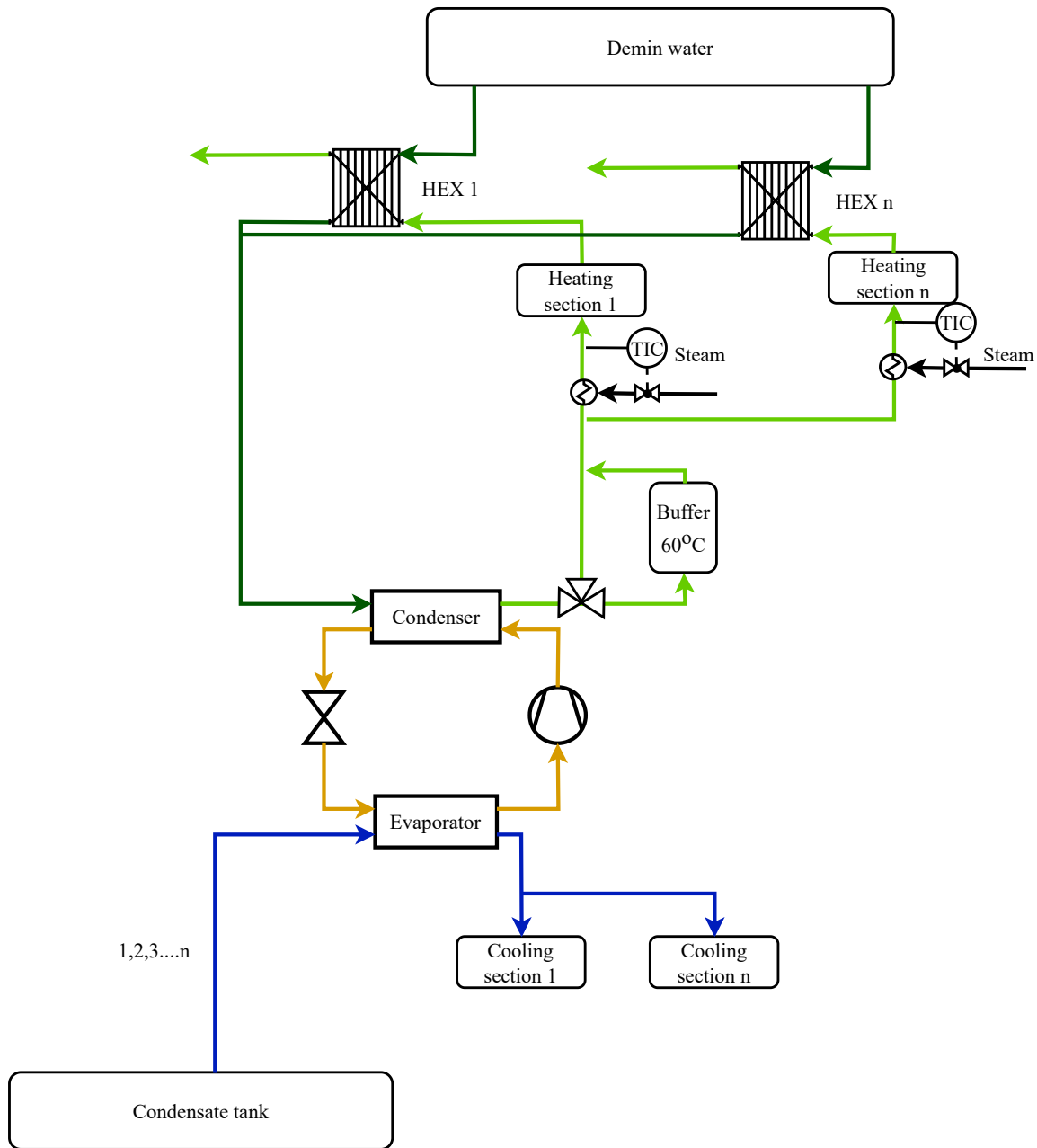


FIGURE 3.8: Concept 2: Centralized heat pump system with integrated buffer and steam backup.

Another significant benefit of this concept is cost reduction. A single, large heat pump is cheaper to install and maintain than ten smaller units, making concept 2 more cost-effective than concept 1 in terms of both capital and operational expenses. Additionally, the simplification of system maintenance with fewer components to monitor and service reduces long-term costs.

However, this concept introduces interdependence between lines. Variations in individual

process lines can impact system-wide temperature dynamics, necessitating additional controls to maintain uniform operating conditions. Additionally, any malfunction in the centralized heat pump system would require reliance on the steam backup system to ensure continued operation of all connected lines.

### **3.4.3 Concept 3: Heat pump per cluster configuration (HPC)**

In this approach, the ten process lines are divided into three clusters: 1-2-3, 4-5-6, and 7-8-9-10, with each cluster sharing a dedicated heat pump system. While individual lines retain separate process streams, heat exchange is performed at the cluster level, balancing thermal loads within the group.

This configuration offers a balance between redundancy and efficiency. By reducing the total number of heat pumps compared to concept 1, it lowers capital and maintenance costs, while still ensuring that a failure in one heat pump only affects a limited subset of lines, thereby maintaining partial redundancy. Furthermore, grouping production lines allows for thermal diversity compensation, where fluctuations in heat demand within a cluster are averaged out, improving heat pump performance.

From a CAPEX cost perspective, concept 3 falls between concept 1 and concept 2. While it requires fewer heat pumps than concept 1, it still involves more equipment than a fully centralized system. The installation and maintenance costs are lower than concept 1 but higher than concept 2. The trade-off lies in moderate capital investment with increased resilience, making it an appealing compromise between system cost and reliability.

However, clustering introduces interdependencies between grouped lines. If one line experiences process disturbances, it may affect the heat pump performance of the entire cluster. Additionally, while clustering improves heat recovery compared to concept 1, it remains less thermally efficient than a fully centralized system (concept 2).

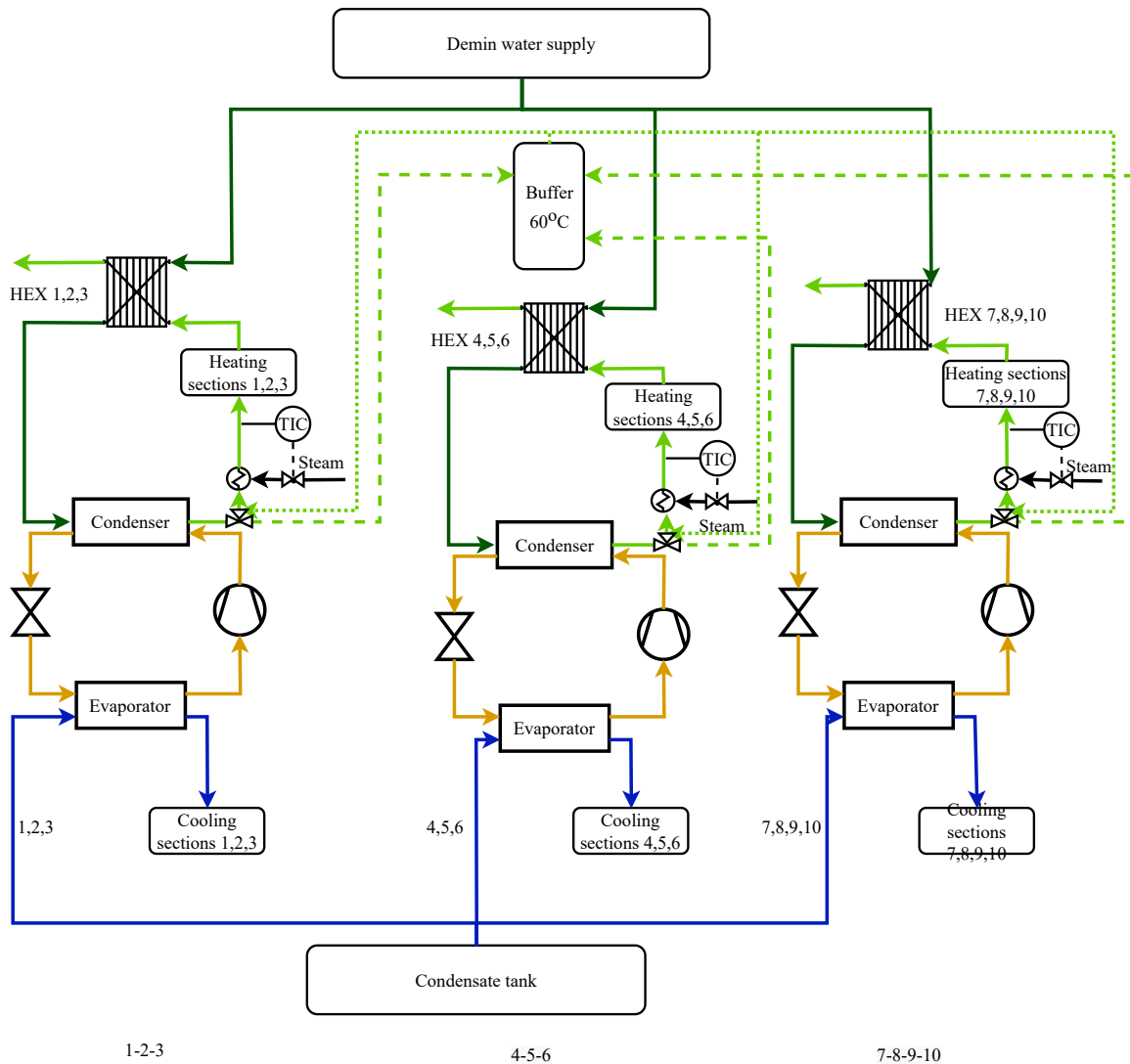


FIGURE 3.9: Concept 3: Clustered heat pump configuration with integrated buffer and steam backup.

### 3.4.4 Concept 4: Cascade heat pump configuration (CaHP)

The fourth concept expands on the centralized approach by implementing a cascade heat pump system, which utilizes two separate heat pump cycles operating in series. The low-temperature cycle extracts heat from process 1, while the high-temperature cycle transfers this heat to process 2 at the required 60°C setpoint.

The key advantage of the cascade approach is its improved thermodynamic efficiency. By dividing the temperature lift across two compression stages, the system reduces compressor work input, leading to a higher COP compared to single-stage heat pump designs. Additionally, this configuration enables the use of refrigerants optimized for specific temperature ranges, further enhancing energy efficiency.

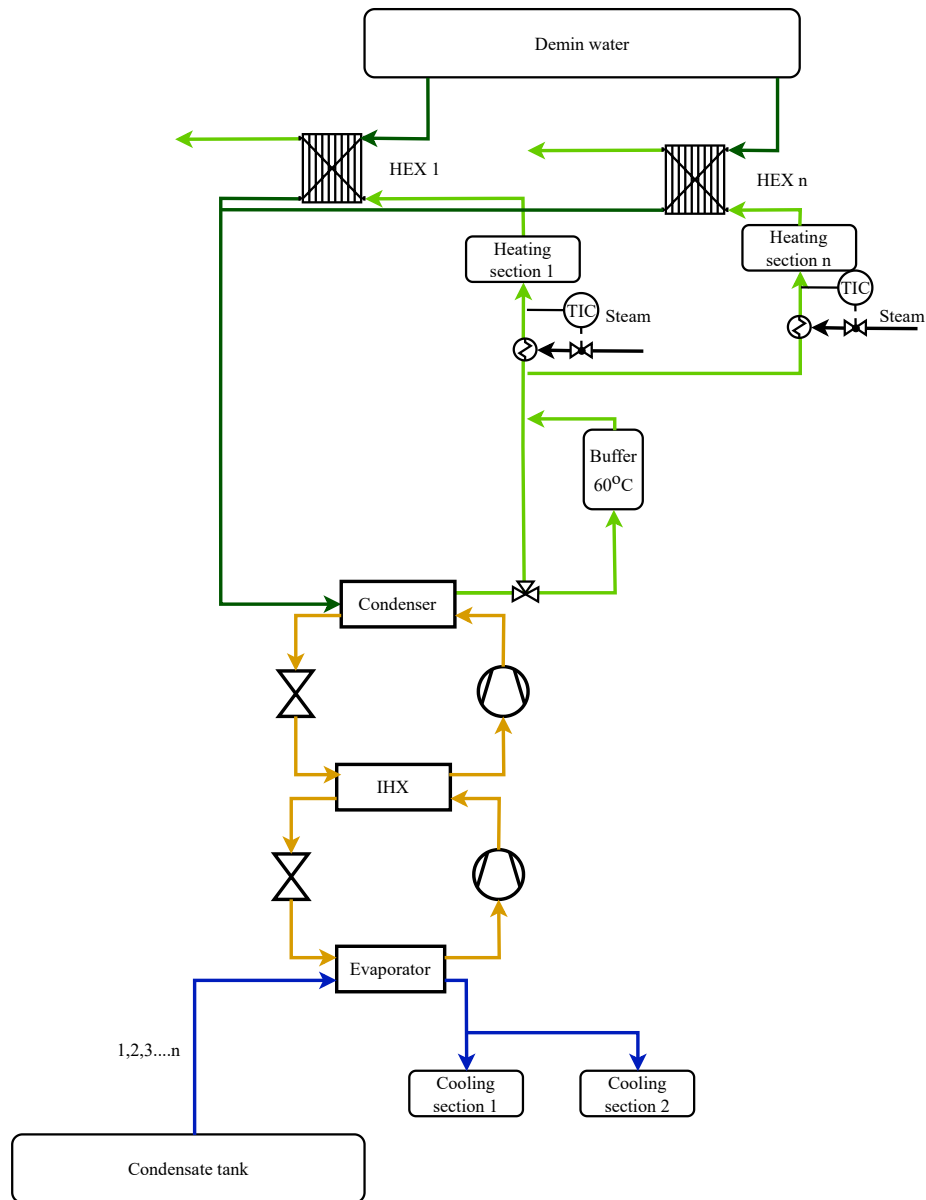


FIGURE 3.10: Concept 4: Cascade heat pump system with integrated buffer and steam backup.

However, cascade systems require a more complex design and higher initial investment costs than concept 2. The need for an intermediate heat exchanger and a two-stage compression process introduces additional control requirements. Furthermore, maintenance demands are higher compared to single-stage systems, as cascade systems require specialized expertise for servicing.



## Chapter 4

# Methodology: Thermodynamic modeling and heat pump integration

*This chapter presents the thermodynamic modeling of heat pump configurations to assess their feasibility for industrial integration. A single vapor compression cycle and a cascade heat pump system are simulated using MATLAB and CoolProp, incorporating key assumptions for accurate performance prediction. The models analyze key parameters such as pressure levels, temperature variations, and system efficiency, ensuring a realistic representation of heat pump behavior under dynamic operating conditions. To ensure reliability, the models are validated against reference thermodynamic data, comparing COP, pressure levels, and mass flow ratios. These validations confirm model accuracy and provide a foundation for system optimization, refrigerant selection, and performance evaluation. The insights gained from this analysis contribute to determining the most efficient heat pump configuration for integration into the existing process.*

## 4.1 Thermodynamic model assumptions and approach simple vapor heat pump

Thermodynamic modeling of the single vapor cycle configuration was undertaken to present the potential of a single vapor heat pump using MATLAB R2024a [21] and CoolProp 6.6.0 [22]. The heat pump cycle was analyzed based on an equation of state (EOS) that defines the thermodynamic properties of the chosen refrigerant under various operating conditions. The open-source application CoolProp facilitated the acquisition of these properties, enhancing the accuracy of the simulation. To simplify the thermodynamic modeling and ensure consistency, the following assumptions were made during the analysis:

- The system is assumed to operate under steady-state conditions.
- Pressure drops in pipes, valves, and heat exchangers are considered negligible.
- The expansion valve process is assumed to be isenthalpic.
- The components of the system are considered perfectly insulated.
- Changes in kinetic and potential energy between the inlet and outlet of components are negligible compared to thermal energy changes.
- The compression process is assumed to be adiabatic, with an isentropic efficiency of 0.7.

The parameters presented in Table 4.1 define the thermodynamic framework for the model. The evaporator and condenser inlet/outlet temperatures ( $T_{e,i}$ ,  $T_{c,i}$ ,  $T_{c,o}$ ) establish the thermal boundaries of the system, while the temperature differentials ( $\Delta T_c$  and  $\Delta T_e$ ) characterize the heat exchanger performance. The isentropic efficiency ( $\eta_{iso}$ ) influences the compressor work input, whereas the specific heat capacity ( $c_p$ ) is utilized in energy balance calculations. The evaporator-side mass flow rate ( $\dot{m}_e$ ) is used to determine the heat absorption at the evaporator, thereby affecting the evaporator outlet temperature and pressure. Similarly, the condenser-side mass flow rate ( $\dot{m}_c$ ) determines the total heat rejection in the condenser, impacting the overall thermal exchange within the cycle.

TABLE 4.1: Constant Properties in the simple vapor heat pump model.

Parameter	Value
Refrigerant type	R134a
$\eta_{iso}$ (Isentropic Efficiency)	0.7
$T_{e,i}$ (Evaporator Inlet Temperature)	35 °C
$T_{c,i}$ (Inlet Temperature Condenser)	50 °C
$T_{c,o}$ (Outlet Temperature Condenser)	60 °C
$\Delta T_c$ (Temperature Difference in Condenser)	5 °C
$\Delta T_e$ (Temperature Difference in Evaporator)	5 °C
$c_p$ (Specific Heat Capacity)	4182 J/kg·K
$\dot{m}_e$ (Water mass flow rate on the evaporator side)	1.81 kg/s
$\dot{m}_c$ (Water mass flow rate on the condenser side)	1.11 kg/s
Tolerance	1e-2

The thermodynamic cycle of the single vapor heat pump is outlined in Figure 2.2. The cycle follows the four key thermodynamic states:

1. Compressor inlet or evaporator outlet.
2. Condenser inlet or compressor outlet.
3. Condenser outlet.
4. Evaporator inlet.

The analysis involved calculating the thermodynamic properties of the refrigerant at the four key states of the cycle through an iterative approach. The process began by assuming an initial value for the evaporator pressure ( $P_1$ ). The condenser pressure ( $P_2$ ) was calculated based on the condensation temperature, determined as the sum of the condenser outlet temperature ( $T_{c,o}$ ) and the temperature difference in the condenser ( $\Delta T_c$ ).

Once  $P_1$  and  $P_2$  were defined, the thermodynamic properties of the refrigerant, such as enthalpy, entropy, and temperature, were calculated at all four states. For the compression process between state 1 and state 2, the entropy was assumed constant ( $s_1 = s_2$ ) to represent ideal isentropic compression. To account for real-world deviations, the isentropic efficiency was applied to adjust the enthalpy at state 2 ( $h_2$ ), as described in Equation (2.12). At state 3, the refrigerant was modeled as a saturated liquid, and its enthalpy ( $h_3$ ) was determined based on the calculated condenser pressure. At the expansion valve, the isenthalpic nature of the process ensured that  $h_4 = h_3$ . The enthalpy at state 1 ( $h_1$ ) was then calculated using the energy balance at the evaporator, along with the evaporator outlet temperature ( $T_{e,o}$ ), determined as described in Equation (2.10).

Using the calculated  $T_{e,o}$ , the evaporator pressure was derived and compared to the initially assumed value of  $P_1$ . If the calculated and assumed pressures differed by more than the predefined tolerance, the assumed evaporator pressure was adjusted, and the calculations were repeated. This iterative process continued until the assumed and calculated evaporator pressures converged.

Once convergence was achieved, the model's output included key performance metrics such as the heat released to the sink ( $\dot{Q}_{out}$ ), the work input to the compressor ( $\dot{W}_{in}$ ), and the COP. These were calculated using the relationships described in the Section 2.3.1, including Equations (2.14), (2.12), and (2.15).

The iterative procedure is summarized in the flowchart shown in Figure 4.1. This approach ensured that the model accurately represented the thermodynamic behavior of the heat pump, providing a consistent basis for evaluating its performance under the specified operating conditions.

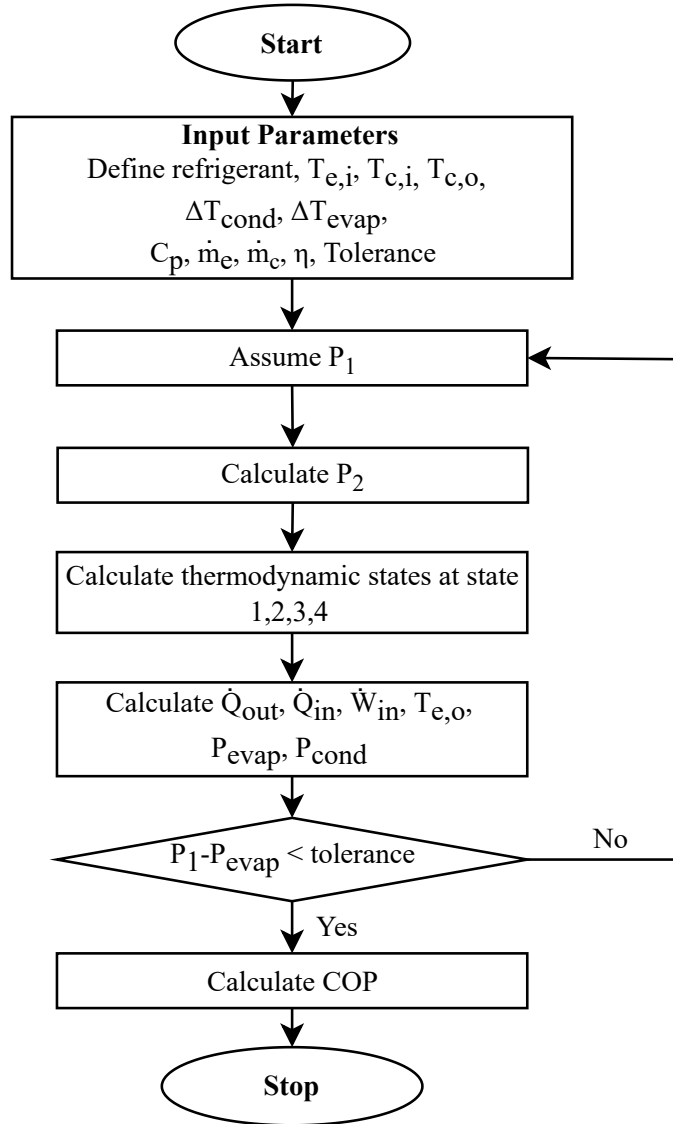


FIGURE 4.1: Flowchart of the thermodynamic model for the simple vapor cycle.

## 4.2 Model validation simple vapor heat pump

In the thermodynamic simple-vapor model, verification was carried out by comparing the model's outputs with reference data obtained from TLK Energy phase diagrams [23]. TLK Energy provides detailed thermodynamic data for various refrigerants, including refrigerant-specific  $\log(p)$ - $h$  diagrams. These diagrams enable visualization of the refrigerant cycle, making TLK Energy a reliable computational benchmarking tool for comparing modeled refrigerant cycles in terms of pressure, temperature, and COP. However, as TLK Energy also relies on established thermodynamic equations, this validation serves as a computational consistency check rather than an independent experimental validation.

The model's boundary conditions were defined as follows: the condensing temperature was set

as a fixed input, while the evaporating temperature was determined through energy balance calculations. A uniform temperature difference of 5 °C was assumed for both the condenser and evaporator heat exchangers. Additionally, an isentropic efficiency of 0.7 was applied to the compressor across all simulations. For R134a, the model predicted an evaporating temperature of 25.1 °C, while for other refrigerants (R1234yf, R290, R1270), the evaporating temperature was 25.2 °C, and for R717, it was 25.0 °C. The condensing temperature remained consistent at 65 °C for all cases. The results of this validation can be found in Table 4.2.

TABLE 4.2: Comparison of COP, pressures, and superheated temperatures (Model vs. Reference).

Refrigerant	COP (Model)	COP (Reference)	P1 (bar) (Model)	P1 (bar) (Reference)	P2 (bar) (Model)	P2 (bar) (Reference)	T (°C) (Model)	T (°C) (Reference)
<b>R134a</b>	4.86	4.85	6.68	6.67	18.90	18.90	75.8	75.8
<b>R290</b>	4.71	4.72	9.56	9.57	23.43	23.43	75.5	75.5
<b>R1270</b>	4.66	4.66	11.59	11.60	27.94	27.94	80.2	80.2
<b>R1234yf</b>	4.54	4.53	6.86	6.86	18.35	18.35	68.7	68.7
<b>R717</b>	5.34	5.33	10.03	10.03	29.48	29.48	130.1	130.3

The validation focused on comparing key outputs from the model with those provided by the reference source, specifically:

- Evaporating pressure (P1): The model’s predictions for P1 showed excellent agreement with the reference values, with deviations of less than 0.01 bar across all refrigerants. This indicates that the model accurately represents the thermodynamic state of the working fluid at the evaporator outlet.
- Condensing pressure (P2): The calculated condensing pressures were also consistent with the reference data, confirming the correct application of energy balance equations and thermodynamic property calculations.
- Superheated temperature at compressor outlet: The predicted superheated temperatures closely matched the reference values, validating the accuracy of enthalpy calculations across the cycle.
- COP: The COP values predicted by the model were compared with the reference data provided by TLK Energy [23] for both heat pump and refrigeration cycles with a maximal difference of 0.01. Minor deviations in COP can be attributed to differences in how the model and the reference source handle property interpolation and numerical precision.

The strong correlation between model outputs and reference data demonstrates the computational validity of the developed thermodynamic model. However, since both the model and the reference rely on theoretical equations rather than empirical measurements, future experimental validation is necessary to confirm real-world applicability.

A graphical representation of the validation results in the form of log(p)-h diagrams is provided in Appendix A, offering a visual comparison of modeled refrigerant cycles with their reference counterparts.

### 4.3 Thermodynamic model assumptions and approach cascade heat pump

The thermodynamic model for the cascade heat pump builds upon the single vapor cycle model described in Section 4.1, extending its principles to a dual-stage configuration. The model enables efficient operation across large temperature differences, enhancing both system performance and mechanical reliability. The cascade system consists of two interconnected cycles: a low-temperature cycle (Cycle A) and a high-temperature cycle (Cycle B), coupled via an intermediate heat exchanger (IHX). The IHX facilitates heat transfer between the two refrigerant loops while maintaining separate pressure levels, allowing the overall temperature lift to be divided into two smaller stages. This configuration is schematically illustrated in Figure 2.4.

The model adopts the core assumptions of the single vapor cycle, such as steady-state operation, negligible pressure drops, adiabatic compression with isentropic efficiency, isenthalpic expansion, and negligible changes in kinetic and potential energy. Additional assumptions unique to the cascade configuration include maintaining a constant temperature difference ( $\Delta T_{\text{IHX}}$ ) across the IHX to ensure effective thermal energy transfer. The input parameters and system properties, including those specific to the cascade system, are detailed in Table 4.3.

TABLE 4.3: Expanded list of input parameters and constant properties for the cascade heat pump model, including a temperature range for  $T_3$ .

Parameter	Value
Refrigerant 1	R134a
Refrigerant 2	R134a
$\eta_1$ (Isentropic Efficiency, Lower Cycle)	0.7
$\eta_2$ (Isentropic Efficiency, Upper Cycle)	0.7
$T_{e,i}$ (Evaporator Inlet Temperature)	35 °C
$T_{c,i}$ (Inlet Temperature Condenser)	50 °C
$T_{c,o}$ (Outlet Temperature Condenser)	60 °C
$\Delta T_{\text{cond}}$ (Temperature Difference in Condenser)	5 °C
$\Delta T_{\text{evap}}$ (Temperature Difference in Evaporator)	5 °C
$\Delta T_{\text{IHX}}$ (Temperature Difference in Intermediate Heat Exchanger)	5 °C
$T_3$ (Range for IHX Intermediate Temperature)	30 °C to 60 °C
$c_p$ (Specific Heat Capacity)	4182 J/kg·K
$\dot{m}_e$ (Water Mass Flow Rate on Evaporator Side)	1.81 kg/s
$\dot{m}_c$ (Water Mass Flow Rate on Condenser Side)	1.11 kg/s
Tolerance	1e-2

The cascade heat pump modeling involves an iterative process to calculate the thermodynamic properties and performance metrics for both cycles while ensuring consistency between the two stages.

The process begins with an initial assumption for the evaporator pressure ( $P_1$ ) in the low-temperature cycle. The condenser pressure ( $P_4$ ) for the high-temperature cycle is calculated

based on the outlet temperature of the condenser ( $T_{c,o}$ ) and the temperature difference in the condenser ( $\Delta T_{\text{IHX}}$ ). The IHX intermediate temperature ( $T_3$ ) is incrementally updated within the specified range (Table 4.3), and pressures  $P_2$  and  $P_3$  are calculated. The condensing pressure of Cycle A ( $P_2$ ) is determined from the condensing temperature ( $T_3$ ) of cycle A. The evaporating pressure of Cycle B ( $P_3$ ) is calculated based on the evaporating temperature ( $T_5$ ), which is defined by:

$$T_5 = T_3 - \Delta T_{\text{IHX}}. \quad (4.1)$$

Thermodynamic properties, such as enthalpy, entropy, and temperature, are evaluated at the eight key states of the cascade system using an equation of state. The mass flow rate for the high-temperature cycle ( $\dot{m}_B$ ) is calculated based on the heat output from the condenser, as outlined in Equation (2.22). The IHX energy balance is then used to determine the mass flow rate for the low-temperature cycle ( $\dot{m}_A$ ) by ensuring the heat released by Cycle A matches the heat absorbed by Cycle B, in accordance with Equation (2.23).

The work input for each compressor ( $\dot{W}_{\text{in,A}}$  and  $\dot{W}_{\text{in,B}}$ ) is determined from the enthalpy differences across the compressors, as described in Equations (2.18) and (2.21), respectively. Using the calculated evaporator outlet temperature ( $T_{e,o}$ ) for Cycle A, the evaporator pressure ( $P_1$ ) is updated and compared with the initially assumed value. If the deviation exceeds the predefined tolerance, the assumed pressure is adjusted, and the calculations are repeated. This iterative process continues until convergence is achieved for  $P_1$ , ensuring consistency between the two cycles.

The COP is calculated using Equation (2.24) for the entire range  $T_3$ . The optimal value of  $T_3$  is identified as the one that maximizes the COP while maintaining consistent operating conditions for both cycles. The iterative modeling process is summarized in the flowchart shown in Figure 4.2.

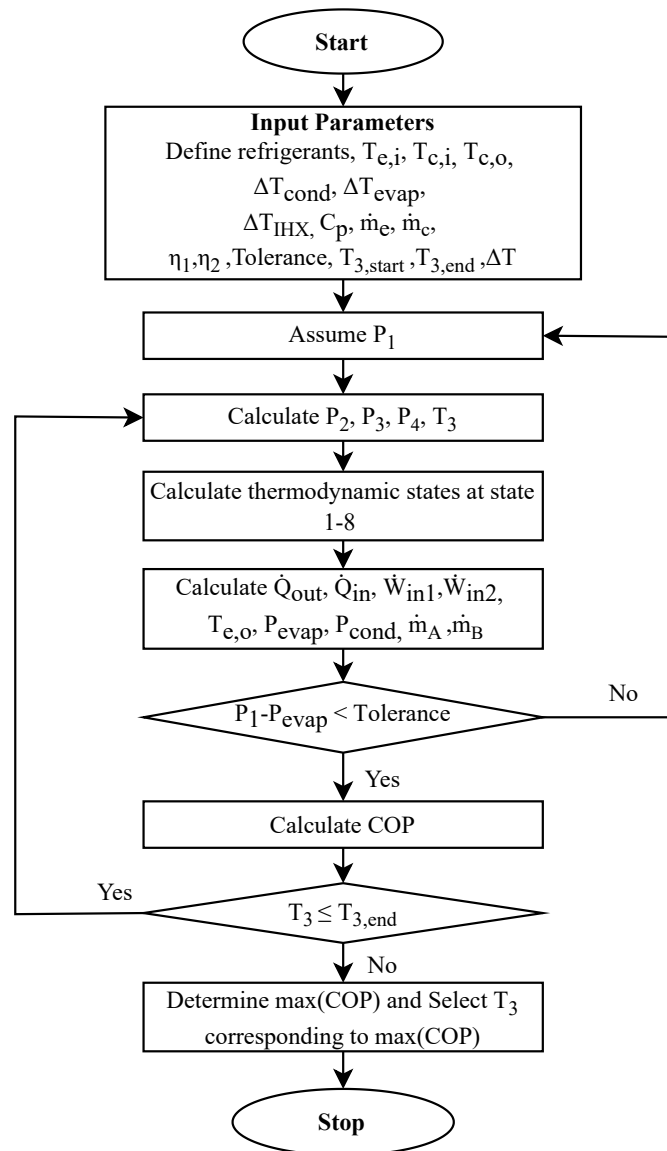


FIGURE 4.2: Flowchart of the thermodynamic model for the cascade cycle.

## 4.4 Model validation cascade heat pump

To validate the accuracy and performance of the cascade heat pump model, its results were compared to those presented in the study by Getu and Bansal [24] on the thermodynamic analysis of an R744-R717 cascade refrigeration system. The operating conditions in the reference paper were replicated for this validation, including a condensing temperature in the upper cycle ( $T_C = 40^\circ\text{C}$ ), an evaporating temperature in the lower cycle ( $T_E = -50^\circ\text{C}$ ), a cascade temperature difference ( $\Delta T_{\text{CAS}} = 5 \text{ K}$ ), and varying subcooling levels ( $\Delta T_{\text{sub}} = 0, 5, 10 \text{ K}$ ).

The comparison highlights the agreement between the reference study and the validated model, particularly in the behavior of the COP as a function of the intermediate temperature at the cascade heat exchanger outlet ( $T_{\text{CAS,E}}$ ). Both the reference and validated results show that the COP increases to a maximum before decreasing as  $T_{\text{CAS,E}}$  ranges from  $-25^\circ\text{C}$  to  $0^\circ\text{C}$ . The influence of subcooling ( $\Delta T_{\text{sub}}$ ) is also evident, with higher subcooling levels (10 K) producing higher COP values across the entire temperature range. Figure 4.3 presents these trends, where the reference results are shown on the left and the validated model's results are on the right.

The mass flow ratio ( $\dot{m}_H/\dot{m}_L$ ) similarly demonstrates close alignment between the reference study and the validated model. As  $T_{\text{CAS,E}}$  increases, the mass flow ratio decreases consistently in both cases. Subcooling again plays a key role, shifting the mass flow ratio upwards with higher values of  $\Delta T_{\text{sub}}$ . This behavior reflects the thermodynamic coupling between the two refrigerant loops. These trends are depicted in Figure 4.4, where the left diagram corresponds to the reference data, and the right diagram illustrates the validated model.

The strong alignment between the validated model and the reference study confirms the robustness and reliability of the thermodynamic approach. By accurately reproducing the COP and mass flow ratio trends under identical conditions, the validation establishes the model's suitability for further parametric studies and optimization of cascade heat pump systems. These findings not only verify the correctness of the thermodynamic calculations but also underline the potential of cascade systems using carbon dioxide and ammonia for high-performance applications. It is important to note that this validation was conducted specifically for the R744-R717 cascade cycle to ensure alignment with the established reference case. The performance evaluation of alternative refrigerant pairs was carried out separately to assess their suitability for industrial implementation.

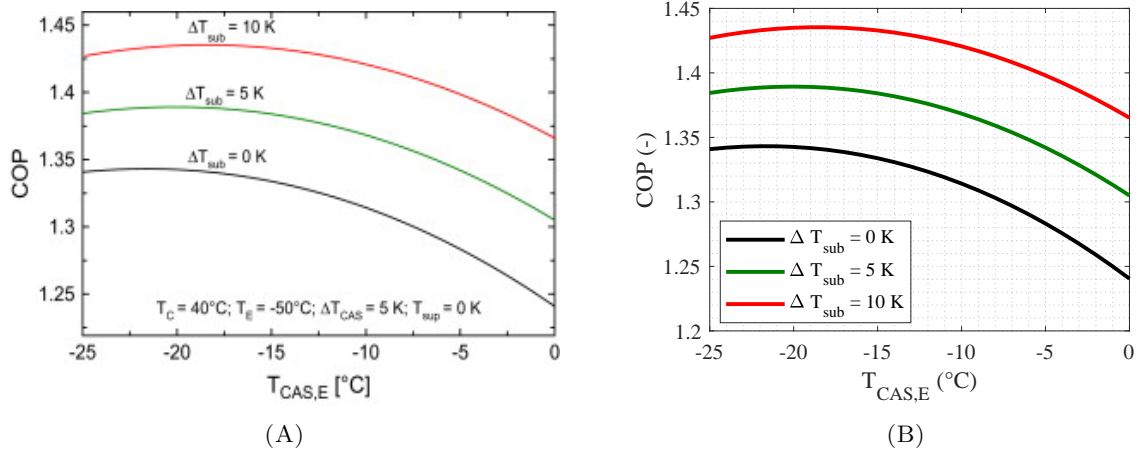


FIGURE 4.3: Comparison between reference model (A) and validated models (B) for COP trends as a function of intermediate temperatures under varying subcooling conditions with a condensing temperature in the upper cycle of  $T_C = 40^\circ\text{C}$ , an evaporating temperature in the lower cycle of  $T_E = -50^\circ\text{C}$  and a cascade temperature difference of  $\Delta T_{CAS} = 5\text{ K}$ .

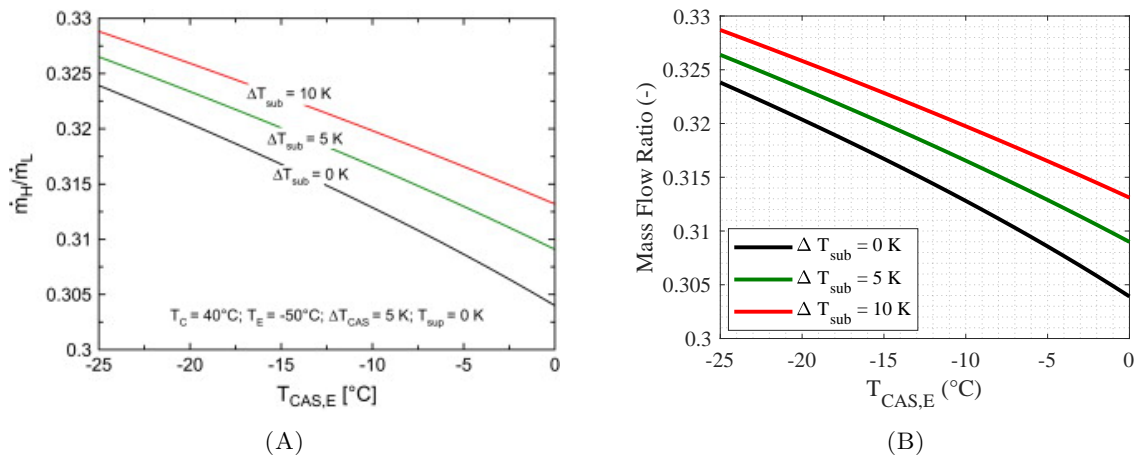


FIGURE 4.4: Comparison of mass flow ratio trends from reference study (A) and validated model (B) as a function of intermediate temperatures under varying subcooling conditions with a condensing temperature in the upper cycle of  $T_C = 40^\circ\text{C}$ , an evaporating temperature in the lower cycle of  $T_E = -50^\circ\text{C}$  and a cascade temperature difference of  $\Delta T_{CAS} = 5\text{ K}$ .

## Chapter 5

# Thermodynamic analysis

*Optimizing energy efficiency in industrial processes is crucial for reducing both operational costs and environmental impact. As part of Teijin Aramid's effort to improve thermal energy management, this chapter evaluates different heat pump configurations to determine the most effective and sustainable solution. The analysis begins by assessing the impact of inlet temperatures and mass flow rates on heat pump efficiency, followed by a comparative study of simple vapor and cascade cycles. A screening of refrigerants is conducted to identify low-GWP alternatives suitable for industrial integration. Finally, COP trends and operational costs are examined across different system configurations, leading to the selection of the centralized and cascade heat pump systems as the most viable solutions for implementation.*

## 5.1 Impact of parameter variation on system performance

This section investigates the influence of key operational parameters on the performance of the single vapor compression heat pump, focusing on the COP. Two primary categories of parameters are analyzed: inlet temperatures and mass flow rates.

### 5.1.1 Influence of inlet temperatures

The impact of variations in inlet temperatures at both the condenser and evaporator sides is summarized in Figure 5.1. An increase in the inlet temperature on the condenser side reduces the heat transfer rate required within the condenser, as the smaller temperature gradient minimizes the thermal demand necessary to achieve the desired outlet temperature. This reduction in thermal load causes an increase in the evaporator outlet temperature, thereby elevating the evaporating pressure of the refrigerant due to the reduced heat absorption requirements. Under steady-state conditions, where the condensing pressure remains constant, the resulting decrease in the pressure ratio across the compressor significantly reduces the compressor's work input. This improvement in compressor efficiency enhances the overall thermodynamic performance of the system, leading to an increase in COP.

Similarly, increasing the evaporator side inlet temperature raises the outlet temperature of the evaporator side water, further increasing the evaporating pressure. This elevated evaporating pressure also reduces the pressure ratio, thereby improving system efficiency and increasing COP. The trends for both heating and cooling modes are illustrated in Figure 5.1.

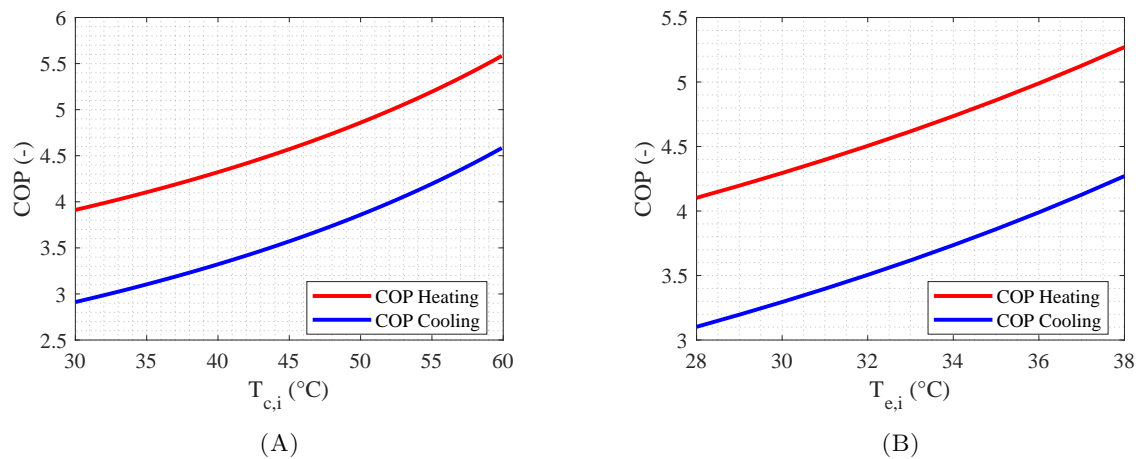


FIGURE 5.1: Impact of inlet water temperatures on COP performance for both condenser and evaporator sides, focusing on (A) the effect of condenser-side inlet temperature at an evaporating temperature of 30°C and (B) the effect of evaporator-side inlet temperature at a condensing temperature of 65°C

### 5.1.2 Influence of mass flow rates

The effect of mass flow rate variations on the condenser and evaporator sides is presented in Figure 5.2. For the condenser side, increasing the mass flow rate leads to a higher heat transfer rate, resulting in greater heat rejection to the sink. To maintain the system's energy balance, the evaporator is required to absorb a proportionally larger amount of heat from the source. This increased heat absorption reduces the evaporating pressure, as the system must operate at a lower temperature to extract the additional heat. Consequently, the pressure ratio across the compressor increases, as the condensing pressure remains constant. This higher pressure ratio necessitates greater work input from the compressor, further reducing the system's overall efficiency and leading to a decline in COP.

Conversely, an increase in the evaporator-side mass flow rate raises the outlet temperature of the evaporator-side water, thereby increasing the evaporating pressure. With the condensing pressure and heat transfer rate on the condenser side remaining constant, the reduced pressure ratio decreases the compressor's energy consumption, improving the COP.

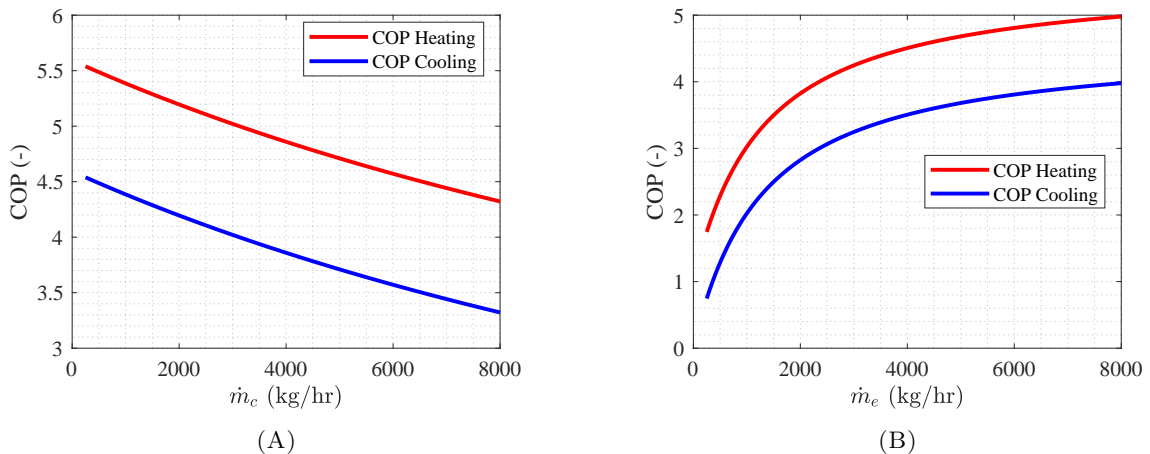


FIGURE 5.2: Impact of water mass flow rate variations on COP performance for both condenser and evaporator sides, showing (A) the effect of condenser side mass flow rate on COP at an evaporating temperature of 30°C and a condensing temperature of 65°C, and (B) the effect of evaporator side mass flow rate on COP under the same temperature conditions.

## 5.2 Comparative analysis of simple vapor and cascade cycles

A comparative analysis was conducted to evaluate the performance of the simple vapor cycle and the cascade cycle, both employing R134a as the refrigerant in both the low-temperature cycle and high-temperature cycle. The study aimed to assess the impact of varying the intermediate heat exchanger (IHX) temperature difference ( $\Delta T_{\text{IHX}}$ ) on the COP of the cascade cycle, as well as to benchmark the cascade cycle against the simple vapor cycle under identical conditions.

The analysis involved a systematic comparison of the two cycles while varying the inlet

temperature at the condenser side. The IHX in the cascade cycle was tested with  $\Delta T_{\text{IHX}}$  values of 3K, 4K, and 5K, which directly influence the interaction between the high-temperature and low-temperature stages in the cascade configuration. The performance of the cascade cycle was analyzed for these three  $\Delta T_{\text{IHX}}$  values and compared with the simple vapor cycle, which lacks an intermediate heat exchanger.

The COP results for the simple vapor and cascade cycles are presented in Figure 5.3.

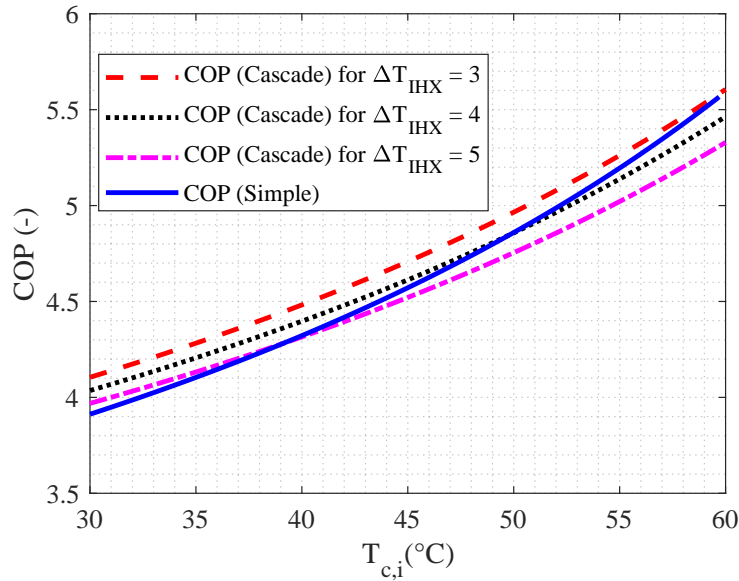


FIGURE 5.3: Comparison of COP performance for cascade and simple heating systems as a function of condenser inlet temperature and internal heat exchanger temperature differences ( $\Delta T_{\text{IHX}}$ ).

The cascade cycle demonstrates superior performance compared to the simple vapor cycle, but the extent of this advantage depends significantly on the intermediate temperature difference ( $\Delta T_{\text{IHX}}$ ). For  $\Delta T_{\text{IHX}} = 3$  K, the cascade cycle outperforms the simple vapor cycle across the entire range of  $T_{\text{cond},\text{in}}$ . This consistent advantage is attributed to the minimized thermal losses in the IHX, which enhances the efficiency of the cascade cycle.

For  $\Delta T_{\text{IHX}} = 4$  K, the cascade cycle's COP surpasses that of the simple vapor cycle only when  $T_{c,i}$  is lower than approximately  $49.7^\circ\text{C}$ . Similarly, for  $\Delta T_{\text{IHX}} = 5$  K, the cascade cycle overtakes the simple vapor cycle at  $T_{c,i}$  values below  $39.1^\circ\text{C}$ . This trend highlights the sensitivity of the cascade cycle's performance to the intermediate temperature difference. Larger  $\Delta T_{\text{IHX}}$  values increase thermal losses in the IHX, reducing the efficiency of the cascade cycle at lower condenser inlet temperatures.

The results emphasize the importance of optimizing  $\Delta T_{\text{IHX}}$  in the cascade cycle design. While smaller  $\Delta T_{\text{IHX}}$  values improve the COP across a broader temperature range, they may also introduce practical challenges, such as increased heat exchanger size and cost. The selection of  $\Delta T_{\text{IHX}}$  should therefore balance performance benefits with practical feasibility.

The comparative study demonstrates that the cascade cycle, under specific conditions, offers

significant performance improvements over the simple vapor cycle. For smaller intermediate temperature differences, such as  $\Delta T_{\text{IHX}} = 3 \text{ K}$ , the cascade cycle consistently outperforms the simple vapor cycle. However, as  $\Delta T_{\text{IHX}}$  increases, the performance advantage diminishes at lower condenser inlet temperatures, underscoring the need for careful optimization of the intermediate temperature difference. This analysis provides valuable insights for selecting and designing efficient heat pump configurations tailored to specific operating conditions.

Next to that, the results of this analysis align with established thermodynamic principles. As expected, the cascade cycle performs better in terms of COP than the simple vapor cycle when the condenser inlet temperature is lower, because distributing the temperature lift across two compression stages reduces the compression ratio and improves overall efficiency. The lower compression ratio in each stage decreases the work required per compressor and enhances the system's COP. However, at higher condenser inlet temperatures, the single-stage cycle can achieve a higher COP, since the smaller temperature difference to the final condensing temperature reduces the compression work required in a single step. This confirms that the cascade cycle is most beneficial in conditions where a high temperature lift is needed, whereas for smaller temperature lifts, a single-stage cycle can be more efficient.

This behavior is consistent with previous studies on cascade refrigeration and heat pump systems, which have shown that cascade cycles are particularly effective for applications requiring large temperature differences, while single-stage cycles tend to be more efficient when the temperature lift is moderate [25].

### 5.3 Screening of refrigerants

The performance of a heat pump depends on the choice of refrigerant. This section screens potential refrigerants for both a simple vapor heat pump and a cascade heat pump, considering thermodynamic performance, environmental impact, and safety. The screening focuses on refrigerants suitable for a condensing temperature of  $65^\circ\text{C}$  and an evaporating temperature of  $25^\circ\text{C}$ . For the cascade heat pump, different refrigerant pairs are evaluated based on COP and lower cycle condensing temperature ( $T_3$ ), with an intermediate heat exchanger (IHX) temperature difference of  $\Delta T_{\text{IHX}} = 5\text{K}$ . Instead of selecting a single refrigerant, this screening provides an overview of viable options and trade-offs for heat pumps in industrial settings.

#### 5.3.1 Screening of refrigerants for the simple vapor heat pump integration

The initial list of refrigerants, as presented in Table 2.1, has been narrowed down in this section based on key criteria including critical temperature, normal boiling point (NBP), and the availability of thermodynamic data. The refined selection considers only refrigerants that meet the operational requirements of a heat pump with a condensing temperature of  $65^\circ\text{C}$  and an evaporating temperature of  $25^\circ\text{C}$ , ensuring compatibility with the system's thermal lift.

Several recent studies [26, 27] have identified R1224yd(Z), R1336mzz(E), and R1336mzz(Z) as promising low-GWP refrigerants for high-temperature heat pump applications, demonstrating favorable thermodynamic performance and environmental benefits. However, these

refrigerants are not currently available in CoolProp, limiting their implementation in this study. Consequently, their performance could not be evaluated within the simulation framework used in this research.

The updated table, Table 5.1, presents the refrigerants that are most suitable for this application. These refrigerants were selected based on their ability to operate efficiently under the given conditions while also adhering to safety and environmental regulations.

TABLE 5.1: Available and suitable refrigerants for the simple vapor heat pump.

Type	Refrigerant	$T_{cr}$ (°C)	$P_{cr}$ (MPa)	NBP (°C)	ODP	GWP	Safety	COP
<b>HFC</b>	<b>R134a</b>	<b>101.2</b>	<b>4.06</b>	<b>-25.9</b>	<b>0</b>	<b>1430</b>	<b>A1</b>	<b>4.86</b>
HFC	R161	102.2	5.09	-37.5	0	12	A3	4.99
HFC	R152a	113.3	4.52	-24.0	0	140	A2	5.14
HFO	R1234yf	94.7	3.38	-29.0	0	<1	A2L	4.54
HFO	R1243zf	103.8	3.52	-25.5	0	0.8	A2L	4.82
HFO	R1234ze(E)	109.4	3.64	-19.0	0	<1	A2L	4.87
HFO	R1234ze(Z)	150.1	3.53	9.8	0	<1	A2L	5.33
HCFO	R1233zd(E)	166.5	3.62	18.0	0.00034	1	A1	5.34
HC	R1270	91.1	4.55	-42.1	0	3	A3	4.66
HC	R290	96.7	4.25	-42.0	0	3	A3	4.71
HC	R600a	134.7	3.66	-11.0	0	3	A3	5.07
HC	R600	152.0	3.80	-0.5	0	3	A3	5.22
Natural	R717	132.3	11.33	-33.0	0	0	B2L	5.34

R134a, an HFC refrigerant, serves as a benchmark due to its widespread use in heat pump systems and its favorable thermodynamic performance. However, its high GWP of 1430 motivates the exploration of low-GWP alternatives.

In terms of environmental performance, the selected refrigerants comply with international sustainability standards. R152a, although efficient and operationally compatible, has a GWP of 140, which is significantly higher than most of the other options listed but remains within acceptable regulatory limits. In contrast, natural refrigerants such as R600, R600a, and R717 stand out for their negligible GWP, aligning with global goals for sustainability. However, their safety classifications (A3 for R600 and R600a and B2L for R717) demand careful implementation and adherence to safety protocols, particularly in large-scale systems.

The synthetic refrigerants R1234ze(E) and R1234ze(Z) emerge as particularly promising options. Both have low GWP values, excellent thermodynamic properties, and favorable safety classifications (A2L). Among these, R1234ze(Z) is particularly notable for its high COP value compared to the rest of the refrigerants listed in the table. While R1233zd(E) offers advantages in terms of safety (A1 classification) and low environmental impact, its high normal boiling point could present challenges in applications requiring lower evaporating temperatures.

### 5.3.2 Screening of refrigerants for the cascade heat pump

In cascade heat pump systems, the selection of refrigerants for the lower and upper cycles significantly influences overall efficiency and operational feasibility. The first refrigerant in

each pair operates in the lower cycle, where it evaporates at a lower temperature, while the second refrigerant operates in the upper cycle, where it undergoes condensation and heat rejection. To ensure effective thermal coupling, an intermediate heat exchanger (IHX) is employed with a temperature difference of  $\Delta T_{\text{IHX}} = 5\text{K}$ . The choice of refrigerant affects key performance indicators such as the COP and the condensing temperature of the lower cycle ( $T_3$ ). To establish a benchmark, R134a was selected as a reference refrigerant for both cycles. The R134a/R134a configuration resulted in a COP of 4.75 and a condensing temperature of 48.8°C. This serves as a comparative basis for evaluating the performance of alternative refrigerant pairs in the cascade system. The comparison between different pairs of refrigerants can be found in Table 5.2.

TABLE 5.2: Comparison of refrigerant combinations, COP values, and  $T_3$  temperatures.

Refrigerants	COP	$T_3$ (°C)
R134a / R134a	4.75	48.8
R717 / R717	5.04	48.6
R600 / R600	4.90	48.7
R600a / R600a	4.92	48.6
R290 / R290	4.63	48.8
R1234ze(Z) / R1234ze(Z)	5.08	48.8
R1233zd(E) / R1233zd(E)	5.09	48.7
R600 / R717	5.03	46.9
R717 / R600	5.03	50.5
R600/ R1233zd(E)	5.06	47.0
R1233zd(E)/ R600	5.05	50.5
R600 / R1234ze(Z)	5.05	47.1
R1234ze(Z) / R600	5.05	50.4
R1234ze(Z) / R1233zd(E)	5.06	49.8
R1234ze(Z) / R717	5.07	50.6

The analysis reveals a range of COP values between 4.63 and 5.09 across different refrigerant combinations. Hydrocarbon-based refrigerants, such as R290 and R600, exhibit moderate efficiency, with R290/R290 yielding the lowest COP of 4.63. Conversely, refrigerant pairs incorporating R1233zd(E) and R1234ze(Z) achieve the highest COP values, indicating superior thermodynamic properties for these fluids in a cascade configuration. The combination R1233zd(E)/R1233zd(E) reaches the highest COP of 5.09, suggesting minimal exergy losses and effective heat transfer.

Condensing temperatures ( $T_3$ ) vary from 46.9°C to 50.6°C, with R600/R717 resulting in the lowest condensing temperature, while R717/R600 and R1234ze(Z)/R717 exhibit the highest. The use of R717 (ammonia) in the upper cycle leads to increased temperature lift, which may

enhance heat rejection but also impose higher pressure requirements.

## 5.4 Evaluation of COP trends across individual, clustered, and integrated heat pump configurations

Efficient heat pump operation depends on the balance between mass flow rates, temperature lift, and system configuration. This analysis evaluates various the different concepts to determine their impact on heat pump performance. Table 5.3 presents data on individual process lines, cluster formations, and the four heat pump concepts. For each concept, refrigerant R134a is used as a reference for comparison.

Each process line requires heating to 60°C at the condenser side, meaning the evaporator conditions are adjusted accordingly to maintain thermal balance. The average mass flow rates of the process fluid over a one-year period, along with key performance metrics such as COP, work input ( $\dot{W}_{in}$ ), and total heat output ( $\dot{Q}_{heat}$ ), are presented in Table 5.3.

The first section of the table lists the performance parameters for each process line (1–10). Since the evaporator inlet temperature ( $T_{e,i}$ ) remains constant for all lines, the evaporator outlet temperature ( $T_{e,o}$ ) varies depending on the required heating demand and the corresponding refrigerant pressure and phase change characteristics.

Below the individual lines, the cluster groups (1-2-3, 4-5-6, 7-8-9-10) are introduced. These clusters aggregate multiple lines, with their corresponding condenser inlet temperature ( $T_{c,i}$ ) determined using the weighted average temperature Equation (6.3). The cluster-based approach is utilized in Concept 3, where three heat pumps serve predefined process groups instead of separate units for each line.

The final four rows summarize the four proposed heat pump system configurations:

- Concept 1: Each line is equipped with an individual heat pump.
- Concept 2: A single centralized heat pump is used for all lines.
- Concept 3: Three heat pumps are deployed, each serving a specific cluster.
- Concept 4: A cascade heat pump configuration is implemented, leveraging heat recovery through a secondary cycle.

For concepts 2, 3, and 4, the mixed condenser inlet temperature was determined using the weighted average approach with Equation (6.3), with concept 3 applying this method separately for each cluster.

TABLE 5.3: Performance parameters for different heating configurations.

Line	$\dot{m}_e$ (kg/s)	$\dot{m}_c$ (kg/s)	$T_{e,i}$ (°C)	$T_{e,o}$ (°C)	$T_{c,i}$ (°C)	COP <sub>h</sub>	COP <sub>c</sub>	$\dot{W}_{in}$ (kW)	$\dot{Q}_{heat}$ (kW)
1	1.67	1.05	34.4	30.9	53.0	4.97	3.97	6.2	30.7
2	1.56	1.13	34.4	30.4	53.0	4.90	3.90	6.7	33.0
3	1.11	1.10	34.4	30.5	55.0	4.91	3.91	4.7	23.0
4	1.60	1.52	34.4	16.1	33.0	3.51	2.51	48.9	171.4
5	1.15	1.18	34.4	19.4	40.0	3.75	2.75	26.3	98.7
6	1.49	1.14	34.4	29.6	52.0	4.79	3.79	8.0	38.1
7	2.33	1.18	34.4	26.6	40.0	4.44	3.44	22.2	98.3
8	0.91	1.12	34.4	18.3	42.0	3.67	2.67	22.9	84.2
9	1.53	1.15	34.4	28.5	50.0	4.66	3.66	10.4	48.3
10	0.81	1.16	34.4	20.6	47.0	3.86	2.86	16.3	63.0
1-2-3	4.34	3.28	34.4	30.6	53.7	4.84	3.84	17.9	86.7
4-5-6	4.24	3.84	34.4	21.5	40.8	3.93	2.93	78.4	30.8
7-8-9-10	5.57	4.61	34.4	24.8	44.8	4.24	3.24	69.2	293.8
Concept 1	14.15	11.72	34.4	NaN	NaN	3.99	2.99	172.5	688.8
Concept 2	14.15	11.72	34.4	25.5	45.9	4.32	3.32	159.6	688.8
Concept 3	14.15	11.72	34.4	NaN	NaN	4.16	3.16	165.6	688.8
Concept 4	14.15	11.72	34.4	25.5	45.9	4.31	3.32	159.8	688.8

#### 5.4.1 COP variations across individual lines

For individual lines (1 to 10), the heating COP ranges from 3.51 (line 4) to 4.97 (line 1). This variation is largely attributed to differences in condenser inlet temperatures ( $T_{c,i}$ ), mass flows and corresponding compressor work input. Lines operating at higher  $T_{c,i}$  values tend to exhibit higher COP values, as the required temperature lift across the compressor is reduced, leading to lower work input. Conversely, lines with lower  $T_{c,i}$ , such as line 4 (33 °C condenser inlet temperature), experience a larger temperature difference, increasing the work input and thereby reducing COP.

#### 5.4.2 COP trends in clustered configurations

The clustered configurations (1-2-3, 4-5-6, and 4-8-9-10) aggregate multiple lines into a single system. The weighted average  $T_{c,i}$  values for each cluster were calculated based on mass flow rates and inlet temperatures. The corresponding COP values for these configurations exhibit a trend consistent with the individual lines. Notably, cluster 1-2-3, which has the highest weighted  $T_{c,i}$  (53.7 °C), achieves a COP of 4.81, which is comparable to the highest COP values among the individual lines. Meanwhile, cluster 4-5-6, with a lower  $T_{c,i}$  of 40.8 °C, shows a reduced COP of 3.93, highlighting the sensitivity of system performance to temperature lift.

#### 5.4.3 COP performance in system concepts

The bottom section of the table presents four integrated system concepts, where multiple lines are combined into a larger-scale heat pump system. The results indicate that concept 1 and concept 3, which operate without precise temperature control, exhibit lower COP values of

3.99 and 4.16, respectively. Concept 2 which account for a weighted condenser inlet temperature (45.9°C), show improved COP values of 4.32, whereas concept 4 with the same weighed condenser inlet temperature results in a COP of 4.31. The weighted temperature approach used in Concepts 2 and 4 leads to better efficiency by balancing temperature lifts, reducing compressor work input, and thereby improving overall heat pump performance. Concept 4, the cascade heat pump configuration, initially demonstrated a COP of 4.31 with a  $T_{\text{IHX}}$  of 5 °C. However, further analysis was conducted to evaluate the impact of different intermediate heat exchanger temperature differences ( $T_{\text{IHX}}$ ) on system efficiency. By adjusting  $T_{\text{IHX}}$  to 4 °C, 3 °C, and 2 °C, a trend was observed in which lower  $T_{\text{IHX}}$  values resulted in changes to system performance. Specifically, at  $T_{\text{IHX}} = 4$  °C, the COP increased slightly to 4.39, whereas at  $T_{\text{IHX}} = 3$  °C and 2 °C, COP reached 4.39 and 4.48, respectively. The improved COP at lower  $T_{\text{IHX}}$  values is attributed to reduced exergy losses across the intermediate heat exchanger, minimizing the temperature lift required at each stage of the cascade cycle. However, as  $T_{\text{IHX}}$  is further reduced, the improvements in COP become smaller due to the increasing thermal resistance in the heat exchanger, which limits further efficiency increases.

## 5.5 Economic analysis of heat pump configurations

The economic viability of different heat pump configurations is assessed based on their operational costs and the financial feasibility of implementation. The analysis considers both the annual cost savings compared to steam-based heating and the investment constraints imposed by a five-year payback period.

### 5.5.1 Operational cost comparison

A key aspect of evaluating the feasibility of different heat pump configurations is the associated operational costs. The cost of steam is €34.15 per ton, while electricity is priced at €123.43 per MWh. Additionally, the latent heat of steam at 3 bar is 2163 kJ/kg, which is used to calculate the energy required for steam-based heating. These values form the basis for the cost analysis of steam and electricity consumption across the four heat pump concepts. Table 5.4 summarizes the annual energy costs for steam and electricity consumption across the four heat pump concepts analyzed in this study. Steam costs remain constant at €343.000 per year across all configurations, as the demand for backup steam is independent of the specific heat pump design. However, electricity costs vary depending on the system configuration, directly influencing the total operational expenditure.

Among the analyzed concepts, the centralized heat pump system (Concept 2) exhibits the lowest electricity cost, followed closely by the cascade heat pump system (Concept 4). These configurations achieve energy cost reductions of approximately 50% in both cases, relative to steam-based heating. The efficiency gains in these concepts are attributed to improved temperature matching and reduced compression work, leading to lower electricity consumption.

TABLE 5.4: Annual energy costs for steam and electricity for the different heat pump concepts.

Cost Type	Annual Cost (€)
Steam cost (all concepts)	343.000
Electricity cost - Concept 1	186.500
Electricity cost - Concept 2	172.600
Electricity cost - Concept 3	179.100
Electricity cost - Concept 4	172.800

Conversely, the independent heat pump configuration (Concept 1) incurs the highest electricity cost, demonstrating a 46% reduction compared to steam-based heating. This result highlights the inefficiency of operating multiple standalone units, which increases redundancy and energy consumption. The clustered heat pump configuration (Concept 3), where lines are grouped into clusters, offers a 48% cost reduction, falling between the fully independent and fully centralized approaches.

These trends align with the expected thermodynamic behavior of the systems. The cascade heat pump system (Concept 4) benefits from staged compression, enhancing the COP, while the centralized system (Concept 2) minimizes redundant heat pump operation, optimizing electricity consumption.

The electricity costs associated with Concept 4 depend on the selected  $T_{\text{IHX}}$  value, as lower  $T_{\text{IHX}}$  results in higher system efficiency and reduced electricity consumption. Table 5.5 presents the updated annual electricity cost estimates for Concept 4 at different  $T_{\text{IHX}}$  settings. At a  $T_{\text{IHX}}$  of 2°C, the annual electricity costs decrease to €163.200, compared to €172.800 at 5°C. Relative to steam-based heating, this lowest-temperature configuration achieves a total cost reduction of approximately 52%.

TABLE 5.5: Effect of  $T_{\text{IHX}}$  variation on  $\dot{W}_{\text{in}}$  and annual electricity costs for Concept 4.

$T_{\text{IHX}}(^{\circ}\text{C})$	$\dot{W}_{\text{in}}(\text{kW})$	Annual Cost (€)
5	159.8	172.800
4	156.8	169.500
3	153.9	166.400
2	150.9	163.200

### 5.5.2 Economic feasibility

The analysis demonstrates that while the proposed heat pump configurations achieve cost reductions compared to steam-based heating, the financial feasibility remains a critical factor to determine whether the project is viable. With a required payback period of five years in Teijin Aramid, the total allowable investment for the heat pump system, including CAPEX, installation, labor, maintenance, and additional infrastructure, is constrained by the total

cost savings over that period.

Concept 2, which exhibits the lowest operational costs, results in annual savings of €170.400, leading to a total five-year savings of €852.000. This indicates that the full cost of implementing a heat pump system must remain below this threshold to meet the required payback period. However, industrial heat pump installations, particularly for large-scale applications, often require substantial capital investment. Based on discussions with industry experts at company X during a site visit to a heat pump installation facility, industrial-scale heat pump installations have demonstrated that actual investment costs have been observed to be substantially higher than initial estimates with total investments frequently reaching several million euros. A notable example is a 3 MW heat pump system, which was initially projected to cost €6 million but ultimately required an investment of €18 million. Given that the required system capacity at Teijin Aramid is approximately 700 kW, a proportionally scaled investment would likely surpass the available budget, posing a significant challenge to financial feasibility.

Further calculations indicate that reducing the intermediate heat exchanger temperature difference ( $T_{\text{IHX}}$ ) from 5°C to 2°C in the cascade heat pump configuration (Concept 4) increases cost savings to €179.800 per year, resulting in a total five-year savings of €899.000. Although this represents a slight improvement, the total savings still fall short of covering the expected investment costs associated with an industrial-scale heat pump system.

Additionally, the cascade heat pump configuration introduces further capital expenditures due to the need for an intermediate heat exchanger and a more complex system architecture. Lowering  $T_{\text{IHX}}$  to enhance efficiency also increases the cost of the heat exchanger itself, further impacting overall investment requirements. These findings suggest that, despite the operational cost benefits, the initial investment for an industrial heat pump system remains a limiting factor within the defined payback period. Achieving financial feasibility may require alternative financing mechanisms, external subsidies, or an extended payback period to justify the investment.

## 5.6 Selection of heat pump configurations for implementation

The evaluation of heat pump integration concepts demonstrates that centralized (Concept 2) and cascade (Concept 4) configurations provide the best balance between energy efficiency, feasibility, and cost-effectiveness. The centralized system uses a single large heat pump to serve all process lines, stabilizing temperature fluctuations and improving overall efficiency. This reduces electricity consumption, enhances COP, and simplifies maintenance, making it a cost-effective solution for large-scale applications. However, since all lines depend on the same system, any failure would require switching to the steam backup, making system reliability a key consideration.

The cascade system further improves efficiency by dividing the temperature lift across two stages, reducing compressor work and enabling the use of refrigerants optimized for different temperature levels. Adjusting the intermediate heat exchanger temperature difference ( $T_{\text{IHX}}$ ) enhances heat recovery, decreasing exergy losses and improving overall system performance.

However, the performance gain compared to the centralized system is relatively small, while the increased system complexity and higher capital investment (CAPEX) make implementation more challenging. As a result, for Teijin, the centralized configuration (Concept 2) is the most attractive solution, providing the best trade-off between performance, cost, and operational feasibility.



## Chapter 6

# Effect of mixing on the performance of heat pumps

*Mixing in heat pump systems, where streams with differing temperatures are combined, significantly influences system performance, energy efficiency, and thermodynamic behavior. This chapter investigates the impact of various mixing strategies on the performance of heat pumps, with a focus on industrial processes at Teijin Aramid. Given the variability in temperatures of process 2, the study evaluates whether it is more effective to mix streams or treat them individually. Each strategy is assessed in terms of its effects on the COP, exergy destruction, and system efficiency. By comparing mixing and non-mixing configurations, this chapter identifies optimal heat pump configurations for industrial applications, balancing energy efficiency and operational simplicity.*

## 6.1 Introduction to mixing strategies in heat pump systems

In Section 3.2, different heat pump integration concepts were introduced to improve thermal efficiency in the industrial processes at Teijin. Among these concepts, mixing occurs in all configurations except for the case in which each production line has its own dedicated heat pump (concept 1). The results presented in Section 5.5 indicate that concepts incorporating mixing achieve a higher COP than concept 1, which does not involve mixing. However, conventional thermodynamic principles suggest that mixing may introduce additional irreversibilities, potentially reducing overall system performance [9]. Moreover, the impact of mixing is influenced by its specific implementation, whether at the inlet or outlet, and whether it occurs on the evaporator or condenser side. These variations may yield contrasting effects on efficiency. Given these complexities and the potential for conflicting outcomes, a comprehensive investigation is required to quantify the effects of mixing under different conditions and to determine the circumstances under which mixing enhances or diminishes heat pump performance.

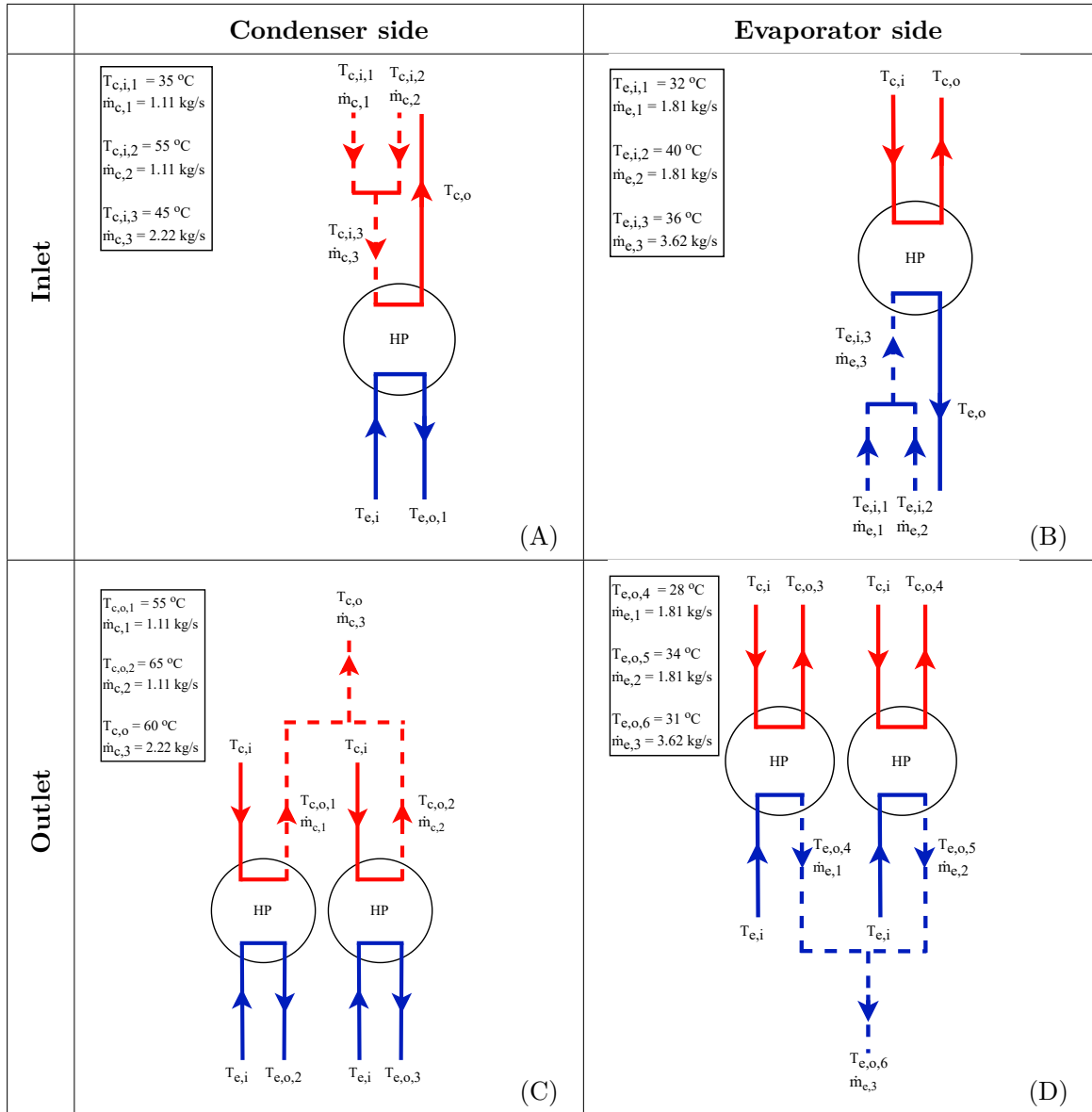
To systematically assess the role of mixing, this chapter investigates four fundamental mixing scenarios, categorized based on the mixing location (condenser side or evaporator side) and the mixing position (inlet or outlet). The four cases analyzed are:

- (A) **Inlet mixing at the condenser side:** Two streams, each with a mass flow rate of 1.11 kg/s, mix before entering the condenser. The inlet temperatures are  $T_{c,i,1} = 35^\circ\text{C}$  and  $T_{c,i,2} = 55^\circ\text{C}$ , resulting in a mixed temperature of  $T_{c,i,3} = 45^\circ\text{C}$  and a combined mass flow of 2.22 kg/s.
- (B) **Inlet mixing at the evaporator side:** Two evaporator inlet streams, each with a mass flow rate of 1.81 kg/s, mix before entering the heat pump. Their respective temperatures are  $T_{e,i,1} = 32^\circ\text{C}$  and  $T_{e,i,2} = 40^\circ\text{C}$ , leading to a mixed temperature of  $T_{e,i,3} = 36^\circ\text{C}$  and a combined mass flow of 3.62 kg/s.
- (C) **Outlet mixing at the condenser side:** Two separate outlet streams from the condenser, each with a mass flow of 1.11 kg/s, mix after exiting their respective heat pumps. Their outlet temperatures are  $T_{c,o,1} = 55^\circ\text{C}$  and  $T_{c,o,2} = 65^\circ\text{C}$ , resulting in a mixed outlet temperature of  $T_{c,o} = 60^\circ\text{C}$  and a combined flow rate of 2.22 kg/s.
- (D) **Outlet mixing at the evaporator side:** Two evaporator outlet streams mix after passing through the heat pump. Each stream has a mass flow rate of 1.81 kg/s, with outlet temperatures of  $T_{e,o,2} = 28^\circ\text{C}$  and  $T_{e,o,3} = 34^\circ\text{C}$ , leading to a mixed outlet temperature of  $T_{e,o} = 31^\circ\text{C}$  and a total mass flow of 3.62 kg/s.

These cases are analyzed first under constant mass flow conditions to isolate the effect of temperature mixing. However, in Teijin's industrial process, mass flows also vary dynamically. Therefore, the analysis is extended to examine the inlet mixing case at the condenser side combined with variations in mass flows.

These mixing strategies are visualized in Table 6.1 where each label (A), (B), (C), and (D) corresponds directly to the scenarios described below. The dashed lines in the diagrams represent the mixing process, where streams with different temperatures are combined to form a single stream with an intermediate temperature.

TABLE 6.1: Overview of inlet and outlet mixing configurations for the condenser and evaporator sides of the heat pump. (A) Inlet mixing at the condenser side with inlet temperatures of 35°C and 55°C, each stream having a mass flow of 1.11 kg/s. (B) Inlet mixing at the evaporator side with inlet temperatures of 32°C and 40°C, each stream having a mass flow of 1.81 kg/s. (C) Outlet mixing at the condenser side with outlet temperatures of 55°C and 65°C, each stream having a mass flow of 1.11 kg/s. (D) Outlet mixing at the evaporator side with outlet temperatures of 28°C and 34°C, each stream having a mass flow of 1.81 kg/s.



The specific mixing strategy directly influences the inlet and outlet temperatures of the streams, which in turn impacts the thermodynamic performance of the heat pump system. These configurations serve as the foundation for assessing the effect of mixing on the system's COP. For each scenario, the COP is determined based on the weighted average temperatures of the mixed streams and compared to non-mixing cases. The key parameters and fixed values used in this analysis are summarized in Table 6.2.

Parameter	Description	Value	Unit
$\dot{m}_c$	Sink-side mass flow rate	1.11	kg/s
$\dot{m}_{c,1}$	Sink-side mass flow rate 1	1.11	kg/s
$\dot{m}_{c,2}$	Sink-side mass flow rate 2	1.11	kg/s
$\dot{m}_{c,3}$	Sink-side mass flow rate 3	2.22	kg/s
$\dot{m}_e$	Source-side mass flow rate	1.81	kg/s
$\dot{m}_{e,1}$	Source-side mass flow rate 1	1.81	kg/s
$\dot{m}_{e,2}$	Source-side mass flow rate 2	1.81	kg/s
$\dot{m}_{e,3}$	Source-side mass flow rate 3	3.62	kg/s
Refrigerant	Working fluid used in the heat pump	R134a	-
$\eta_{iso}$	Isentropic efficiency of the compressor	0.7	-
$c_p$	Specific heat capacity of the working fluid	4182	J/kg·K
$\Delta T_{cond}$	Temperature difference in the condenser	5	°C
$\Delta T_{evap}$	Temperature difference in the evaporator	5	°C
$T_{c,i}$	Condenser side inlet temperature	50	°C
$T_{c,o}$	Condenser side outlet temperature	60	°C
$T_{e,i}$	Evaporator side inlet temperature	35	°C
$T_{e,o}$	Evaporator side outlet temperature	30	°C
$T_{c,i,1}$	Condenser side inlet temperature 1	35	°C
$T_{c,i,2}$	Condenser side inlet temperature 2	55	°C
$T_{c,i,3}$	Condenser side inlet temperature 3	45	°C
$T_{c,o,1}$	Condenser side outlet temperature 1	55	°C
$T_{c,o,2}$	Condenser side outlet temperature 2	65	°C
$T_{e,i,1}$	Evaporator side inlet temperature 1	32	°C
$T_{e,i,2}$	Evaporator side inlet temperature 2	40	°C
$T_{e,i,3}$	Evaporator side inlet temperature 2	36	°C
$T_{e,o,4}$	Evaporator side outlet temperature 4	28	°C
$T_{e,o,5}$	Evaporator side outlet temperature 5	34	°C
$T_{e,o,6}$	Evaporator side outlet temperature 6	31	°C

TABLE 6.2: Summary of fixed parameters, mass flow rates, and input/output temperatures in the heat pump model.

## 6.2 Thermodynamic principles of mixing

Mixing in heat pump systems significantly influences key thermodynamic properties, including entropy generation and exergy destruction. Since mixing is inherently irreversible, it leads to an increase in entropy ( $\Delta S_{\text{mix}}$ ) and a corresponding loss of available exergy, quantified as exergy destruction ( $\dot{E}_{\text{des}}$ ). The entropy generation during mixing is expressed as [9]:

$$\Delta S_{\text{mix}} = \sum_{j=1}^n \dot{m}_j s_j - \dot{m}_{\text{tot}} s_{\text{mix}}, \quad (6.1)$$

where  $\dot{m}_{\text{tot}}$  and  $s_{\text{mix}}$  are the total mass flow and specific entropy of the mixed stream, respectively, while  $\dot{m}_j$  and  $s_j$  are the mass flow and specific entropy of the individual streams before mixing.

The corresponding exergy destruction, which quantifies the loss of available work potential due to irreversibilities, is determined by:

$$\dot{E}_{\text{des}} = T_0 \cdot \Delta S_{\text{mix}}, \quad (6.2)$$

where  $T_0$  denotes the ambient or dead-state temperature, which serves as the thermodynamic reference in exergy analysis. It represents the temperature at which a system is in equilibrium with its surroundings, meaning no useful work can be extracted.

To evaluate the impact of mixing on the heat pump system, the temperature of the mixed stream is determined as a weighted average of the inlet stream temperatures:

$$T_{\text{mix}} = \frac{\sum_{j=1}^n (c_{p,j} \dot{m}_j T_j)}{\sum_{j=1}^n c_{p,j} \dot{m}_j}, \quad (6.3)$$

where  $c_{p,j}$  is the specific heat at stream  $j$ . The mass flows of stream  $j$  is given by  $\dot{m}_j$  and  $T_j$  is the temperature of stream  $j$ .

## 6.3 Integration of mixing in the heat pump model

This study analyzes a simple vapor compression heat pump governed by fundamental thermodynamic principles, with the energy balance equations and COP calculations detailed in Section 2.3.1. The methodology used to analyze mixing at the condenser side follows an identical approach to that described in the aforementioned section, with the heat transfer and system performance evaluated based on the resulting mixed inlet temperature.

For mixing on the evaporator side, the same thermodynamic framework applies; however, adjustments are required to account for the shift in energy balance constraints. Specifically, when mixing occurs at the evaporator inlet, the resultant mixed temperature influences the heat absorption process, thereby affecting the condenser outlet temperature ( $T_{c,o}$ ). This effect is incorporated by modifying the energy balance equation, where the heat extracted by the evaporator, as expressed in Equation (2.10), is used in conjunction with Equation 2.13 to determine the corresponding temperature shift at the condenser outlet.

**Mixing at the inlet** For inlet mixing, the weighted average temperature is calculated prior to entering the heat pump using Equation (6.3). This influences the heat transfer rate ( $\dot{Q}_{\text{out}}$  or  $\dot{Q}_{\text{in}}$ ), depending on whether mixing occurs at the evaporator or condenser. Once the heat transfer rate is known, the COP of the heat pump is calculated using Equation (2.4).

In the case of non-mixing at the inlet, the streams are processed independently, each passing through its own heat pump. Instead of using the mixed temperature, the calculations for heat transfer rate and work input are performed separately for each stream. The total heat delivered in the non-mixing case is expressed as:

$$\dot{Q}_{\text{heat},j} = \sum_{j=1}^n \dot{m}_{c,j} c_{p,j} (T_{c,o} - T_{c,i,j}), \quad (6.4)$$

where  $\dot{m}_{c,j}$  the mass flow of the sink side is per stream  $j$ ,  $T_{c,o}$  the required outlet temperature of the heat pump and  $T_{c,i}$  the weighted average temperature at the inlet of the heat pump.

The total work input is defined as:

$$\dot{W}_{\text{in}} = \sum_{j=1}^n \dot{W}_{\text{in},j}, \quad (6.5)$$

where  $\dot{W}_{\text{in},j}$  represents the work input of stream  $j$ .

**Mixing at the outlet** Outlet mixing occurs when streams with different temperatures combine after exiting their respective heat pumps. The mixed outlet temperature is determined using Equation (6.3). Unlike inlet mixing, it does not impact the internal heat pump performance, as mixing occurs after heat exchange. The total heat output and work input remain unchanged, and COP is calculated similarly to the non-mixing case of inlet mixing.

Non-mixing refers to a configuration where each stream maintains its distinct outlet temperature, with no interaction between separate heat pump units. In this scenario, the total heat delivered and total work input are obtained by summing the individual stream contributions, and no additional temperature averaging occurs.

## 6.4 Results and discussion

The following section shows the effects of mixing and non-mixing configurations on the performance of a simple vapor compression heat pump system. The analysis encompasses both the condenser and evaporator sides, assessing the influence of inlet and outlet temperature variations on the system's COP. Initially, the impact of inlet mixing is evaluated for both sides, focusing on the thermodynamic consequences of combining inlet streams at different temperatures. Subsequently, the implications of outlet mixing are investigated, analyzing the effect of merging streams after they have undergone heat exchange within the heat pump. Finally, a comprehensive exergy analysis is performed for all four scenarios to quantify thermodynamic efficiency and system irreversibilities.

### 6.4.1 Inlet temperature mixing cases

**Condenser side** To assess the impact of inlet mixing on heat pump performance, two scenarios are considered: one with separate processing of two streams (35 °C and 55 °C, each 1.11 kg/s) and one where these streams are mixed into a single stream at 45 °C. The thermodynamic consequences of these configurations are analyzed below.

Analysis of inlet mixing and non-mixing two streams of 35 °C and 55 °C with both a mass flow of 1.11 kg/s

The table below summarizes the results of the performance comparison for mixing and non-mixing inlet streams at the inlet of the condenser side:

$T_{c,i}$ (°C)	$\dot{m}_c$ (kg/s)	$\dot{Q}_{\text{heat}}$ (kW)	$\dot{W}_{\text{in}}$ (kW)	$T_{e,o}$ (°C)	COP
35	1.11	116.1	28.3	23.4	4.1
55	1.11	23.2	4.5	32.5	5.2
45 ( $T_{\text{mix}}$ )	2.22	139.4	30.4	27.8	4.6
35 & 55 (Non-mix.)	2.22	139.4	32.8	23.4 & 32.5	4.3

The COP for each configuration was calculated using Equation (2.4).

**Mixing streams** For the mixed case, the two inlet streams (35 °C and 55 °C) are combined into a single stream with a weighted average temperature of 45 °C calculated by Equation (6.3). The COP for the mixed configuration is calculated as:

$$COP_{\text{mix}} = \frac{139.4}{30.4} = 4.6. \quad (6.6)$$

**Non-mixed streams** For the non-mixed case, the streams are processed separately by two heat pumps. Each stream maintains its original temperature before entering its respective heat pump.

The COP for the stream at 35 °C can be determined by:

$$COP_{35} = \frac{116.1}{28.3} = 4.1, \quad (6.7)$$

and for the stream at 55°C:

$$COP_{55} = \frac{23.2}{4.5} = 5.2. \quad (6.8)$$

The total COP for the non-mixed case, considering both streams, is:

$$COP_{\text{non-mix}} = \frac{116.1 + 23.2}{28.3 + 4.5} = 4.3. \quad (6.9)$$

The mixed configuration demonstrates a COP of 4.6, compared to 4.3 for the non-mixed case. These results highlight the advantage of mixing inlet streams in terms of energy efficiency compared to the non-mixing case.

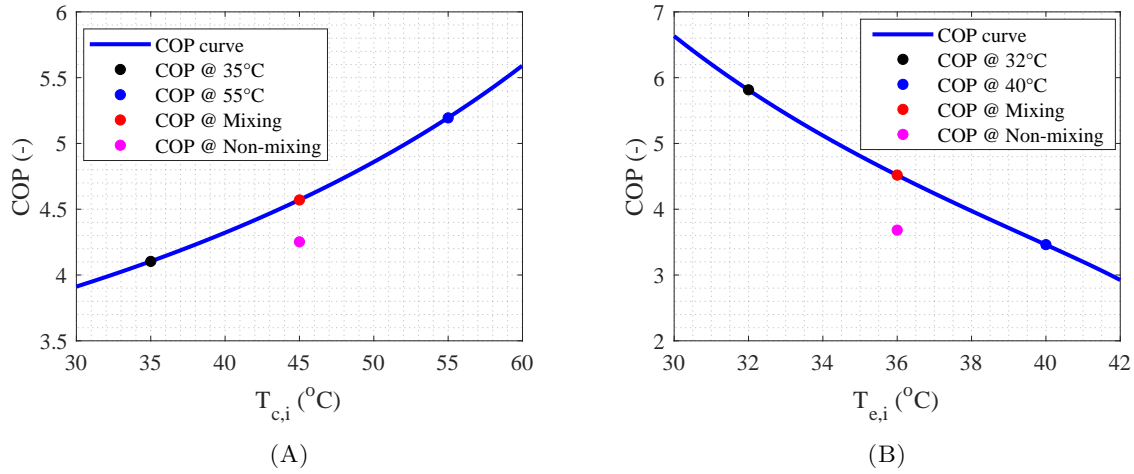


FIGURE 6.1: COP curve as a function of inlet temperatures and under mixing and non-mixing configurations. (A) Evaluates inlet streams on the condenser side, where two streams at 35 °C and 55 °C, each with a mass flow of 1.11 kg/s, are heated in the condenser. The process fluid enters the evaporator at 35 °C, while the refrigerant condenses at a fixed temperature of 65 °C. The corresponding refrigerant evaporating temperatures are 18.4 °C for the 35 °C stream, 27.5 °C for the 55 °C stream, and 22.8 °C for the mixed case (45 °C inlet). (B) Examines inlet streams on the evaporator side, where two streams at 32 °C and 40 °C, each with a mass flow of 1.81 kg/s, are cooled in the evaporator. The refrigerant evaporates at a constant temperature of 25 °C, while the process fluid enters the condenser at 50 °C. The corresponding refrigerant condensing temperatures are 58.9 °C for the 32 °C stream, 77.9 °C for the 40 °C stream, and 67.5 °C for the mixed case (36 °C inlet).

The results in Figure 6.1(A) show that the mixed configuration achieves a higher COP than the non-mixed case. This outcome is primarily due to the distribution of work input across the two streams.

In the non-mixed configuration, the streams at 35 °C and 55 °C are processed separately by individual heat pumps. While the 55 °C stream requires relatively little work input to reach the target outlet temperature of 60 °C, the 35 °C stream demands significantly more energy to achieve the same temperature increase. The additional work required to heat the low-temperature stream outweighs the savings gained from the high-temperature stream, leading to a higher total work input and a lower overall COP.

Conversely, in the mixed configuration, the two streams are combined before entering the heat pump, resulting in a single stream at 45 °C. This approach eliminates the extreme energy demand of the 35 °C stream, allowing for a more balanced distribution of work input. Since the heat pump now operates with a more moderate temperature difference, the total work input is lower, improving efficiency and increasing the COP.

**Evaporator side** The analysis of inlet mixing at the evaporator side follows the same approach as the condenser-side case, evaluating two streams with inlet temperatures of 32 °C and 40 °C, each with a mass flow rate of 1.81 kg/s, under both mixed and non-mixed configurations. As shown in Figure 6.1(B), the mixed configuration achieves a higher COP than the non-mixed case, primarily due to the redistribution of cooling demand across the streams.

The observed decrease in COP with increasing evaporator inlet temperature, as shown in Figure 6.1(B), is attributed to the fixed evaporating temperature of 25 °C, which is constrained by the required outlet temperature of 30 °C and a heat exchanger temperature difference of 5 °C. As the evaporator inlet temperature rises, the condenser outlet temperature increases accordingly, leading to a higher condensing temperature. This results in an increased pressure ratio, as the evaporating pressure remains constant while the condensing pressure rises. Consequently, the compressor requires more work input, reducing the overall COP.

In the non-mixed configuration, the streams at 32 °C and 40 °C are processed separately by individual heat pumps. While the 32 °C stream requires relatively little cooling to reach the target evaporator outlet temperature of 30 °C, the 40 °C stream requires significantly more heat extraction to achieve the same outlet temperature. The greater cooling demand of the higher-temperature stream leads to increased compressor work, which outweighs the efficiency gained from the low-temperature stream. Consequently, the total work input of the non-mixing case is higher, resulting in a lower overall COP.

In contrast, in the mixed configuration, the two streams are combined before entering the heat pump, forming a single stream at 36 °C. This eliminates the extreme cooling demand of the 40 °C stream while slightly increasing the cooling requirement of the 32 °C stream. As a result, the system experiences a more balanced cooling load, reducing the overall compressor work. This leads to improved efficiency and an increased COP of 4.5 compared to the non-mixed configuration, which achieves a COP of 3.7 due to the higher work input required for separate stream processing.

### 6.4.2 Outlet temperature mixing cases

**Condenser side** To analyze the impact of mixing at the outlet streams on the condenser side, two cases are compared: one involving outlet streams at 55 °C and 65 °C, each with a mass flow rate of 1.11 kg/s. These are compared with a non-mixing configuration where both streams independently reach 60 °C. These cases are discussed below:

Analysis of outlet mixing and non-mixing two streams of 55 °C and 65 °C with both a mass flow of 1.11 kg/s

The table below summarizes the results of the performance comparison for mixing and non-mixing streams at the outlet of the condenser side:

$T_{c,o}$ (°C)	$\dot{m}_c$ (kg/s)	$\dot{Q}_{\text{heat}}$ (kW)	$\dot{W}_{\text{in}}$ (kW)	$T_{e,o}$ (°C)	COP
55	1.11	23.2	3.8	32.4	6.1
65	1.11	69.7	17.3	28.1	4.0
60 & 60 (Non-mix.)	2.22	92.9	19.1	30.1 & 30.1	4.9
60 ( $T_{\text{mix}}$ )	2.22	92.9	21.1	32.4 & 28.1	4.4

The COP for each configuration was calculated using Equation (2.4).

**Mixing streams** For the mixed case, the two streams (55 °C and 65 °C) are combined at the outlets of the heat pumps into a single stream with a weighted average temperature of 60 °C calculated by Equation (6.3). The COP for the mixed configuration is calculated in the following ways:

For the stream at 55 °C:

$$COP_{55} = \frac{23.2}{3.8} = 6.1 \quad (6.10)$$

For the stream at 65°C:

$$COP_{65} = \frac{69.7}{17.3} = 4.0 \quad (6.11)$$

The total COP for the non-mixed case, considering both streams, is:

$$COP_{\text{mix}} = \frac{23.2 + 69.7}{3.8 + 17.3} = 4.4 \quad (6.12)$$

**Non-mixed streams** In this case, the streams are processed separately by two heat pumps. Each stream maintains its original temperature before entering its respective heat pump.

$$COP_{\text{non-mix}} = \frac{92.9}{19.1} = 4.9 \quad (6.13)$$

The mixed configuration demonstrates a COP of 4.4, compared to 4.9 for the non-mixed case. These results indicate that mixing outlet streams leads to a reduction in energy efficiency compared to the non-mixing case.

The results shown in Figure 6.2(A) indicate that the non-mixed configuration achieves a higher COP than the mixed case, which contrasts with the trends observed for inlet mixing.

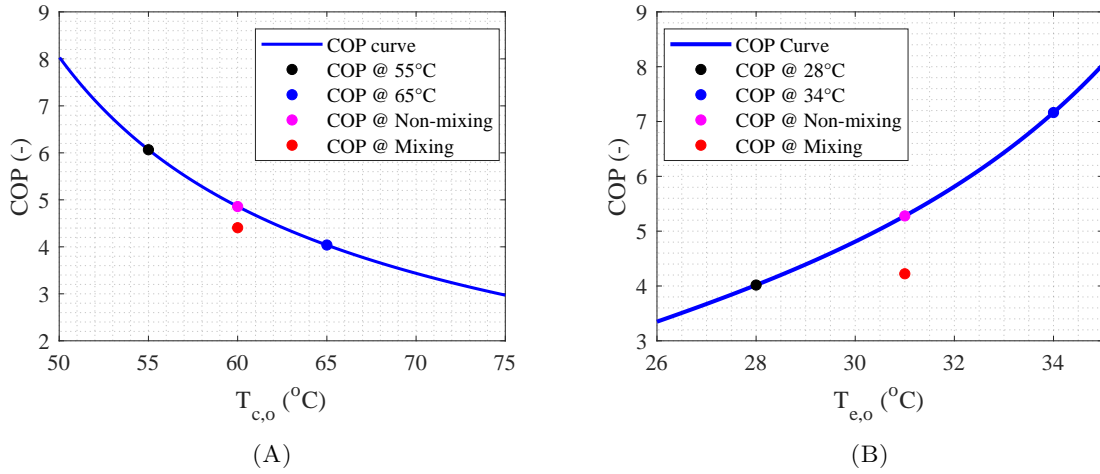


FIGURE 6.2: COP curves as functions of outlet temperatures for mixing and non-mixing configurations: (A) Evaluates condenser outlet temperatures for streams at 55 °C and 65 °C (mixing) and 60 °C (non-mixing). The process fluid enters the evaporator at 35 °C, and enters the condenser at a temperature of 50 °C. The corresponding refrigerant evaporating temperatures are 27.4 °C for the 55 °C stream, 23.1 °C for the 65 °C stream, and 25.1 °C for the non-mixed 60 °C streams. (B) Examines evaporator outlet temperatures for streams at 28 °C and 34 °C (mixing) and 31 °C (non-mixing). The process fluid enters the evaporator at a temperature of 35 °C, and enters the condenser at 50 °C. The corresponding refrigerant condensing temperatures are 70.1 °C for the 28 °C stream, 56.9 °C for the 34 °C stream, and 63.0 °C for the non-mixed 31 °C case.

This outcome can be explained by the distribution of heating demand between the streams.

The decrease in the COP curve with increasing condenser outlet temperature, as shown in Figure 6.1(A), is due to the higher heat demand at the condenser while the inlet temperatures remain fixed. As the outlet temperature increases, more heat must be supplied, which requires additional heat extraction from the evaporator. To maintain this balance, the evaporating temperature decreases, while the condensing temperature rises, leading to a higher pressure ratio across the compressor. This increased pressure ratio results in greater compressor work input, ultimately reducing the COP as the condenser outlet temperature rises.

In the mixed configuration, the two streams are processed separately, each reaching its designated outlet temperature before being combined. The stream exiting at 65 °C exhibits a significantly higher heat demand compared to the 55 °C stream, as it requires greater thermal input to reach its outlet temperature from the fixed condenser inlet temperature of 50 °C. While the 55 °C stream undergoes a relatively minor temperature increase, the energy savings associated with its lower heat demand are insufficient to offset the substantially greater energy input required for the 65 °C stream. Consequently, the total compressor work remains high, leading to a reduction in overall COP for the mixed case compared to the non-mixed case.

Conversely, in the non-mixed configuration, both streams are heated to a uniform outlet temperature of 60 °C, which results in a more balanced heat demand distribution. By avoiding the excessive energy requirement associated with separately heating the higher-temperature stream, the total work input is reduced, yielding a higher COP compared to the mixed case.

**Evaporator side** A similar analysis is conducted for outlet mixing at the evaporator side, where two streams exit the evaporator at 28 °C and 34 °C. These streams mix at the evaporator outlet, forming a single stream at 31 °C. The results indicate that the non-mixed configuration achieves a higher COP than the mixed case, consistent with the trends observed for condenser-side outlet mixing. This is shown in Figure 6.2(B).

The observed increase in the COP curve with a higher evaporator outlet temperature results from a reduced cooling load at the evaporator. With constant inlet temperatures, less heat extraction leads to a lower heat rejection at the condenser, decreasing the condensing temperature and pressure. Simultaneously, the higher evaporator outlet temperature raises the evaporating pressure. Combined with a lower condensing temperature and pressure, this results in a reduced pressure ratio across the compressor. This lowers the work input, improving efficiency and increasing COP.

In the mixing configuration, the 28 °C and 34 °C streams combine into a single 31 °C stream at the evaporator outlet. The 28 °C stream requires greater heat extraction, as more energy must be removed from the stream cooling from 35 °C to 28 °C compared to the stream cooling from 35 °C to 34 °C, resulting in higher compressor work. Meanwhile, the 34 °C stream, which requires less cooling, does not offset this increased energy demand. The increased work input from the low-temperature stream outweighs the benefit of the higher-temperature stream, resulting in a lower overall COP compared to the non-mixed configuration.

Conversely, in the non-mixed configuration, both streams are cooled directly to 31 °C, ensuring a uniform thermal load distribution across the system. By avoiding the additional cooling demand imposed by the lower-temperature stream in the mixing case, the compressor work input remains more balanced. This results in a more efficient heat extraction process, reducing the overall energy requirement and yielding a higher COP compared to the mixing configuration.

### 6.4.3 Inlet mixing extended analysis: Mass flow variation on condenser and evaporator side

The results from the initial temperature mixing cases discussed in Sections 6.4.1 and 6.4.2 demonstrated that inlet mixing improved COP, whereas outlet mixing led to efficiency losses. However, these cases were analysed under the assumption of constant mass flow rates. In reality, industrial systems such as in the case of Teijin experience fluctuating mass flows, which can significantly impact system performance.

While previous analyses considered various temperature conditions, this extended investigation focuses exclusively on the inlet mixing case at the condenser side with 35 °C and 55 °C streams, referred to as the reference scenario. In this case, the system operates with a constant mass flow rate of 1.11 kg/s on the condenser side and 1.81 kg/s on the evaporator side. Under these conditions, the COP of the 35 °C stream is 4.1, the 55 °C stream is 5.2, the mixing case is 4.6, and the non-mixing case is 4.3. In the mixing case, the two inlet streams at 35 °C and 55 °C are combined into a single stream at 45 °C, due to their equal mass flow rates, and processed by a single heat pump. In contrast, in the non-mixing case, each stream is processed separately, with the total system COP calculated by summing the heating capacities and dividing them by the total work input.

TABLE 6.3: Reference case.

$T_{c,i}$ (°C)	$\dot{m}_c$ (kg/s)	$\dot{m}_e$ (kg/s)	$\dot{Q}_{\text{heat}}$ (kW)	$\dot{W}_{\text{in}}$ (kW)	$T_{e,o}$ (°C)	COP
35	1.11	1.81	116.1	28.3	23.4	<b>4.1</b>
55	1.11	1.81	23.2	4.5	32.5	<b>5.2</b>
45 ( $T_{\text{mix}}$ )	2.22	3.62	139.4	30.4	27.8	<b>4.6</b>
35 & 55 (Non-mix.)	2.22	3.62	139.4	32.8	23.4 & 32.5	<b>4.3</b>

This reference scenario is selected because it aligns with the operating conditions at Teijin and serves as the baseline for all mass flow variation cases in this study. Other cases from the initial analysis, which involved different temperature configurations, are not considered in this extended study..

To expand upon this case, the analysis now incorporates mass flow variations to evaluate their effect on system performance. Specifically, the study examines:

- Variations in mass flow at the evaporator side, while keeping the condenser-side mass flow constant.
- Variations in mass flow at the condenser side, while keeping the evaporator-side mass flow constant.

The considered mass flow variations are summarized in Table 6.4, which categorizes the scenarios based on whether the change takes place on the evaporator or condenser side and whether the mass flow is increased or decreased. This structured approach allows for a systematic evaluation of thermodynamic effects under varying flow conditions.

TABLE 6.4: Classification of mass flow variation scenarios based on increases and decreases in the 35 °C and 55 °C streams for the evaporator and condenser sides.

	Evaporator	Condenser
<b>Increasing</b>	<ul style="list-style-type: none"> <li>The mass flow of the 55 °C stream was increased to <b>2.50 kg/s</b>, while the 35 °C stream remained at 1.81 kg/s.</li> </ul>	<ul style="list-style-type: none"> <li>The mass flow of the 55 °C stream was increased to <b>1.39 kg/s</b>, while the 35 °C stream remained at 1.11 kg/s.</li> </ul>
	<ul style="list-style-type: none"> <li>The mass flow of the 35 °C stream was increased to <b>2.50 kg/s</b>, while the 55 °C stream remained at 1.81 kg/s.</li> </ul>	<ul style="list-style-type: none"> <li>The mass flow of the 35 °C stream was increased to <b>1.39 kg/s</b>, while the 55 °C stream remained at 1.11 kg/s.</li> </ul>
<b>Decreasing</b>	<ul style="list-style-type: none"> <li>The mass flow of the 55 °C stream was reduced to <b>1.11 kg/s</b>, while the 35 °C stream remained at 1.81 kg/s.</li> </ul>	<ul style="list-style-type: none"> <li>The mass flow of the 55 °C stream was reduced to <b>0.83 kg/s</b>, while the 35 °C stream remained at 1.11 kg/s.</li> </ul>
	<ul style="list-style-type: none"> <li>The mass flow of the 35 °C stream was reduced to <b>1.11 kg/s</b>, while the 55 °C stream remained at 1.81 kg/s.</li> </ul>	<ul style="list-style-type: none"> <li>The mass flow of the 35 °C stream was reduced to <b>0.83 kg/s</b>, while the 55 °C stream remained at 1.11 kg/s.</li> </ul>

**Variation in evaporator mass flow ( $\dot{m}_e$ )** To assess the impact of mass flow variations on system performance, the following analysis examines both reductions and increases in evaporator side mass flow. Since the total heat transfer remains constant, the evaporator outlet temperature adjusts accordingly to maintain energy balance. Since the condenser side mass flows remained equal, the mixed inlet temperature was calculated to be 45 °C in all cases. The results are presented in Figure 6.3 for mass flow reductions and Figure 6.4 for mass flow increases. Corresponding performance parameters are detailed in Tables 6.5, 6.6, 6.7 and 6.8.

- **Decrease of mass flow at evaporator side**

As presented in Table 6.5, when the mass flow of the 55 °C stream is reduced, the COP of the 35 °C stream remains unchanged at 4.1, while the COP of the 55 °C stream decreases from 5.2 to 5.0. The COP of the mixing case declines from 4.6 to 4.4, and the non-mixing case decreases from 4.3 to 4.2. Although reducing the mass flow negatively affects system performance, the difference between the mixing and non-mixing cases is reduced.

In contrast, when the mass flow of the 35 °C stream is reduced, as shown in Table 6.6, the COP of this stream decreases significantly from 4.1 to 3.6, whereas the COP of the 55 °C stream remains constant at 5.2. The COP of the mixing case remains at 4.4, while the non-mixing case declines further to 3.8. This indicates that a reduction in the 35 °C stream has a more pronounced negative effect on system performance compared to a reduction in the 55 °C stream.

The 35 °C stream has a greater influence on overall system efficiency, as previously analyzed in Section 6.4.1 on inlet mixing effects at the evaporator side. Since the energy losses associated with the 35 °C stream were already greater than the efficiency gains from the 55 °C stream, further reducing its mass flow intensifies this effect. With

a lower mass flow rate, the same amount of heat must be extracted from a smaller mass, resulting in a lower evaporating temperature. Consequently, the evaporator pressure decreases, while the condenser pressure remains unchanged, leading to an increased compressor pressure ratio and higher work input requirements. Given that the non-mixing case was already less efficient in handling lower-temperature streams, a further reduction in the 35 °C stream's mass flow amplifies this disparity, widening the performance gap between the mixing and non-mixing cases.

Further analysis indicates that if the mass flow of the 55 °C stream is reduced below 0.69 kg/s, the non-mixing case becomes more efficient than the mixing case. This suggests that under conditions of extreme mass flow reduction, the efficiency benefits of mixing are diminished, and non-mixing may become the preferable configuration.

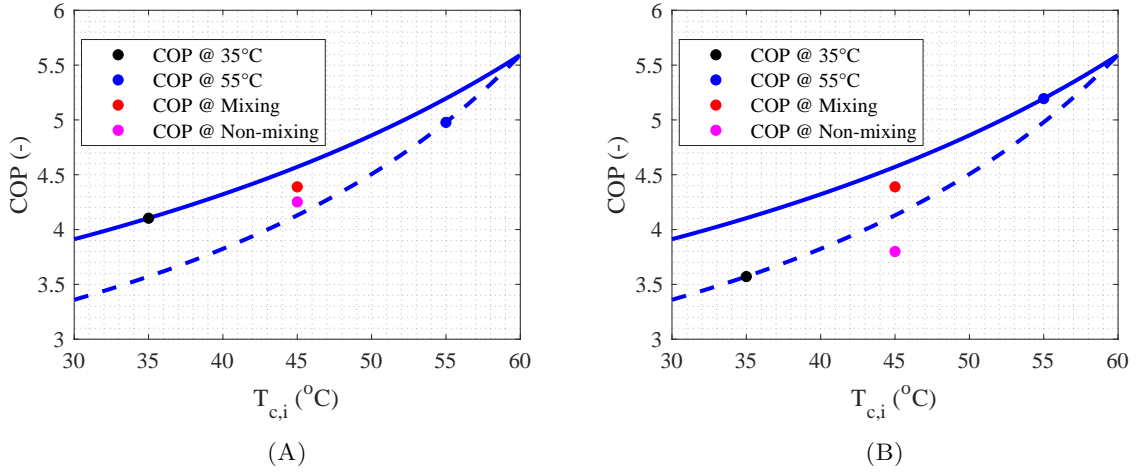


FIGURE 6.3: Effect of evaporator mass flow reduction on COP for mixing and non-mixing configurations: (A) The mass flow rate of the 55 °C stream is reduced from 1.81 to 1.11 kg/s, while the mass flow of the 35 °C stream remains constant at 1.81 kg/s. Under these conditions, the evaporating temperature of the 35 °C stream is 18.4 °C, the evaporating temperature of the 55 °C stream is 26.0 °C, and the evaporating temperature of the mixed stream at 45 °C is 21.2 °C. (B) The mass flow rate of the 35 °C stream is reduced from 1.81 to 1.11 kg/s, while the mass flow of the 55 °C stream remains constant. Under these conditions, the evaporating temperature of the 35 °C stream decreases to 12.0 °C, while the evaporating temperature of the 55 °C stream remains at 27.5 °C. The evaporating temperature of the mixed stream at 45 °C remains 21.2 °C. All cases operates at a condensing temperature of 65 °C.

TABLE 6.5: Performance parameters for varying evaporator side mass flow with a reduction in 55°C stream mass flow from 1.81 to 1.11 kg/s while keeping the 35°C stream mass flow at 1.81 kg/s.

$T_{c,i}$ (°C)	$\dot{m}_c$ (kg/s)	$\dot{m}_e$ (kg/s)	$\dot{Q}_{\text{heat}}$ (kW)	$\dot{W}_{\text{in}}$ (kW)	$T_{e,o}$ (°C)	COP
35	1.11	1.81	116.2	28.3	23.4	4.1
55	1.11	1.11	23.2	4.7	31.0	5.0
45 ( $T_{\text{mix}}$ )	2.22	2.92	139.4	31.8	26.2	4.4
35 & 55 (Non-mix.)	2×1.11	1.81 & 1.11	139.4	33.0	23.4 & 31.0	4.2

TABLE 6.6: Performance parameters for varying evaporator-side mass flow with a reduction in 35 °C stream mass flow from 1.81 to 1.11 kg/s while keeping the 55 °C stream mass flow at 1.81 kg/s.

$T_{c,i}$ (°C)	$\dot{m}_c$ (kg/s)	$\dot{m}_e$ (kg/s)	$\dot{Q}_{\text{heat}}$ (kW)	$\dot{W}_{\text{in}}$ (kW)	$T_{e,o}$ (°C)	COP
35	1.11	1.11	116.2	32.5	17.0	3.6
55	1.11	1.81	23.2	4.5	32.5	5.2
45 ( $T_{\text{mix}}$ )	2.22	2.92	139.4	31.8	26.2	4.4
35 & 55 (Non-mix.)	2×1.11	1.81 & 1.11	139.4	37.0	17.0 & 32.5	3.8

- **Increase of mass flow at evaporator side**

A similar trend is observed when the mass flow is increased. As presented in Table 6.7, when the mass flow of the 35 °C stream is increased, the COP of this stream improves from 4.1 to 4.4, while the 55 °C stream remains constant at 5.2. The mixing case COP increases from 4.6 to 4.7, and the non-mixing case improves from 4.3 to 4.5. Since only the 35 °C stream benefits from the increased mass flow, while the 55 °C stream remains unchanged, the performance gap between the mixing and non-mixing cases narrows.

As shown in Table 6.8, when the mass flow of the 55°C stream is increased, the COP of this stream improves from 5.2 to 5.3, while the 35 °C stream remains constant at 4.1. The mixing case COP remains at 4.7, similar to the previous case, while the non-mixing case remains at 4.3. In this scenario, since only the 55 °C stream benefits, while the 35 °C stream remains unchanged, the performance gap between the mixing and non-mixing cases increases. This contrasts with the case where the mass flow of the 35 °C stream was increased, where the COP improvement was more evenly distributed across the system, leading to a smaller difference in performance between the two configurations.

TABLE 6.7: Performance parameters for varying evaporator side mass flow with an increase in 55 °C stream mass flow from 1.81 to 2.50 kg/s while keeping 35 °C at 1.81 kg/s.

$T_{c,i}$ (°C)	$\dot{m}_c$ (kg/s)	$\dot{m}_e$ (kg/s)	$\dot{Q}_{\text{heat}}$ (kW)	$\dot{W}_{\text{in}}$ (kW)	$T_{e,o}$ (°C)	COP
35	1.11	1.81	116.2	28.3	23.4	4.1
55	1.11	2.50	23.2	4.4	33.2	5.3
45 ( $T_{\text{mix}}$ )	2.22	4.31	139.4	29.6	28.9	4.7
35 & 55 (Non-mix.)	2×1.11	1.81 & 2.50	139.4	32.7	23.4 & 33.2	4.3

TABLE 6.8: Performance parameters for varying evaporator-side mass flow with an increase in 35 °C stream mass flow from 1.81 to 2.50 kg/s while keeping 55 °C at 1.81 kg/s.

$T_{c,i}$ (°C)	$\dot{m}_c$ (kg/s)	$\dot{m}_e$ (kg/s)	$\dot{Q}_{\text{heat}}$ (kW)	$\dot{W}_{\text{in}}$ (kW)	$T_{e,o}$ (°C)	COP
35	1.11	2.50	116.2	26.3	26.4	4.4
55	1.11	1.81	23.2	4.5	32.5	5.2
45 ( $T_{\text{mix}}$ )	2.22	4.31	139.4	29.6	28.9	4.7
35 & 55 (Non-mix.)	2×1.11	2.50 & 1.81	139.4	30.8	26.4 & 32.5	4.5

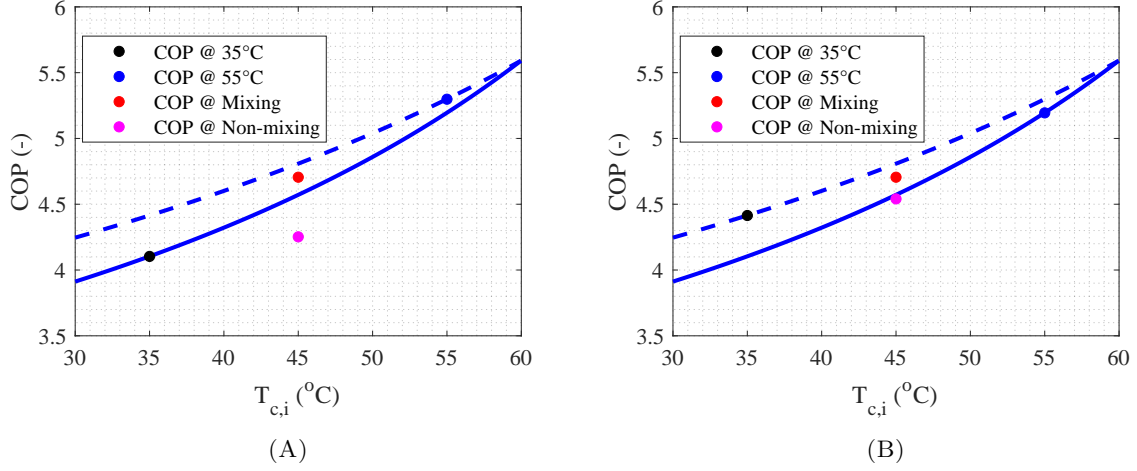


FIGURE 6.4: Effect of evaporator mass flow increase on COP for mixing and non-mixing configurations: (A) The mass flow rate of the 55 °C stream is increased from 1.81 to 2.50 kg/s, while the mass flow of the 35 °C stream remains constant at 1.81 kg/s. Under these conditions, the evaporating temperature of the 35 °C stream is 18.4 °C, the evaporating temperature of the 55 °C stream is 28.2 °C, and the evaporating temperature of the mixed stream at 45 °C is 23.9 °C. (B) The mass flow rate of the 35 °C stream is increased from 1.81 to 2.50 kg/s, while the mass flow of the 55 °C stream remains constant. Under these conditions, the evaporating temperature of the 35 °C stream decreases to 21.4 °C, while the evaporating temperature of the 55 °C stream remains at 27.5 °C. The evaporating temperature of the mixed stream at 45 °C remains 23.9 °C. All cases operates at a condensing temperature of 65 °C.

**Variation in condenser mass flow ( $\dot{m}_c$ )** To evaluate the impact of condenser-side mass flow variations on system performance, this analysis examines both reductions and increases in mass flow. Unlike the evaporator-side analysis, where the mixed inlet temperature remained constant at 45 °C, variations in condenser mass flow alter the weighted average inlet temperature. When the mass flow of the 35 °C stream increases, the mixed inlet temperature decreases below 45 °C, whereas an increase in the 55 °C stream mass flow results in a higher mixed inlet temperature. Since the target outlet temperature is maintained at 60 °C, in accordance with Teijin’s operational conditions, changes in mass flow lead to variations in heat demand. A lower mixed inlet temperature necessitates a greater temperature lift, thereby increasing the compressor work input and reducing system efficiency. Conversely, a higher mixed inlet temperature lowers the required temperature difference, mitigating the workload on the compressor and potentially improving efficiency.

The effects of mass flow increases are illustrated in Figure 6.5, while Figure 6.6 presents the impact of mass flow reductions. The corresponding performance parameters are detailed in Tables 6.9, 6.10, 6.11, and 6.12.

- **Increase of mass flow at condenser side**

As shown in Table 6.9, when the mass flow of the 55 °C stream increases, the COP of the 35 °C stream remains at 4.1, while the COP of the 55 °C stream decreases from 5.2 to 5.1. The average mixed temperature, which was 45 °C in the reference case, increases to 46.1 °C due to the larger contribution of the higher-temperature stream in the weighted average. As a result, the mixing case COP decreases to 4.5, while the

non-mixing case COP remains at 4.3, indicating that the non-mixing configuration is unaffected, whereas the mixing case experiences a slight efficiency reduction.

Similarly, as presented in Table 6.10, when the mass flow of the 35 °C stream increases, the COP of this stream decreases from 4.1 to 3.9, whereas the COP of the 55 °C stream remains unchanged at 5.2. The mixed temperature decreases to 43.8 °C, as the greater mass flow of the lower-temperature stream dominates the weighted average calculation. Consequently, the mixing case COP declines to 4.4, while the non-mixing case COP decreases to 4.0, reflecting a notable reduction in system efficiency compared to the reference case.

The observed decrease in system performance with increased mass flow at the condenser side is primarily due to the higher heat demand at the condenser, as more energy must be transferred to achieve the same outlet temperature with a larger mass flow. Consequently, a greater amount of heat must be extracted at the evaporator side, which lowers the evaporating temperature while the condensing temperature remains constant. This increases the compressor pressure ratio, requiring more work input, leading to a decline in overall COP.

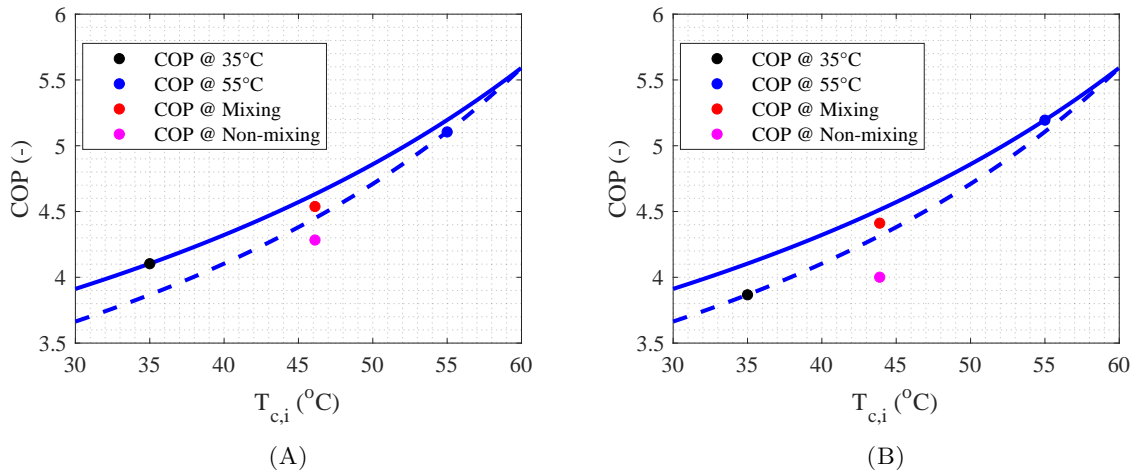


FIGURE 6.5: Effect of condenser mass flow increase on COP for mixing and non-mixing configurations: (A) The mass flow rate of the 55 °C stream is increased from 1.11 to 1.39 kg/s, while the mass flow of the 35 °C stream remains constant at 1.11 kg/s. Under these conditions, the evaporating temperature of the 35 °C stream is 18.4 °C, the evaporating temperature of the 55 °C stream is 26.9 °C, and the evaporating temperature of the mixed stream at 46.1 °C is 22.5 °C. (B) The mass flow rate of the 35 °C stream is increased from 1.11 to 1.39 kg/s, while the mass flow of the 55 °C stream remains constant at 1.11 kg/s. Under these conditions, the evaporating temperature of the 35 °C stream is 15.7 °C, while the evaporating temperature of the 55 °C stream is 27.5 °C. The evaporating temperature of the mixed stream at 43.8 °C is 21.3 °C. All cases operates at a condensing temperature of 65 °C.

TABLE 6.9: Performance parameters for varying condenser-side mass flow with an increase in 55 °C stream mass flow from 1.11 to 1.39 kg/s while keeping the 35 °C stream mass flow at 1.11 kg/s.

$T_{c,i}$ (°C)	$\dot{m}_c$ (kg/s)	$\dot{m}_e$ (kg/s)	$\dot{Q}_{\text{heat}}$ (kW)	$\dot{W}_{\text{in}}$ (kW)	$T_{e,o}$ (°C)	COP
35	1.11	1.81	116.2	28.3	23.4	4.1
55	1.39	1.81	29.0	5.7	31.9	5.1
46.1 ( $T_{\text{mix}}$ )	2.50	3.62	145.2	32.0	27.5	4.5
35 & 55 (Non-mix.)	1.11 & 1.39	2×1.81	145.2	34.0	23.4 & 31.9	4.3

TABLE 6.10: Performance parameters for varying condenser-side mass flow with an increase in 35 °C stream mass flow from 1.11 to 1.39 kg/s while keeping the 55 °C stream mass flow at 1.11 kg/s.

$T_{c,i}$ (°C)	$\dot{m}_c$ (kg/s)	$\dot{m}_e$ (kg/s)	$\dot{Q}_{\text{heat}}$ (kW)	$\dot{W}_{\text{in}}$ (kW)	$T_{e,o}$ (°C)	COP
35	1.39	1.81	145.2	37.5	20.7	3.9
55	1.11	1.81	23.2	4.5	32.5	5.2
43.8 ( $T_{\text{mix}}$ )	2.50	3.62	168.4	38.2	26.3	4.4
35 & 55 (Non-mix.)	1.11 & 1.39	2×1.81	168.4	42.0	20.7 & 32.5	4.0

- **Decrease of mass flow at condenser side**

As presented in Table 6.11, when the mass flow of the 55 °C stream is reduced, the COP of this stream increases from 5.2 to 5.3, while the COP of the 35 °C stream remains unchanged at 4.1. The average mixed temperature decreases to 43.6 °C, as the lower mass flow of the 55 °C stream reduces its influence on the weighted average temperature. This results in a mixing case COP of 4.6 and a non-mixing case COP of 4.2, showing a minor performance improvement compared to the reference case.

Conversely, as shown in Table 6.12, when the mass flow of the 35 °C stream is reduced, the COP of this stream increases from 4.1 to 4.4, while the COP of the 55 °C stream remains unchanged at 5.2. The mixed temperature increases to 46.4 °C, as the 55 °C stream has a greater impact on the weighted average due to its relatively higher mass flow. This leads to a mixing case COP of 4.8 and a non-mixing case COP of 4.5, demonstrating a significant efficiency improvement compared to the reference case.

A comparison of these two mass flow reduction cases reveals that reducing the mass flow of the 35 °C stream leads to greater COP improvements than reducing the mass flow of the 55 °C stream. This occurs because the 35 °C stream has a stronger impact on system performance, and even a small reduction in its mass flow leads to substantial efficiency gains. The lower heat load associated with the 35 °C stream reduces the required temperature lift, thereby decreasing compressor work input and improving overall system efficiency.

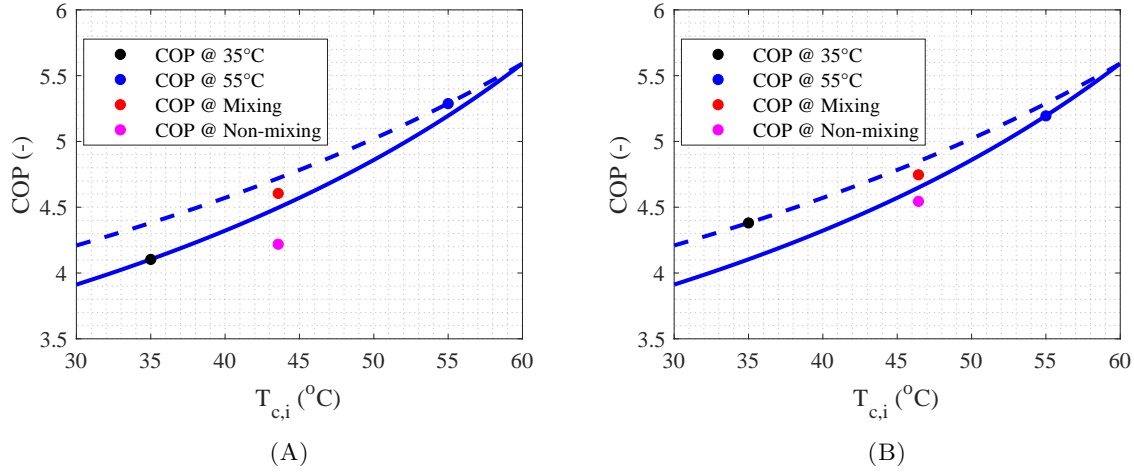


FIGURE 6.6: Effect of condenser mass flow decrease on COP for mixing and non-mixing configurations: (A) The mass flow rate of the 55  $^{\circ}$ C stream is decreased from 1.11 to 0.83 kg/s, while the mass flow of the 35  $^{\circ}$ C stream remains constant at 1.11 kg/s. Under these conditions, the evaporating temperature of the 35  $^{\circ}$ C stream is 18.4  $^{\circ}$ C, the evaporating temperature of the 55  $^{\circ}$ C stream is 28.1  $^{\circ}$ C, and the evaporating temperature of the mixed stream at 43.6  $^{\circ}$ C is 22.8  $^{\circ}$ C. (B) The mass flow rate of the 35  $^{\circ}$ C stream is decreased from 1.11 to 0.83 kg/s, while the mass flow of the 55  $^{\circ}$ C stream remains constant at 1.11 kg/s. Under these conditions, the evaporating temperature of the 35  $^{\circ}$ C stream is 21.1  $^{\circ}$ C, while the evaporating temperature of the 55  $^{\circ}$ C stream is 27.5  $^{\circ}$ C. The evaporating temperature of the mixed stream at 46.4  $^{\circ}$ C is 24.2  $^{\circ}$ C. All cases operates at a condensing temperature of 65  $^{\circ}$ C.

TABLE 6.11: Performance parameters for varying condenser-side mass flow with a reduction in 55  $^{\circ}$ C stream mass flow from 1.11 to 0.83 kg/s while keeping the 35  $^{\circ}$ C stream mass flow at 1.11 kg/s.

$T_{c,i}$ ( $^{\circ}$ C)	$\dot{m}_c$ (kg/s)	$\dot{m}_e$ (kg/s)	$\dot{Q}_{\text{heat}}$ (kW)	$\dot{W}_{\text{in}}$ (kW)	$T_{e,o}$ ( $^{\circ}$ C)	COP
35	1.11	1.81	116.2	28.3	23.4	4.1
55	0.83	1.81	17.4	3.3	33.1	5.3
43.6 ( $T_{\text{mix}}$ )	1.94	3.62	133.6	29.0	27.8	4.6
35 & 55 (Non-mix.)	1.11 & 0.94	2 $\times$ 1.81	133.6	31.6	23.4 & 33.1	4.2

TABLE 6.12: Performance parameters for varying condenser-side mass flow with a reduction in 35  $^{\circ}$ C stream mass flow from 1.11 to 0.83 kg/s while keeping the 55  $^{\circ}$ C stream mass flow at 1.11 kg/s.

$T_{c,i}$ ( $^{\circ}$ C)	$\dot{m}_c$ (kg/s)	$\dot{m}_e$ (kg/s)	$\dot{Q}_{\text{heat}}$ (kW)	$\dot{W}_{\text{in}}$ (kW)	$T_{e,o}$ ( $^{\circ}$ C)	COP
35	0.83	1.81	87.1	19.9	26.1	4.4
55	1.11	1.81	23.2	4.5	32.5	5.2
46.4 ( $T_{\text{mix}}$ )	1.94	3.62	110.4	23.3	29.2	4.8
35 & 55 (Non-mix.)	0.94 & 1.11	2 $\times$ 1.81	110.4	24.4	26.1 & 32.5	4.5

#### 6.4.4 Inlet mixing condenser side extended: Mixing of cascade with simple vapor heat pump

The previous analysis of inlet mixing at the condenser side (Section 6.4.1) compared a mixed configuration, where 35 °C and 55 °C streams were pre-mixed before heating from 45 °C to 60 °C, with a non-mixing case, where each stream was heated separately to 60 °C. Mixing was found to improve COP, as direct heating from 35 °C to 60 °C required significantly higher compressor work, reducing non-mixing efficiency.

To further examine the impact of temperature lift distribution, an alternative heating strategy was introduced. In this approach, the 35 °C stream was heated in incremental steps of 5 °C using a cascade heat pump system, rather than undergoing a single large temperature increase. This stepwise heating strategy was then combined with the original 55 °C to 60 °C heating process, with the objective of determining whether mixing would still provide a COP advantage under this configuration.

As illustrated in Figure 6.7, the mixing process results in an effective inlet temperature of 45 °C, thereby bypassing the first two heating stages in the cascade system. Consequently, in the mixed configuration, the stream is heated directly from 45 °C to 60 °C in 5 °C increments, rather than following the full cascade sequence. The stepwise heating approach is outlined in Table 6.13, which provides an overview of the temperature steps in each configuration. This adjusted approach allows for a more detailed assessment of whether stepwise heating mitigates the performance gap between mixing and non-mixing cases and provides further insight into the thermodynamic efficiency of temperature lift distribution.

TABLE 6.13: Overview of temperature steps in each configuration

Configuration	Temperature Steps
Cascade (35 → 60 °C)	35 → 40 → 45 → 50 → 55 → 60
Single-Stage (55 → 60 °C)	55 → 60
Mixed (45 → 60 °C)	45 → 50 → 55 → 60

The comparison between mixing and non-mixing configurations within the cascade heating approach reveals a notable shift in performance trends. Unlike the initial findings, where mixing improved COP, the cascade configuration demonstrates that the non-mixing case achieves a higher COP than the mixed case. The results, presented in Table 6.14, show that this change is due to the enhanced efficiency of the cascade approach, which optimizes COP by distributing the temperature lift across multiple stages, thereby reducing compressor work at each step and diminishing the relative advantage of mixing.

The stepwise heating process within the cascade system is detailed in Table 6.15, illustrating how incremental temperature increases improve system efficiency. Similarly, Table 6.16 presents the performance breakdown of the mixed case (45 → 60 °C), highlighting how the system behaves when the two streams are pre-mixed before heating.

While the cascade approach provides theoretical validation, it is not considered in the broader

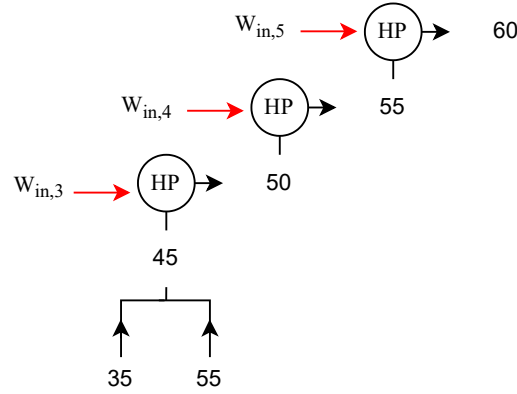


FIGURE 6.7: Mixing of an inlet stream of 35 °C cascade heat pump stream with a 55 °C stream leading to a 45 °C inlet in a cascade configuration

industrial evaluation due to practical constraints. The primary objective of this study is to analyze the integration of heat pumps in dynamically fluctuating industrial processes, ensuring a balance between efficiency, feasibility, and scalability. Although the cascade configuration enhances performance in specific scenarios, it introduces additional complexity in terms of equipment requirements, operational control, and heat exchanger design. Furthermore, this study focuses on comparing mixing and non-mixing configurations within conventional heat pump setups, rather than incorporating additional heat pump stages.

TABLE 6.14: Performance parameters comparing mixing and non-mixing configurations. In the mixing case, a 35 °C stream (heated in 5 °C steps to 60 °C) is mixed with a 55 °C stream to form a 45 °C inlet, while in the non-mixing case, both streams are heated separately to 60 °C.

$T_{c,i}(\text{°C})$	$\dot{Q}_{\text{heat}}(\text{kW})$	$\dot{W}_{\text{in}}(\text{kW})$	COP
35	116.2	19.5	6.0
55	23.2	4.5	5.2
45 ( $T_{\text{mix}}$ )	139.4	25.0	5.6
35 & 55 (Non-mix.)	139.4	24.0	5.8

TABLE 6.15: Performance parameters for cascade heat pump steps.

$T_{c,i}(\text{°C})$	$\dot{m}_c(\text{kg/s})$	$\dot{m}_e(\text{kg/s})$	$\dot{Q}_{\text{heat}}(\text{kW})$	$\dot{W}_{\text{in}}(\text{kW})$	$T_{c,o}(\text{°C})$	COP
35-40	1.11	1.81	23.2	2.04	32.19	11.4
40-45	1.11	1.81	23.2	2.95	29.5	7.9
45-50	1.11	1.81	23.2	3.88	26.9	6.0
50-55	1.11	1.81	23.2	4.83	24.5	4.8
35-60	1.11	1.81	23.2	5.82	22.2	4.0
<b>35-60</b>	<b>1.11</b>	<b>1.81</b>	<b>116.2</b>	<b>19.5</b>	<b>22.2</b>	<b>6.0</b>

TABLE 6.16: Performance of heat pump steps of mixen configuration.

$T_{c,i}$ (°C)	$\dot{m}_c$ (kg/s)	$\dot{m}_e$ (kg/s)	$\dot{Q}_{\text{heat}}$ (kW)	$\dot{W}_{\text{in}}$ (kW)	$T_{e,o}$ (°C)	COP
45-50	2.22	3.62	46.5	6.4	32.4	7.2
50-55	2.22	3.62	46.5	8.3	29.8	5.6
55-60	2.22	3.62	46.5	10.3	27.4	4.5
<b>45-60</b>	<b>2.22</b>	<b>3.62</b>	<b>139.4</b>	<b>25</b>	<b>27.4</b>	<b>5.6</b>

## 6.5 Exergy analysis of mixing strategies

This section extends the analysis presented in Sections 6.4.1 and 6.4.2, which examined mixing and non-mixing configurations under constant mass flow conditions at the condenser and evaporator sides. The objective is to further evaluate the impact of mixing strategies on exergy destruction and exergy efficiency, providing a more comprehensive understanding of their thermodynamic implications.

The analysis follows the theoretical framework established in Section 2.4, where the exergy balance equations and efficiency calculations were introduced. Exergy destruction is quantified across the compressor, condenser, evaporator, and expansion valve using Equation (2.26), while the overall exergy efficiency is determined using Equation (2.31) to assess system performance. The results offer insights into how different mixing strategies influence irreversibilities within the heat pump cycle and whether mixing enhances efficiency or contributes to additional exergy losses.

The input parameters for the analyzed cases are based on those presented in Tables 6.1 and 6.2, which provide the mass flow rates and temperatures for each configuration. In addition to the parameters listed in these tables, this section introduces two additional variables: The pressure of the process fluid at the condenser side is 3 bar. The pressure of the process fluid at the evaporator side is 5.4 bar.

### 6.5.1 Exergy analysis: Inlet side

The impact of inlet mixing on exergy destruction and exergy efficiency is evaluated by comparing mixing and non-mixing configurations at both the condenser and evaporator inlets. Figure 6.8 presents the exergy destruction for each configuration, broken down into the compressor, condenser, evaporator, and expansion valve, while cases (A) and (B) of Table 6.1 provide the corresponding operational conditions. The results demonstrate that mixing inlet streams reduces exergy destruction and improves exergy efficiency, while non-mixing configurations experience greater irreversibilities due to the way heat is processed separately in each stream.

At the condenser inlet, two separate streams at 35 °C and 55 °C (both with a mass flow rate of 1.11 kg/s) are compared against a mixed stream at 45 °C. The non-mixing case exhibits a total exergy destruction of approximately 24.1 kW and an exergy efficiency of 30%, making it the least efficient scenario. This is primarily due to the high exergy destruction in the compressor and condenser, as the 35 °C stream requires significantly more work input to reach the target outlet temperature of 60 °C. Conversely, mixing the inlet streams into a single 45 °C stream reduces total exergy destruction to approximately 21.0 kW, resulting in

a higher exergy efficiency of 33%. The compressor losses are notably lower in this case, as the more balanced thermal conditions reduce the thermal burden on compression, improving the overall performance of the heat pump. However, mixing itself introduces an additional exergy loss, quantified as 1.3 kW at the condenser inlet. Although this mixing loss adds to overall irreversibilities, the total system performance still benefits from inlet mixing due to the reduction in exergy destruction compared to the non-mixing case.

At the evaporator inlet, a similar trend is observed. Two separate streams at 32 °C and 40 °C (each with a mass flow rate of 1.81 kg/s) are compared against a mixed stream at 36 °C. The non-mixing evaporator inlet case results in higher exergy destruction (23.5 kW) and an exergy efficiency of 33%, while the mixing case achieves the lowest exergy destruction (17.1 kW) and the highest exergy efficiency of 36%. The largest reduction in exergy destruction is observed in the compressor, highlighting that mixing significantly reduces the work required for compression and improves overall system performance. The exergy loss due to mixing at the evaporator inlet is 0.4 kW, which is notably lower than at the condenser inlet. This lower value is due to the smaller temperature difference between the two streams (32 °C and 40 °C), leading to less entropy generation during the mixing process. As a result, although mixing introduces some exergy loss, its impact remains minor compared to the overall efficiency improvements achieved through reduced irreversibilities in the system.

These findings confirm that inlet mixing enhances exergy efficiency by minimizing entropy generation, reducing unnecessary heat processing complexities, and lowering exergy destruction through the reduction of temperature differences and irreversibilities.

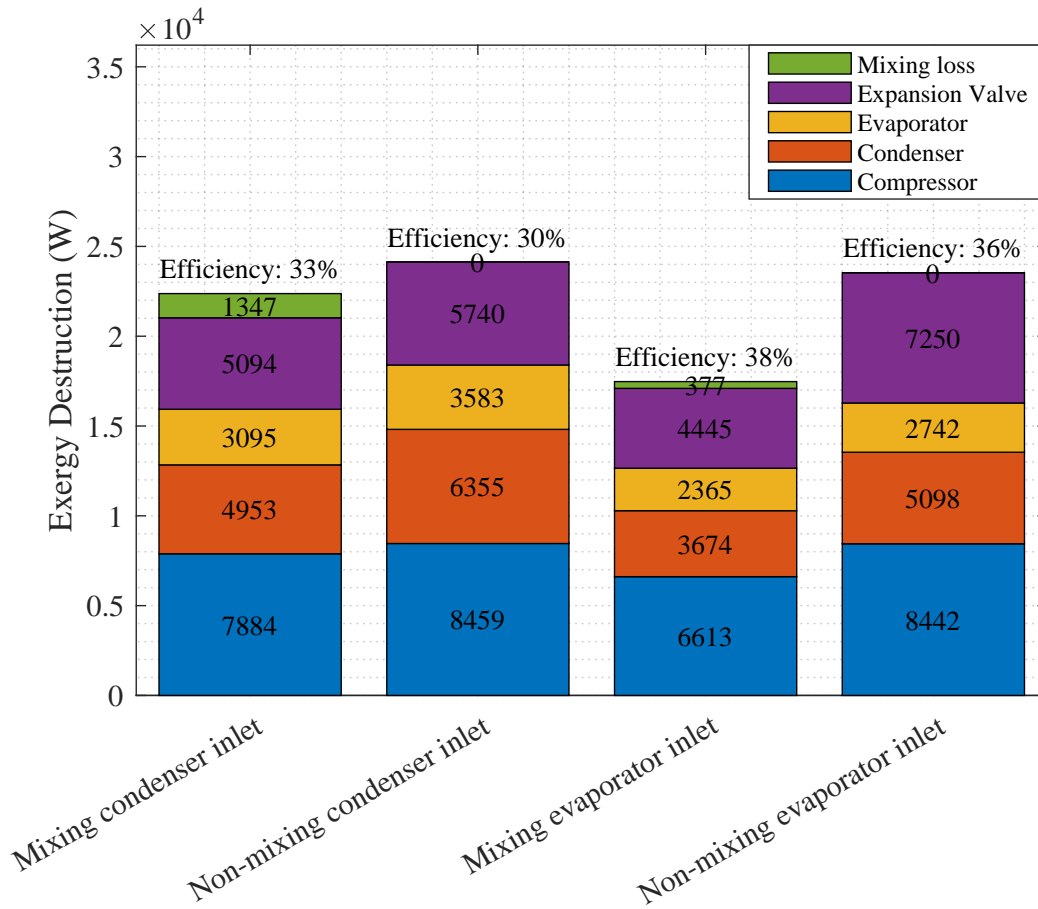


FIGURE 6.8: Exergy destruction for mixing and non-mixing strategies at the condenser side and evaporator side inlets. Exergy destruction is categorized by component (compressor, condenser, evaporator, and expansion valve), and the overall exergy efficiency for each configuration is indicated above the bars. At the condenser inlet, the non-mixing case consists of two separate streams at 35 °C and 55 °C, each with a mass flow rate of 1.11 kg/s, while the mixing case combines these into a single 45 °C stream with a total mass flow of 2.22 kg/s. At the evaporator inlet, the non-mixing case includes two separate streams at 32 °C and 40 °C, each with a mass flow rate of 1.81 kg/s, whereas the mixing case results in a single 36 °C stream with a total mass flow of 3.62 kg/s.

### 6.5.2 Exergy analysis: Outlet side

The impact of outlet mixing on exergy destruction and exergy efficiency is evaluated by comparing mixing and non-mixing configurations at both the condenser and evaporator outlets. Figure 6.9 presents the exergy destruction for each configuration, broken down into the compressor, condenser, evaporator, and expansion valve, while cases (C) and (D) of Table 6.1 provide the corresponding operational conditions. The results demonstrate that outlet mixing leads to higher exergy destruction and lower efficiency compared to the non-mixing case.

At the condenser outlet, the mixing configuration combines two outlet streams at 55 °C and 65 °C (both with a mass flow rate of 1.11 kg/s) into a single mixed stream at 60 °C.

In contrast, the non-mixing case consists of two separate streams, each at 60 °C. The non-mixing configuration results in total exergy destruction of approximately 12.5 kW, leading to an exergy efficiency of 41%. However, in the mixing case, exergy destruction increases to 14.0 kW, reducing efficiency to 39%. The additional exergy loss due to mixing at the condenser outlet is 0.3 kW, arising from the temperature difference between the 55 °C and 65 °C streams. Since this difference is relatively small, the entropy generation remains limited, but still contributes to an overall increase in irreversibilities.

In the non-mixing configuration, both streams are heated from 50 °C to 60 °C, allowing for a balanced heat transfer process with lower exergy losses. In contrast, the mixing case involves heating one stream to 55 °C and the other to 65 °C, requiring a significantly higher temperature lift for the latter. The increased exergy destruction associated with heating the 65 °C stream surpasses the savings gained from the 55 °C stream, leading to a higher overall exergy destruction compared to the non-mixing case.

A similar effect is observed at the evaporator outlet, where the mixing case combines two outlet streams at 28 °C and 34 °C (both with a mass flow rate of 1.81 kg/s) into a single mixed stream at 31 °C. In contrast, the non-mixing case maintains two separate outlet streams at 31 °C. In the non-mixing configuration, total exergy destruction is 9.1 kW, leading to an exergy efficiency of 42%. When mixing occurs, exergy destruction increases to 12.5 kW, reducing efficiency to 38%. The exergy loss due to mixing at the evaporator outlet is 0.2 kW, which is lower than at the condenser outlet. This lower value is due to the smaller temperature difference between the mixed streams (28 °C and 34 °C), resulting in less entropy generation compared to the condenser outlet case.

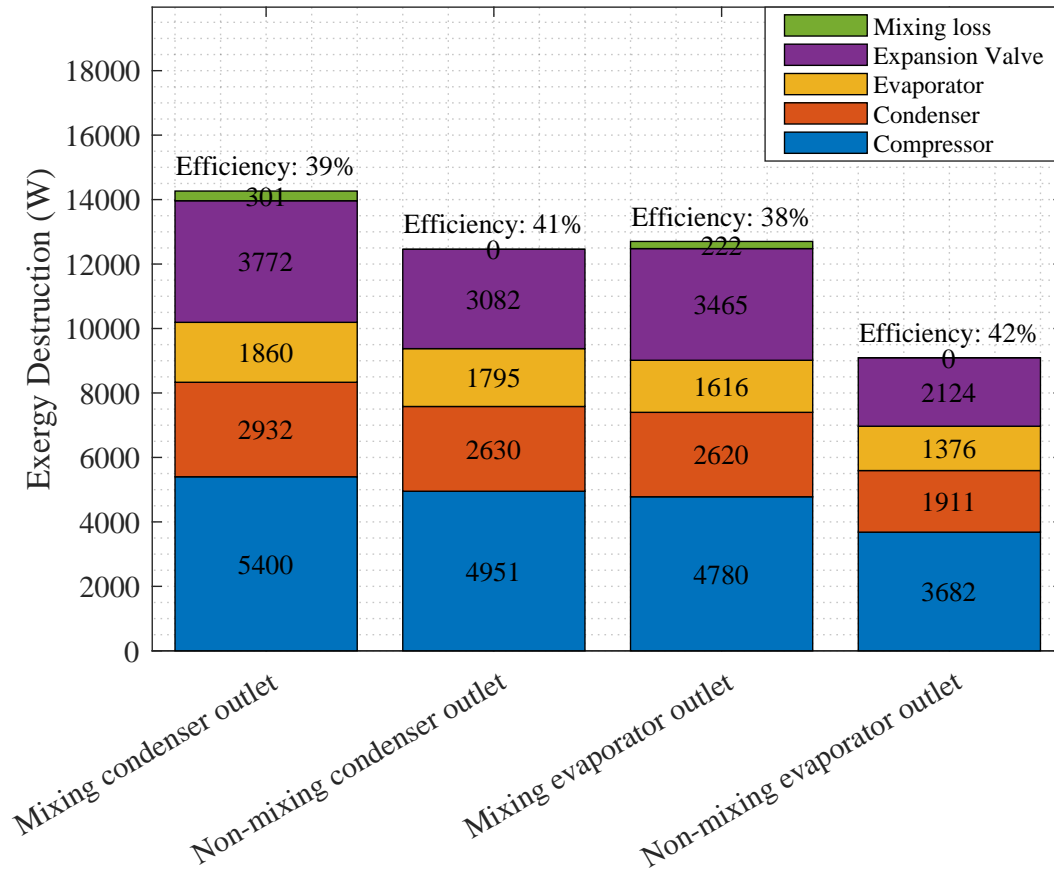


FIGURE 6.9: Exergy destruction for mixing and non-mixing strategies at the condenser side and evaporator side outlets. Exergy destruction is categorized by component (compressor, condenser, evaporator, and expansion valve), with the overall exergy efficiency for each configuration indicated above the bars. At the condenser outlet, the non-mixing case consists of two separate streams, each at 60 °C, while the mixing case combines outlet streams at 55 °C and 65 °C into a single 60 °C stream, with both configurations having a mass flow rate of 1.11 kg/s per stream. At the evaporator outlet, the non-mixing case consists of two separate streams, each at 31 °C, while the mixing case combines outlet streams at 28 °C and 34 °C into a single 31 °C stream, with both configurations having a mass flow rate of 1.81 kg/s per stream.

## 6.6 Conclusion: Influence of mixing strategies on heat pump performance

This chapter has investigated the thermodynamic impact of mixing and non-mixing configurations on heat pump performance, focusing on COP, exergy destruction, and exergy efficiency at both the inlet and outlet of the condenser and evaporator. The results demonstrate that inlet mixing generally improves system efficiency, whereas outlet mixing increases exergy destruction, reducing overall performance. However, an exception to this trend was observed when mixing was applied in a cascade heat pump configuration, where non-mixing resulted in higher efficiency.

The results show that inlet mixing leads to a higher COP and lower exergy destruction due to a more balanced thermal distribution before entering the heat pump. In the non-mixing inlet configuration, the heat pump responsible for the largest temperature lift requires significantly more work input than the one handling a smaller temperature increase. The additional work required for the high-lift heat pump outweighs the efficiency gains from the low-lift heat pump, leading to a lower overall COP. In contrast, mixing the two inlet streams before processing results in a single intermediate-temperature stream, which reduces the overall temperature lift required for compression, lowers exergy destruction, and improves heat pump efficiency. This effect is consistently observed at both the condenser and evaporator inlets.

In contrast, mixing at the outlet leads to higher exergy destruction and a lower COP. When outlet streams mix, the heat pump responsible for the stream requiring the largest temperature increase experiences significantly higher exergy losses, as the greater temperature lift demands more work input. Although the other heat pump, which requires a smaller temperature lift, operates more efficiently, the overall system efficiency declines because the additional losses in the high-lift heat pump outweigh the efficiency benefits of the low-lift heat pump. Conversely, in the non-mixing outlet configuration, both heat pumps directly heat their respective streams to the final outlet temperature, leading to a more balanced heat transfer process, lower irreversibilities, and higher exergy efficiency.

The inlet mixing analysis was extended to investigate mass flow variations, confirming that inlet mixing consistently results in a higher COP compared to non-mixing, even under fluctuating flow conditions. These findings suggest that the efficiency gains of inlet mixing are not limited to specific operating conditions but hold across different flow scenarios.

While inlet mixing improves efficiency in a conventional heat pump setup, the results from the cascade heat pump configuration show the opposite effect. In the non-mixing cascade case, the lower-temperature stream is gradually heated in multiple smaller temperature increments, rather than experiencing a single large temperature lift. This stepwise heating strategy optimizes the distribution of work input across multiple stages, reducing the overall compressor workload and improving efficiency. In contrast, mixing the inlet streams in a cascade system skips some intermediate heating steps, reducing the effectiveness of the staged approach. As a result, the non-mixing case achieves a higher COP than the mixing case in the cascade setup, in contrast to the findings for conventional heat pumps.

## Chapter 7

# Conclusion

*This chapter presents the key findings of this study regarding the feasibility of integrating heat pumps into Teijin Aramid's industrial thermal process. The results demonstrate the potential of heat pump technology to enhance energy efficiency, reduce operational costs, and lower environmental impact. By analyzing various heat pump configurations, evaluating refrigerant selection, and assessing scalability under fluctuating production conditions, this study provides insights into the optimal strategies for sustainable heat recovery. The findings align with broader industrial decarbonization efforts and emphasize the role of heat pumps in achieving energy efficiency targets while maintaining operational feasibility.*

## 7.1 Concluding reflections on research objectives

The chapter is structured according to the sub-research questions, addressing critical process parameters, optimal heat pump configurations, refrigerant selection, scalability considerations, and economic feasibility. Each section highlights the main conclusions drawn from the analysis, supported by quantitative results and comparative evaluations. Each section highlights the main conclusions drawn from the analysis, supported by quantitative results and comparative evaluations. These findings contribute to answering the central research question: *How can heat pump cycles be integrated into industrial fluid heating and cooling processes, characterized by dynamic fluctuations in temperature and mass flow rates, to optimize energy efficiency, operational feasibility, and environmental sustainability in the textile industry?*

### 7.1.1 Critical process parameters and system performance

Temperature variations play a critical role in the integration and operation of a heat pump system. In process 1, the condensate temperature ( $T_{p1}$ ) exhibits fluctuations due to variations in upstream evaporation conditions, leading to non-uniform thermal profiles across process lines. However, since all lines receive condensate from the same storage tank, these variations are in all lines. The current cooling approach could be optimized by implementing pre-cooling strategies earlier in the process. This would reduce the thermal load on the glycol chiller system, thereby decreasing overall energy consumption and improving operational efficiency.

In process 2, the temperature of preheated water ( $T_{p2}$ ) varies significantly between production lines, ranging from 33 °C to 55 °C. These variations in inlet temperature directly influence steam consumption, resulting in inconsistencies in energy usage and inefficiencies in thermal energy management. A heat pump solution should account for these variations to ensure stable and efficient heating, potentially by adjusting system operation based on real-time temperature data.

In addition to temperature variations, mass flow rate fluctuations ( $F_{p1}$  and  $F_{p2}$ ) present further challenges in the design of an optimal heat pump system. In process 1, fluctuations in condensate mass flow occur due to varying product-specific requirements, influencing downstream cooling demand. Similarly, in process 2, the mass flow of preheated water ( $F_{p2}$ ) varies dynamically across production lines, leading to inconsistent heating demand.

By accounting for these factors, the heat pump system can be optimized to enhance energy efficiency, operational reliability, and sustainability within the production process.

### 7.1.2 Optimal heat pump configurations for managing dynamic conditions

This study evaluated four heat pump configurations to determine the most effective solution for managing dynamic temperature ranges and fluctuating mass flow rates in a manufacturing line. The results indicate that centralized (Concept 2) and cascade (Concept 4) heat pump systems provide the best balance between energy efficiency, operational feasibility, and cost-effectiveness.

The centralized system (Concept 2) achieved the lowest operational costs, reducing redundancy by aggregating heat demand across all process lines. This configuration exhibited a COP of 4.32, which is higher than the independent heat pump setup (Concept 1, COP = 3.99) and the clustered configuration (Concept 3, COP = 4.16). However, its reliance on a single heat pump introduces system-wide dependence, requiring backup steam usage in case of failure.

The cascade heat pump system (Concept 4) demonstrated thermodynamic advantages by dividing the temperature lift into two stages, reducing compressor work and improving efficiency. The baseline COP of 4.31 increased with a lower intermediate heat exchanger temperature difference ( $T_{\text{IHX}}$ ), reaching 4.48 at  $T_{\text{IHX}} = 2$  °C. While this system enhances heat recovery and exergy efficiency, its higher capital costs and added system complexity outweigh the marginal performance gains compared to the centralized system. Given this trade-off, the centralized configuration (Concept 2) emerges as the most suitable solution for Teijin, offering the best balance between cost, performance, and implementation feasibility.

### 7.1.3 Impact of refrigerant selection on system efficiency and sustainability

The selection of refrigerants plays a crucial role in optimizing heat pump efficiency, environmental impact, and operational feasibility. For the simple vapor heat pump, R1234ze(Z) and R1233zd(E) emerged as the most promising alternatives to R134a, demonstrating high COP and low GWP while maintaining favorable thermodynamic properties. While natural refrigerants such as R600 and R717 offer excellent environmental performance, their flammability (R600) and toxicity (R717) pose safety challenges that must be carefully managed in industrial applications.

For the cascade heat pump, refrigerant pairing significantly influenced system performance. The R1233zd(E)/R1233zd(E) combination achieved the highest COP (5.09), highlighting its efficiency in staged compression cycles. Meanwhile, R600/R717 exhibited the lowest condensing temperature ( $T_3$ ).

### 7.1.4 Scalability of heat pump systems under fluctuating production conditions

The scalability of industrial heat pump systems was evaluated by analyzing different integration concepts, ranging from independent heat pumps for each production line to centralized configurations that consolidate multiple lines. In the concepts where production lines are combined, inlet mixing occurs, merging multiple mass flows and temperatures before entering the heat pump. This mixing directly influences the thermodynamic performance of the system, affecting the coefficient of performance (COP), exergy destruction, and overall efficiency.

The findings indicate that inlet mixing enhances COP and reduces exergy destruction, resulting in a more efficient heat pump system. This improvement is attributed to the creation of a more balanced inlet temperature, which reduces the required temperature lift and, consequently, the compressor work. In contrast, outlet mixing leads to higher exergy destruction

and lower COP, as it introduces additional irreversibilities in the system. Given that industrial processes, such as those at Teijin, involve dynamically fluctuating mass flows and temperatures, and that inlet mixing has been shown to improve efficiency in these configurations, a centralized heat pump system emerges as the preferable solution. This approach leverages the efficiency gains of inlet mixing, resulting in lower operational costs through a higher COP, reduced exergy destruction, and improved exergy efficiency.

### 7.1.5 Economic feasibility

The integration of heat pumps significantly reduces electricity expenses compared to traditional steam heating, which incurs an annual cost of €343.000. Both the centralized and cascade configurations achieved a 50% reduction in operational costs, demonstrating comparable efficiency gains. The clustered system reduced costs by 48%, while the independent heat pump system yielded the lowest cost savings at 46%. Despite these savings, financial feasibility remains a key constraint due to the required five-year payback period, which limits the total allowable investment for the heat pump system, including CAPEX, installation, maintenance, and infrastructure costs. Concept 2 provides annual savings of €170.400, leading to a total five-year savings of €852.000. Concept 4, with a reduced  $T_{\text{IHX}}$  of 2 °C, slightly increases annual savings to €179.800, resulting in a total five-year savings of €899.000.

However, industrial-scale heat pump systems require substantial capital investment. Based on industry discussions, similar large-scale heat pump projects have demonstrated that real-world costs often exceed initial estimates. Given that the required system capacity at Teijin Aramid is approximately 700 kW, a proportionally scaled investment would likely surpass the available budget, making financial feasibility a significant challenge within the current payback constraints. To improve feasibility, alternative financing mechanisms, external subsidies, or an extended payback period may be necessary to accommodate the high capital investment. While heat pump integration presents a viable strategy for improving energy efficiency and reducing operational costs, achieving financial feasibility remains a challenge unless additional financial support is secured.

## Chapter 8

# Recommendations

*Building on the findings of this study, this chapter provides recommendations for both practical implementation at Teijin Aramid and future research directions. The integration of heat pump technology has demonstrated significant potential for improving energy efficiency, reducing operational costs, and supporting sustainability goals. However, successful implementation requires careful consideration of system optimization, control strategies, and scalability under dynamic production conditions. Additionally, further research is necessary to refine modeling approaches, improve real-time adaptability, and explore alternative refrigerants that align with evolving environmental regulations. This chapter is divided into two sections. The first section provides practical recommendations for Teijin Aramid, whereas the second section outlines key areas for further research. These recommendations are based on the findings of this study and aim to support both immediate implementation and future advancements in heat pump integration.*

## 8.1 Recommendations for Teijin Aramid

Based on the findings of this study, several recommendations are proposed to enhance the efficiency, sustainability, and economic feasibility of heat pump integration at Teijin. These recommendations focus on optimizing energy recovery, improving process stability, and ensuring long-term financial viability.

- **Selection of an appropriate heat pump configuration:** For Teijin’s industrial processes, selecting the right heat pump system is crucial to achieving both operational efficiency and energy savings. Given the dynamic temperature fluctuations, a centralized or cascade heat pump system should be considered to optimize heat recovery and maintain process stability. The centralized system minimizes fluctuations by aggregating thermal loads, improving overall process stability and energy distribution. Meanwhile, the cascade system optimizes performance by distributing the temperature lift across two stages, thereby reducing compressor work and improving COP at higher temperature levels. To maximize energy savings and ensure long-term feasibility, a thorough techno-economic analysis should be conducted to evaluate the practical implementation of these configurations, taking into account factors such as investment costs, energy savings, and system integration feasibility.
- **Optimization of heat exchangers:** As discussed in Section 3.1.3, the heat exchangers currently produce different outlet temperatures across the different process lines, resulting in varying heating demands for the heating process. Some lines require a significantly larger temperature increase than others, leading to higher overall energy consumption. By optimizing the performance of these heat exchangers and ensuring more uniform outlet temperatures, the total amount of heat that needs to be supplied to the heating process can be reduced. This would decrease the thermal load on the heat pump, potentially lowering energy costs and improving overall system efficiency. Standardizing these temperatures could be achieved through targeted upgrades to underperforming heat exchangers, enabling a more balanced and efficient heating process.
- **Refrigerant safety, selection, and environmental compliance:** The refrigerants R1234ze(Z), R1233zd(E), and R717 were identified as the most efficient and sustainable alternatives for integration. However, safety and regulatory requirements should be considered when selecting the final working fluid. A detailed risk assessment and lifecycle analysis should be conducted to ensure compliance with environmental and operational standards.
- **Economic and Operational Feasibility Study:** Although the cost analysis demonstrated that a heat pump system could significantly reduce operational expenses (up to a 52% reduction in electricity costs), a more detailed financial feasibility study should be conducted. This should include long-term maintenance considerations, and an evaluation of available subsidies or financial incentives while considering a longer payback period to improve investment feasibility.

## 8.2 Recommendations for further reseach

Future research should focus on refining technical aspects, exploring new refrigerants, and validating theoretical models with experimental data. The following areas warrant further investigation:

- **Dynamic modeling and transient analysis:** This study was conducted using steady-state modeling, which does not fully capture the impact of fluctuating mass flows and temperature variations. Future research should focus on developing dynamic models to simulate real-time operational changes and assess the performance of heat pump configurations under transient conditions.
- **Refrigerant selection and further research:** Certain newer refrigerants, such as R1336mzz(E) and R1224yd(Z), were not included in this study due to their absence in the CoolProp database. However, these refrigerants exhibit promising thermodynamic properties and environmental advantages. Additionally, the potential of zeotropic refrigerant mixtures should be explored, as they can offer temperature glide benefits and improved efficiency in specific applications. To conduct a more comprehensive evaluation, future studies should consider using REFPROP, which includes a wider range of refrigerants and provides more precise thermophysical data. This would ensure that the most efficient and sustainable refrigerants are considered for future heat pump applications.
- **Experimental validation:** To verify the theoretical findings, an experimental setup or pilot-scale implementation of the heat pump system should be developed. This will help validate the predicted COP values, exergy efficiency, and operational feasibility of the proposed configurations.
- **Advanced control strategies for dynamic conditions:** Since the operational conditions of the industrial process are highly dynamic and not easily predictable, future research should focus on developing robust and adaptive control strategies rather than relying on traditional model-based approaches.

## Appendix A

# Verification of the thermodynamic model

*During the preparation of this work, the author used ChatGPT to refine wording and improve clarity in some sections of the text. After using this tool, the author carefully reviewed and edited the content as needed and takes full responsibility for the final version of the work.*

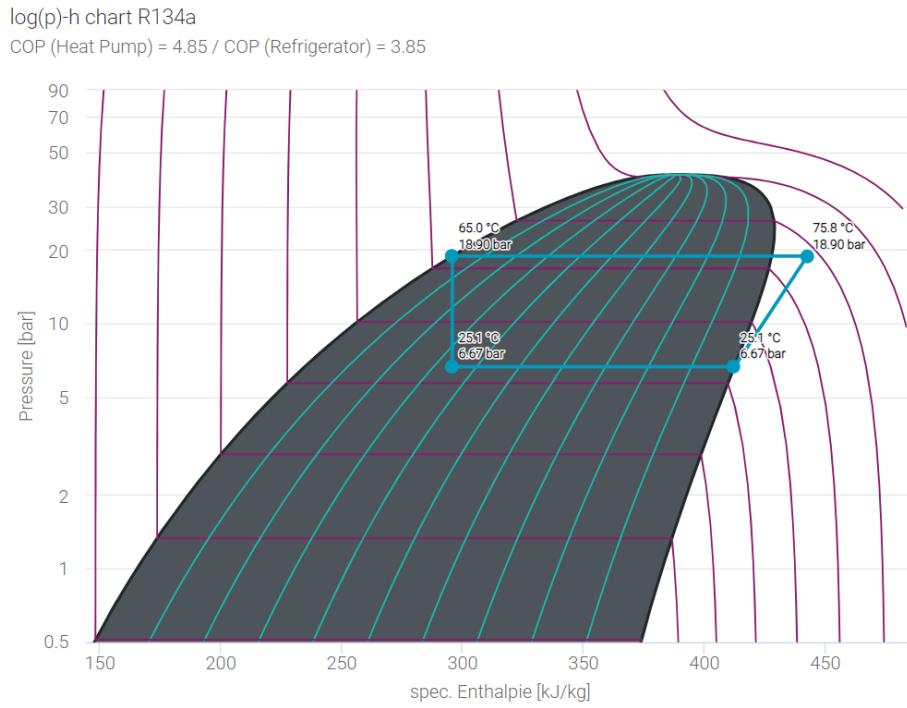


FIGURE A.1: (log)P-h chart R134a (reference)

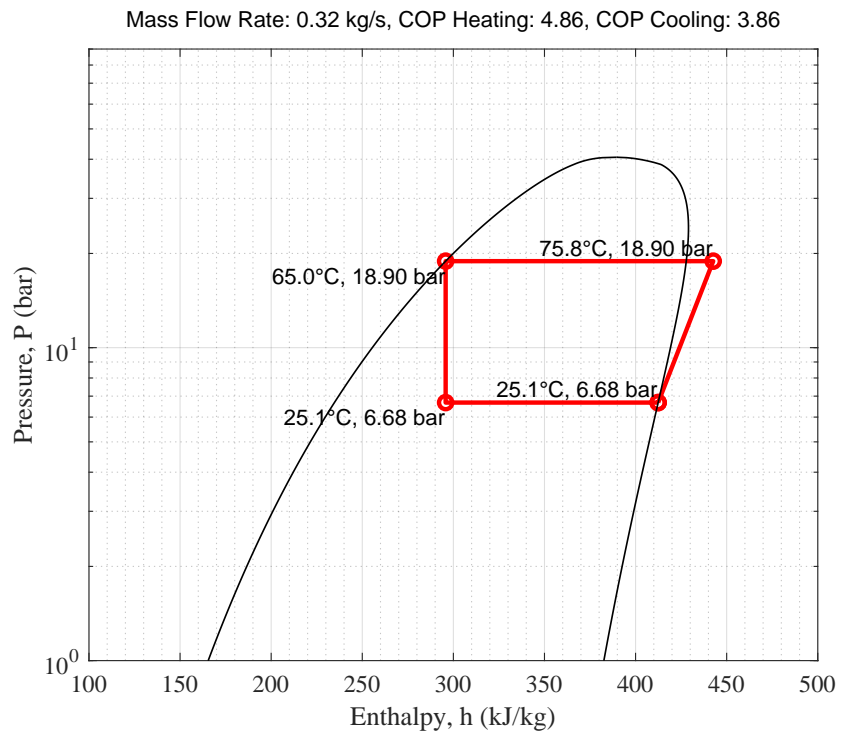


FIGURE A.2: (log)P-h chart R134a (model)

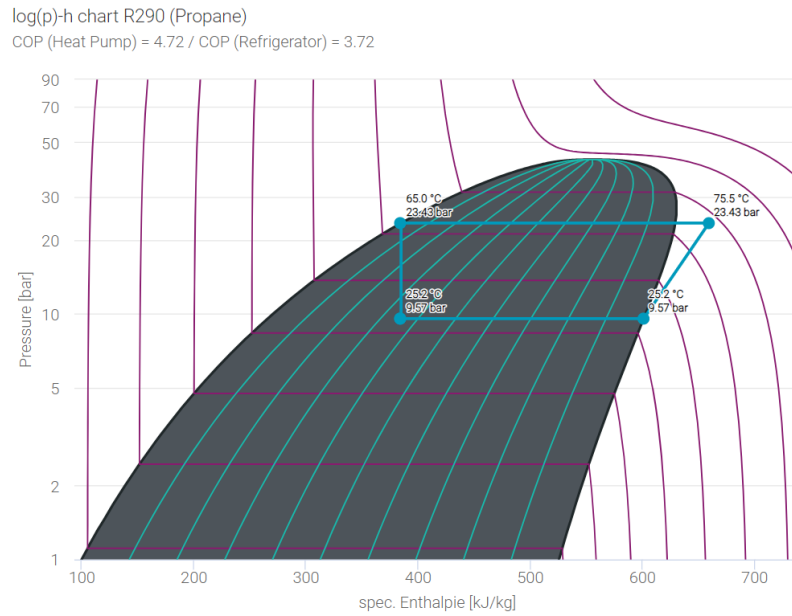


FIGURE A.3: (log)P-h chart R290 (reference)

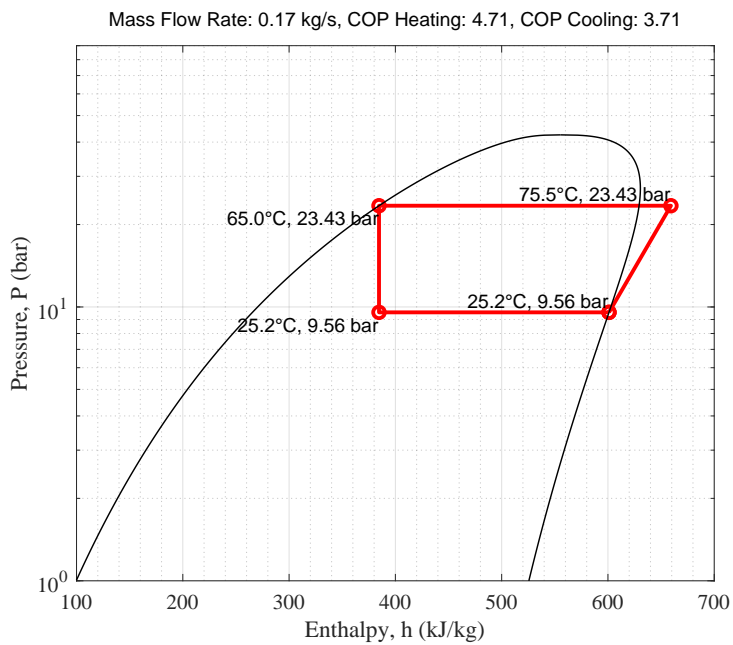


FIGURE A.4: (log)P-h chart R290 (model)

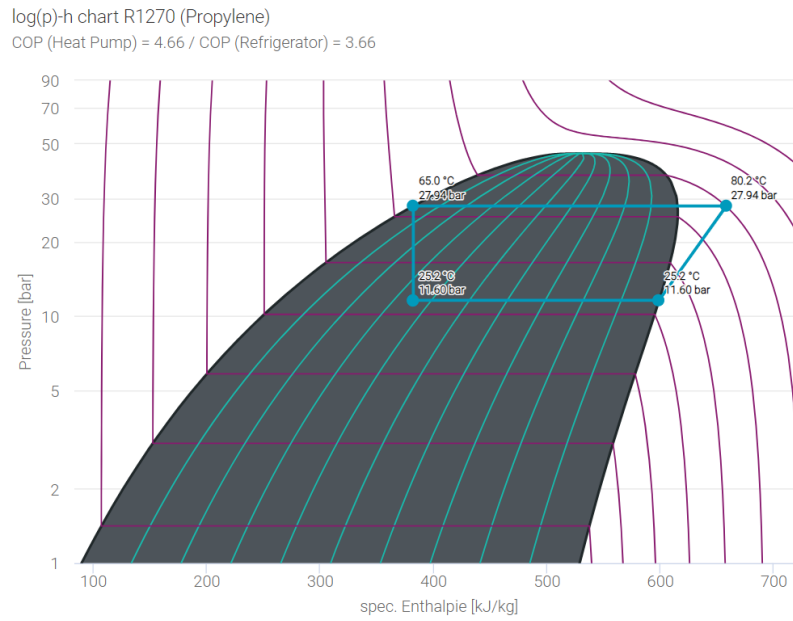


FIGURE A.5: (log)P-h chart R1270 (reference)

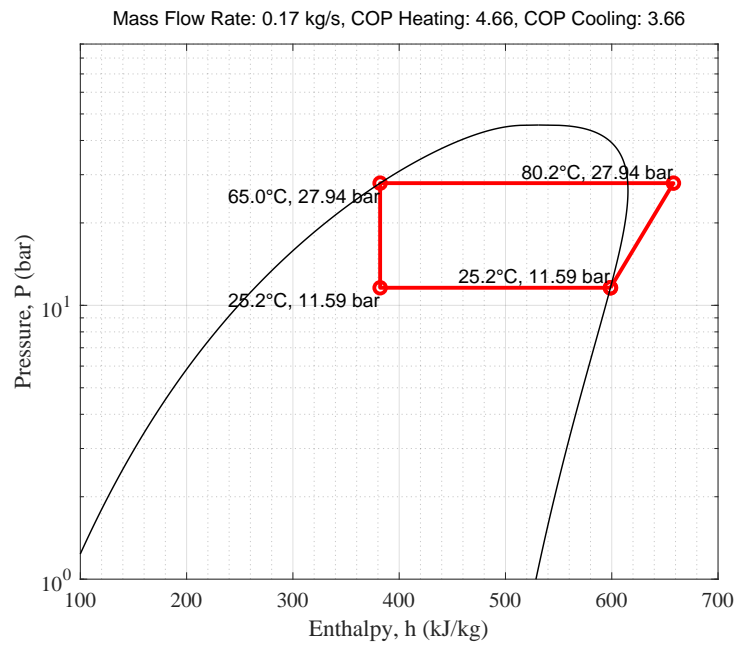


FIGURE A.6: (log)P-h chart R1270 (model)

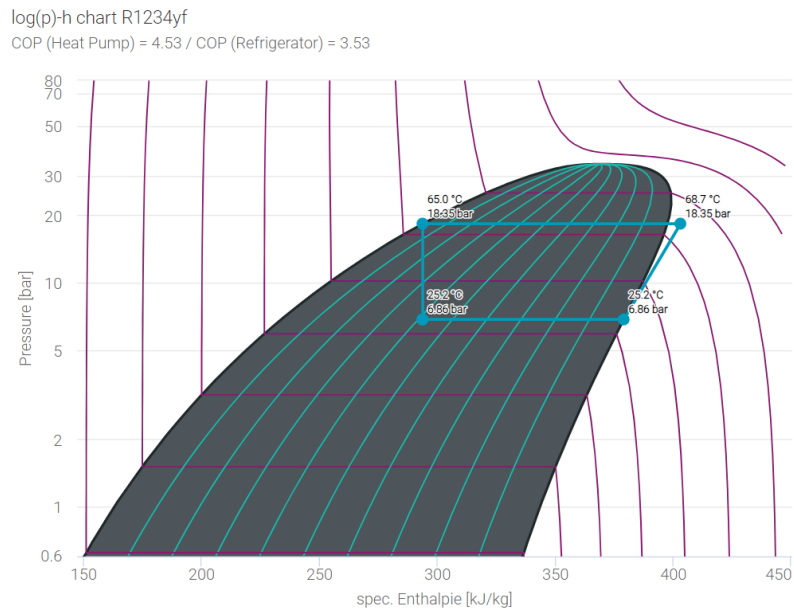


FIGURE A.7: (log)P-h chart R1234yf (reference)

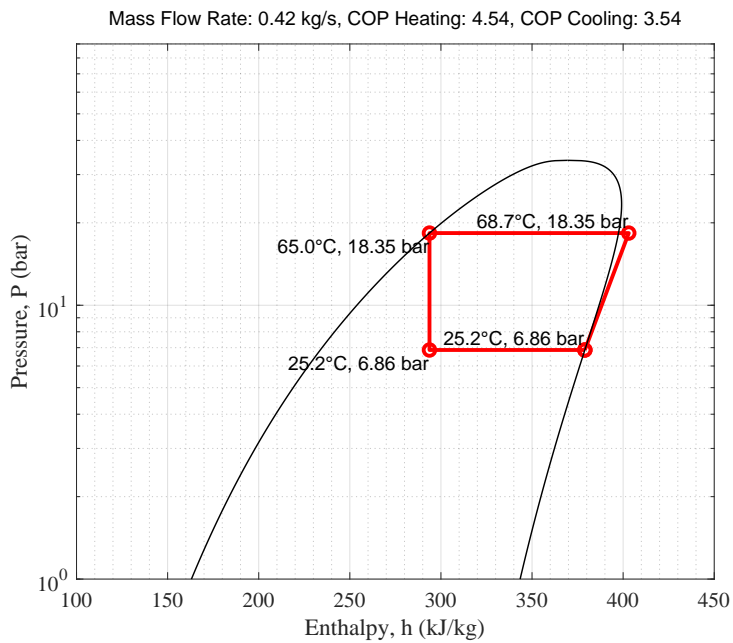


FIGURE A.8: (log)P-h chart R1234yf (model)

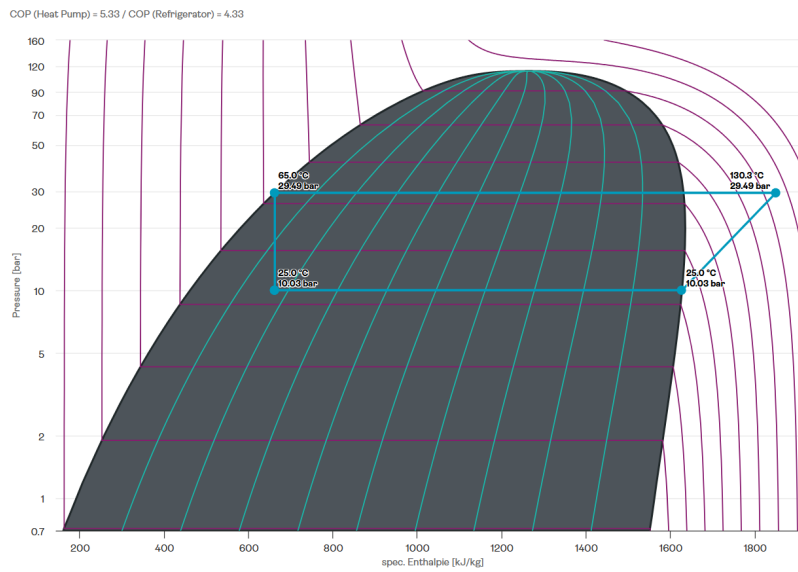


FIGURE A.9: (log)P-h chart R717 (reference)

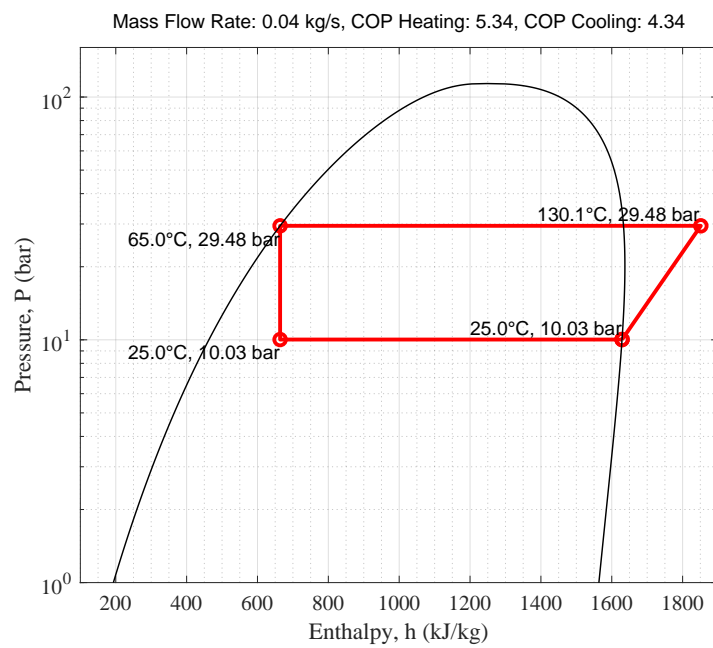


FIGURE A.10: (log)P-h chart R717 (model)

# Bibliography

- [1] International Energy Agency (IEA), “Tracking clean energy progress 2023.” <https://www.iea.org/reports/tracking-clean-energy-progress-2023>, 2023. Licence: CC BY 4.0.
- [2] K. Adamson, T. G. Walmsley, J. K. Carson, Q. Chen, F. Schlosser, L. Kong, and D. J. Cleland, “High-temperature and transcritical heat pump cycles and advancements: A review,” *Renewable and Sustainable Energy Reviews*, vol. 167, p. 112798, 2022.
- [3] Y. Dong and R. Wang, “When and how to use cascade high temperature heat pump—its multi-criteria evaluation,” *Energy Conversion and Management*, vol. 309, p. 118435, 2024.
- [4] D. Wu, B. Hu, and R. Wang, “Vapor compression heat pumps with pure low-GWP refrigerants,” *Renewable and Sustainable Energy Reviews*, vol. 138, p. 110571, 2021.
- [5] C. Arpagaus, F. Bless, J. Schiffmann, and S. S. Bertsch, “Multi-temperature heat pumps: A literature review,” *International Journal of Refrigeration*, vol. 69, pp. 437–465, 2016.
- [6] M. J. Atkins, M. R. Walmsley, and J. R. Neale, “The challenge of integrating non-continuous processes—milk powder plant case study,” *Journal of Cleaner Production*, vol. 18, no. 9, pp. 927–934, 2010.
- [7] J. V. Walden and P. Stathopoulos, “The impact of heat pump load flexibility on its process integration and economics,” *Journal of Cleaner Production*, vol. 462, p. 142643, 2024.
- [8] J. V. Walden, B. Wellig, and P. Stathopoulos, “Heat pump integration in non-continuous industrial processes by dynamic pinch analysis targeting,” *Applied Energy*, vol. 352, p. 121933, 2023.
- [9] Y. Cengel, *Thermodynamics: An Engineering Approach*. McGraw-Hill Education, 2014.
- [10] R. de Boer, A. Marina, B. Zühlsdorf, C. Arpagaus, M. Bantle, V. Wilk, B. Elmegaard, J. Corberán, and J. Benson, “Strengthening industrial heat pump innovation: Decarbonizing industrial heat,” tech. rep., TNO, 2020.
- [11] J. V. Walden and R. Padullés, “An analytical solution to optimal heat pump integration,” *Energy Conversion and Management*, vol. 320, p. 118983, 2024.
- [12] T. Zhu, J. Liang, J. E. Thorsen, O. Gudmundsson, W. Rohlf, and B. Elmegaard, “A heat pump system for simultaneous comfort floor cooling and domestic hot water,” in *14th IEA Heat Pump Conference 2023: Heat Pumps—Resilient and Efficient*, 2023.

- [13] RVO, “Best practice industriële warmtepompen.” <https://www.rvo.nl/sites/default/files/2022-12/Elektrificatie%20in%20de%20industrie%20-%20Best%20practice%20Warmtepompen.pdf>. [Accessed 06-09-2024].
- [14] O. Bamigbetan, T. M. Eikevik, P. Neksa, and M. Bantle, “Review of vapour compression heat pumps for high temperature heating using natural working fluids,” *International journal of refrigeration*, vol. 80, pp. 197–211, 2017.
- [15] L. Rajapaksha, “Influence of special attributes of zeotropic refrigerant mixtures on design and operation of vapour compression refrigeration and heat pump systems,” *Energy conversion and Management*, vol. 48, no. 2, pp. 539–545, 2007.
- [16] K. Uddin, S. Arakaki, and B. B. Saha, “Thermodynamic analysis of low-GWP blends to replace R410A for residential building air conditioning applications,” *Environmental Science and Pollution Research*, vol. 28, pp. 2934–2947, 2021.
- [17] H. Jouhara, A. Żabnieńska-Góra, B. Delpech, V. Olabi, T. El Samad, and A. Sayma, “High-temperature heat pumps: Fundamentals, modelling approaches and applications,” *Energy*, p. 131882, 2024.
- [18] M. Sadeghi, T. Petersen, Z. Yang, B. Zühlsdorf, and K. S. Madsen, “Thermal and economic performance assessment of different high temperature heat pump layouts for upgrading district heating to process heating of steam production at 160 °C,” *Energy*, vol. 313, p. 133832, 2024.
- [19] GETEC Group, “GETEC Energy Services - Cover Page.” <https://www.getec-energyservices.com/en/short-menu/cover-page/>, 2024. Accessed: 2024-11-18.
- [20] B. Linhoff and H. March, “Introduction to pinch technology,” tech. rep., Linhoff March Ltd, 1998. .
- [21] T. M. Inc., “Matlab version: 24.1.0 (r2024a),” 2024.
- [22] I. H. Bell, J. Wronski, S. Quoilin, and V. Lemort, “Pure and pseudo-pure fluid thermophysical property evaluation and the open-source thermophysical property library coolprop,” *Industrial & engineering chemistry research*, vol. 53, no. 6, pp. 2498–2508, 2014.
- [23] TLK Energy, “Pressure-Enthalpy Diagrams for Refrigerants,” 2024.
- [24] H. Getu and P. Bansal, “Thermodynamic analysis of an R744–R717 cascade refrigeration system,” *International journal of refrigeration*, vol. 31, no. 1, pp. 45–54, 2008.
- [25] H. W. Jung, H. Kang, W. J. Yoon, and Y. Kim, “Performance comparison between a single-stage and a cascade multi-functional heat pump for both air heating and hot water supply,” *International Journal of Refrigeration*, vol. 36, no. 5, pp. 1431–1441, 2013.
- [26] D. Zhou, Z. Meng, Y. Liu, S. Dong, F. Zhang, C. Ding, Z. Huo, and M. Wang, “Theoretical study of low-GWP refrigerants in high-temperature heat pump systems,” *International Journal of Low-Carbon Technologies*, vol. 18, pp. 881–886, 2023.

- [27] C. Arpagaus, S. Paranjape, L. Brendel, L. D. Simoni, K. Kontomaris, and S. S. Bertsch, “Experimental investigation of R1336mzz(E) in a high-temperature heat pump,” 2022.